AFAPL-TR-71-18

MECHANISM OF MIXING OF TWO NONREACTING GASES

PAUL JAMES ORTWERTH

TECHNICAL REPORT AFAPL-TR-71-18

OCTOBER 1971

AIR FORCE AERO PROPULSION LABORATORY
AIR FORCE SYSTEMS COMMAND
WRIGHT-PATTERSON AIR FORCE BASE, OHIO

136

NOTICE

When Government drawings, specifications, or other data are used for any purpose other than in connection with a definitely related Government procurement operation, the United States Government thereby incurs no responsibility nor any obligation whatsoever; and the fact that the government may have formulated, furnished, or in any way supplied the said drawings, specifications, or other data, is not to be regarded by implication or otherwise as in any manner licensing the holder or any other person or corporation, or conveying any rights or permission to manufacture, use, or sell any patented invention that may in any way be related thereto.

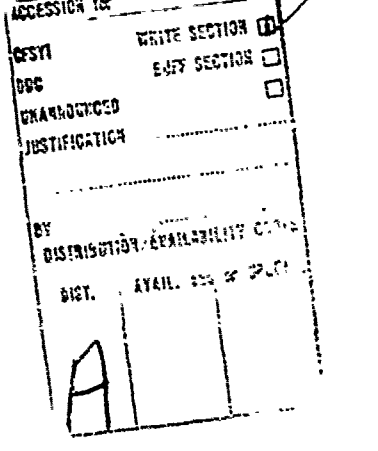

Copies of this report should not be returned unless return is required by security considerations, contractual obligations, or notice on a specific document.

AIR FORCE: 1-12-71/100

UNCLASSIFIED
Security Classification

DOCUMENT CONTROL DATA - R & D
(Security classification of title, body of abstract and indexing annotation must be entered when the overall report is classified)

1 ORIGINATING ACTIVITY (Corporate author)
Air Force Aero Propulsion Laboratory
Wright-Patterson Air Force Base, Ohio 45433

2a. REPORT SECURITY CLASSIFICATION
Unclassified

2b. GROUP

3 REPORT TITLE
MECHANISM OF MIXING OF TWO NONREACTING GASES

4 DESCRIPTIVE NOTES (Type of report and inclusive dates)

5 AUTHOR(S) (First name, middle initial, last name)
Paul James Ortwerth

6 REPORT DATE	7a. TOTAL NO OF PAGES	7b. NO OF REFS
October 1971	134	17

8a. CONTRACT OR GRANT NO	9a. ORIGINATOR'S REPORT NUMBER(S)
b. PROJECT NO 3012	AFAPL-TR-71-18
c. Task No. 301206	9b. OTHER REPORT NO(S) (Any other numbers that may be assigned this report)
d.	

10 DISTRIBUTION STATEMENT
This document has been approved for public release and sale; its distribution is unlimited.

11 SUPPLEMENTARY NOTES	12 SPONSORING MILITARY ACTIVITY
	Air Force Aero Propulsion Laboratory Wright-Patterson Air Force Base, Ohio 45433

13 ABSTRACT

The turbulence phenomena associated with the mixing of fuel and air in a supersonic combustion ramjet are studied. The turbulence generated by coaxial and normal jet fuel injection is studied by analyzing a control volume in which fuel and air are mixed. These two modes of fuel injection are examined for various initial conditions in order to compare their respective characteristics and determine the design advantages of each mode.

The results of this analysis show that large turbulence energies can be generated, much larger than the energy added by the jet. Thus one draws a mental picture of the fuel jet exciting the flow into a turbulent state. This turbulence energy if frozen into the flow causes losses in thrust and specific impulse. These losses are calculated as flight speed varies for both modes of fuel injection. A universal plot for a diatomic gas $\gamma = 1.4$ was determined for which specific impulse losses are found to be a function of relative turbulence intensity and flight speed. These losses are large but not catastrophic as previously reported by Dr. James Swithenbank of the University of Sheffield, England.

Experimental results from a compressible turbulent shear flow experiment, the decay of a supersonic free jet, having important theoretical implications and are used in formulating a new theoretical model for turbulent shear flow. A basic relationship between the local "eddy viscosity" and the square root of the local turbulent kinetic energy has been found for incompressible and supersonic jets. This result plus a correlation of the turbulent energy dissipation rate allows the formulation of a turbulent flow model that includes calculation of the turbulent kinetic [illegible] field as well as the mean velocity, mean temperature, and mean concentration fields.

DD FORM 1 NOV 65 1473

UNCLASSIFIED
Security Classification

13. ABSTRACT (Contd)

A fuel injector designed to maximize the turbulent kinetic energy was tested to verify the existing mixing rate correlations. This fuel injector, a normal jet, of high Mach number and rectangular cross section exhibited slightly larger penetration distances than predicted by a recent correlation developed by Povinelli at the NASA Lewis Flight Propulsion Laboratory. The mixing rate, as measured by decay of the maximum concentration, was nearly an order of magnitude faster than predicted by the correlation due to Henry at the NASA Langley Research Center. Further, it is postulated that the mixing length of this injector may be independent of initial conditions. The results of this study are directly applicable to the design of supersonic combustion ramjet engines.

14 KEY WORDS	LINK A		LINK B		LINK C	
	ROLE	WT	ROLE	WT	ROLE	WT
Ramjets, Scramjets Supersonic Mixing Turbulence Kinetic Energy in Supersonic Flow						

*U.S.Government Printing Office: 1971 756-080/215

AFAPL-TR-71-18

MECHANISM OF MIXING OF TWO NONREACTING GASES

PAUL JAMES ORTWERTH

FOREWORD

This report is based on dissertation previously submitted by the author to The Ohio State University in partial fulfillment of the requirements for the degree of Doctor of Philosophy. Only those changes necessary to make the thesis meet the requirements of an AFAPL Technical Report have been made. The work was accomplished at the Air Force Aero Propulsion Laboratory as part of Project 3012, "Special Ramjets." This report was submitted by the author 11 March 1971.

This technical report has been reviewed and is approved.

J. F. REGAN
Col, USAF
Ramjet Engine Division
Air Force Aero Propulsion Laboratory

ABSTRACT

The turbulence phenomena associated with the mixing of fuel and air in a supersonic combustion ramjet are studied. The turbulence generated by coaxial and normal jet fuel injection is studied by analyzing a control volume in which fuel and air are mixed. These two modes of fuel injection are examined for various initial conditions in order to compare their respective characteristics and determine the design advantages of each mode.

The results of this analysis show that large turbulence energies can be generated, much larger than the energy added by the jet. Thus one draws a mental picture of the fuel jet exciting the flow into a turbulent state. This turbulence energy if frozen into the flow causes losses in thrust and specific impulse. These losses are calculated as flight speed varies for both modes of fuel injection. A universal plot for a diatomic gas $\gamma = 1.4$ was determined for which specific impulse losses are found to be a function of relative turbulence intensity and flight speed. These losses are large but not catastropic as previously reported by Dr. James Swithenbank of the University of Sheffield, England.

Experimental results from a compressible turbulent shear flow experiment, the decay of a supersonic free jet, have important theoretical implications and are used in formulating a new theoretical model for turbulent shear flow. A basic relationship between the local "eddy viscosity" and the square root of the local turbulent kinetic energy has been found for incompressible and supersonic jets. This result plus a correlation of the turbulent energy dissipation rate allows the formulation of a turbulent flow model that includes calculation of the turbulent kinetic energy field as well as the mean velocity, mean temperature, and mean concentration fields.

A fuel injector designed to maximize the turbulent kinetic energy was tested to verify the existing mixing rate correlations. This fuel injector, a normal jet, of high Mach number and rectangular cross section exhibited slightly larger penetration distances than predicted by a recent correlation developed by Povinelli at the NASA Lewis Flight Propulsion Laboratory. The mixing rate,

as measured by decay of the maximum concentration, was nearly an order of magnitude faster than predicted by the correlation due to Henry at the NASA Langley Research Center. Further, it is postulated that the mixing length of this injector may be independent of initial conditions. The results of this study are directly applicable to the design of supersonic combustion ramjet engines.

TABLE OF CONTENTS

SECTION		PAGE
I	INTRODUCTION	1
	1.1 Background	1
	1.2 Purpose	2
II	THEORETICAL RELATIONSHIPS FOR TURBULENCE PRODUCTION AND PERFORMANCE LOSSES	3
	2.1 Discussion	3
	2.2 Analysis of Internal Flow	3
	2.3 Comparison of Normal and Coaxial Fuel Injection	11
	2.3.a Coaxial Injection	12
	2.3.b Normal Injection	14
	2.3.c Total Pressure Losses	14
	2.4 Compressible Homogeneous Turbulence	16
	2.5 Solution of the Compressible Equations of Motion for Coaxial and Normal Injection	22
	2.6 Frozen Flow	25
	2.7 Relative Performance	27
	2.8 Summary of Design Considerations	28
III	TURBULENT FIELD EQUATIONS FOR COAXIAL MIXING	29
	3.1 Compressible Mixing	29
	3.2 Turbulent Stress Tensor	29
	3.3 Dynamic Equations for Mean Motion	31
	3.4 Transformation of Equations	36
	3.5 Numerical Treatment of Differential Equations	37
	3.6 Equations of Motion on the Axis	39
	3.7 The Inverse Transformation	41
	3.8 Summary of Theoretical Considerations	41
IV	DESCRIPTION OF EXPERIMENTS	43
	4.1 Supersonic Free Jet	43
	4.1.a Nozzles	43
	4.1.b Instrumentation	43
	4.1.c Procedure	44
	4.1.d Accuracy of the Measurements	44
	4.2 Coaxial Supersonic Mixing	45
	4.2.a Instrumentation	46
	4.2.b Procedure	46
	4.2.c Accuracy	47

TABLE OF CONTENTS (Contd)

SECTION		PAGE
	4.3 Normal Jet Penetration and Mixing	47
	4.3.a Procedure	47
V	EXPERIMENTAL RESULTS	49
	5.1 Structure of Free Jet	49
	5.1.a Velocity Profiles	49
	5.1.b Total Temperature	49
	5.1.c Static Pressure Defect	50
	5.1.d Eddy Viscosity and Prandtl Number	50
	5.1.e Dissipation	51
	5.2 Coaxial Mixing	52
	5.2.a Pitot Pressures and Static Pressure	52
	5.2.b Concentration	52
	5.2.c Velocity Profile	52
	5.2.d Turbulence	52
	5.2.e Scale of Turbulence	53
	5.3 Normal Injection	53
	5.3.a Optical Measuremont Penetration	53
	5.3.b Concentration Measurement	54
	5.4 Summary of Important Experimental Results	55
VI	NUMERICAL RESULTS FOR FREE JETS	56
	6.1 Description of Turbulence Program Empirical Input	56
	6.2 Solutions for Incompressible Flow	57
	6.3 Solutions for Compressible Flows with Constant Total Temperature	58
	6.4 Flow With Excess Total Enthalpy	58
VII	CONCLUSIONS	60
APPENDIXES		
A.	Table of Experimental Conditions Free Jet Experiments	61
B.	Figures	63
REFERENCES		110

ILLUSTRATIONS

SKETCH		PAGE
1.	Control Volume for Constant Area Mixing	4
2.	Control Volume for Flow Over Flame Holder	10
3.	Control Volume for Coaxial Mixing	12
4.	Control Volume for Normal Jet Mixing	12
5.	Control Volume for Turbulence Decay	15
6.	Compressible Mixing Model	17
7.	Control Volume for Turbulent Combustion and Expansion	25
8.	Definition of Differences	37
9.	Schlieren Photograph of a Normal Sonic Jet	48

FIGURE		
1.	Schlieren of Free Jet Showing Turbulent and Nonturbulent Regions	64
2.	Turbulence Production in Internal Flow	65
3.	Effects of Initial Conditions on Turbulence Production	66
4.	Specific Impulse Losses Due to Freezing Turbulence Generated by Mixing	67
5.	Effect of Fuel Injection Mode on Combustor Total Pressure Losses	68
6.	Effect of Fuel Injection Mode on Performance	69
7.	Free Jet Exit Mach Number Profile	70
8.	Free Jet Exit Total Temperature Profiles	71
9.	Schematic Drawing of Instrumentation	72
10.	Comparison of Combination Probe and Naval Ordnance Laboratory Probe Data	73
11.	Accuracy of Mass Flow Rate at Nozzle Exit	74
12.	Accuracy of Exit Momentum Flux	75

ILLUSTRATIONS (Contd)

FIGURE		PAGE
13.	Accuracy of Normalized Jet Momentum	76
14.	Accuracy of Normalized Enthalpy	77
15.	Free Jet Centerline Velocity Decay	78
16.	Similarity of Radial Velocity Profiles of Free Jet	79
17.	Experimental Velocity Half Width; $\bar{T}_o/T_\infty = 1.0$	80
18.	Experimental Velocity Half Width; $\bar{T}_o/T_\infty > 1$	81
19.	Free Jet Centerline Total Temperature Decay	82
20.	Similarity Profile of Normalized Enthalpy Free Jet	83
21.	Normalized Enthalpy Half Width	84
22.	Experimental Free Jet Centerline Static Pressure	85
23.	Free Jet Centerline Turbulent Kinetic Energy	86
24.	Eddy Viscosity Correlation With Turbulent Pressure	87
25.	Turbulent Kinetic Energy Decay	88
26.	Coaxial Mixing Pitot and Static Pressure Profile	89
27.	Profile of Helium Mole Fraction	90
28.	Computed Mach Number Profile	91
29.	Computed Velocity Profile	92
30.	Autocorrelation Coefficients $\frac{Z}{D_j}$ 10	93
31.	Eulerian Time Scale	94
32.	Integral Scale of Turbulence	95
33.	Schlieren Photographs of Helium Penetration into a Mach 2.5 Airstream (Jet to Stream Total Pressure Ratio)	96
34.	Schlieren Photographs of Helium Penetration into a Mach 3.0 Airstream (Jet to Stream Total Pressure Ratio)	97
35.	Observed Penetration Height	98

ILLUSTRATIONS (Contd)

FIGURE		PAGE
36.	Profile of Helium Concentration	99
37.	Experimental Mixing Rate of the Normal Injector	100
38.	Effect of Compressibility on Eddy Viscosity	101
39.	Data Used to Determine Mach Number Dependence of Eddy Viscosity	102
40.	Comparison of Computed and Measured Turbulent Kinetic Energy from Reference 15	103
41.	Comparison of Theoretical and Experimental Centerline Velocity Decay; $T_o/T_\infty = 1$	104
42.	Comparison of Velocity and Normalized Enthalpy Decay	105
43.	Comparison of Velocity and Normalized Enthalpy Decay	106
44.	Theoretical and Experimental Free Jet Decay	107
45.	Theoretical and Experimental Free Jet Decay	108
46.	Comparison of Theoretical and Experimental Relative Turbulence Intensity on the Centerline	109

SYMBOLS

A	area
A_B	baffle cross sectional area
A_e	cross sectional area at exit of nozzle
A_f	cross sectional area of fuel at injection station
A_0	constant in pressure polynomial
A_1	cross sectional area of air flow at station 1
A_2	cross section area at station 2
A_3	cross section area at station 3
A_5	coefficient of fifth order term in pressure polynomial
A_{10}	coefficient of tenth order term in pressure polynomial
A_{12}	coefficient of twelfth order term in pressure polynomial
$\tilde{A}$	nondimensional area
a	"viscosity" in transformed equations
B_g	geometrical blockage of flame holder
b	width of mixing zone in Prandtl eddy viscosity formula
C_D	drag coefficient
C_f	friction coefficient
C_h	Stanton number, nondimensional heat transfer coefficient
C_p	specific heat at constant pressure
$\bar{C}_p$	time average specific heat
D	drag
D_e	effective diffusion coeffient
D_{eff}	diameter of a circle of cross sectional area A_f
$\mathcal{D}_f$	mass flow function at injection plane

$$\mathcal{D}_f = M_f \left(1 + \frac{\gamma-1}{2} M_f^2\right)^{-\frac{(\gamma+1)}{2(\gamma-1)}}$$

SYMBOLS (Contd)

D_j	jet diameter
D_1	mass flow function at station 1 $$D_1 = M_1 \left(1 + \frac{\gamma-1}{2} M_1^2\right)^{-\frac{(\gamma+1)}{2(\gamma-1)}}$$
d	dissipation of turbulent kinetic energy by molecular viscous shear forces
d_e	effective rate of conversion of kinetic energy into thermal energy
d_k	dissipation rate of turbulence kinetic energy
e_f	specific internal energy of jet fluid at injection station
e_1	specific internal energy of air at station 1
e_2	specific internal energy of mixture at station 2
e_3	specific internal energy of mixture at station 3
$\vec{e}_1, \vec{e}_2, \vec{e}_3$	unit vectors for (X_1, X_2, X_3) coordinates
F	stream thrust
F_e	stream thrust at nozzle exit
F_{X_1}	X_1 component of stream thrust
F_1	stream thrust at station 1
F_2	stream thrust at station 2
$\tilde{F}_1$	nondimensional stream thrust $\frac{F_1}{P_1 A_1}$
$\tilde{F}_2$	nondimensional stream thrust $\frac{F_2}{P_1 A_1}$
$\frac{f}{a}$	fuel air ratio
H	total enthalpy

SYMBOLS (Contd)

H_{AW}	adiabatic wall enthalpy
H_W	gas enthalpy at wall
$\overline{H}$	time averaged total enthalpy
h	specific enthalpy
h_T	specific enthalpy of turbulence
$\overline{h}$	time averaged specific enthalpy
h'	fluctuating specific enthalpy
h'_{ai}	fluctuating enthalpy of air in i-th eddy
h'_{fi}	fluctuating enthalpy of fuel in i-th eddy
$\overline{\overline{I}}$	identity tensor
K	turbulent kinetic energy per unit mass
k	molecular thermal conductivity
k_e	effective thermal conductivity
$\overline{k}$	time average conductivity
L_d	dissipation scale of turbulence
L_e	effective Lewis number
L_k	Lewis number for turbulent diffusion of K
L'	length of eddy
ℓ_{mix}	mixing length of turbulence in eddy viscosity law
M_e	Mach number at nozzle exit
M_f	Mach number of fuel at injection plane
M_1	Mach number of air at station 1
m_a	molecular weight of air
m_f	molecular weight of fuel

SYMBOLS (Contd)

m	normal coordinate mesh indice for numerical analysis of differential equations
$\dot{m}$	mass flow rate
n	downstream mesh indice for numerical analysis of differential equations
n	number of eddies crossing station 2 per unit time through area L^{12}
n_a	number of eddies containing air
n_f	number of eddies containing fuel
$\vec{n}$	outer normal unit vector to surface element
$\vec{n}_1$	outer normal to control volume at station 1
$\vec{n}_2$	outer normal to control volume at station 2
P	static pressure
P_T	turbulence static pressure
P_r	effective Prandtl number
P_∞	static pressure outside mixing zone
P_0	total pressure
P_{0_f}	total pressure of fuel at injection station
P_{0_1}	total pressure of air at station 1
$\bar{P}_1$	static pressure at station 1
	time average static pressure
$\bar{P}_0$	time average total pressure
$\bar{P}_{0_T}$	time average total pressure in turbulent flow with frozen turbulence energy
$\bar{P}_3$	mean static pressure at station 3
q_f	dynamic pressure of fuel at injection plane

SYMBOLS (Contd)

q_1	dynamic pressure of air at station 1
$\vec{q}$	heat flux vector
$\vec{q}_T$	turbulent heat flux vector
R	specific gas constant
r	radial coordinate in cylindrical polar coordinates
S	surface of integration
S_c	effective Schmidt number
T	static temperature
T	time period for time averaging
T_E	Eulerian integral time scale of turbulence
T_T	turbulence temperature
T_{O_T}	effective total temperature in frozen turbulent flow
T_O	total temperature
t_i	integration time for i-th eddy
U	X_1 coordinate velocity of $\vec{U}$
U	r coordinate velocity in cylindrical polar coordinates
U_i	velocity of i-th eddy
U_1	air velocity at station 1
$\overline{U}_2$	average velocity at station 2
$\overline{U}_3$	average velocity at station 3
$\overline{U}$	time average of velocity
U'	fluctuating velocity
U'	root mean square turbulence velocity
U_i'	fluctuating velocity of i-th eddy

SYMBOLS (Contd)

$\vec{U}$	vector velocity (U, V, W)
V	volume of integration
V	X_2 coordinate velocity
V	θ coordinate velocity in cylindrical polar coordinates
$\overline{V}$	mass average velocity
V'	fluctuating component of velocity V
W	X_3 coordinate velocity
W	z coordinate velocity in cylindrical polar coordinates
W_{max}	largest value of W at a given station
$\overline{W}$	time average velocity in cylindrical polar coordinates
W'	fluctuating component of velocity W
X	variable of polynomial
X_0	last distance from normal injector for which concentration was 100%
X_1, X_2, X_3	rectangular coordinates
Y_f	mass fraction of fuel in mixture
Y_i	mass fraction of species i
$\overline{Y_i}$	time average mass fraction of species i
Y_0	penetration height based on zero concentration point
Y_1	mass fraction of air in mixture
$\tilde{z}$	transformed streamwise coordinate
z	streamwise coordinate

GREEK SYMBOLS

γ	ratio of specific heat
ϵ	momentum parameter, 1 for coaxial mixing, 0 for normal injection

GREEK SYMBOLS (Contd)

ϵ	eddy viscosity
ϵ_D	eddy mass diffusion coefficient
ϵ_T	eddy thermal diffusion coefficient
ϵ_K	eddy difussion coefficient for turbulent energy
η	nondimensional parameter $\eta = \frac{f}{a} \frac{\bar{\rho}_{a_1}}{\rho_{f_1}}$
θ	nondimensional total enthalpy $\frac{\bar{H}}{h_{a_1}}$
Λ	integral scale of turbulence
μ	molecular viscosity coefficient
$\bar{\mu}$	time average viscosity
μ_e	effective viscosity coefficient
μ_T	turbulent viscosity coefficient
ρ	density
ρ_a	density of air
ρ_1	density of air at station 1
ρ'_{a_i}	fluctuating density of air in i-th eddy
$\bar{\rho}$	time average air density
ρ_f	density of fuel
$\bar{\rho}_f$	time average fuel density
ρ_{f_1}	density of fuel at station 1
ρ_{f_i}	density of fuel in i-th eddy
ρ'_{f_i}	fluctuating density of fuel in i-th eddy
ρ_{a_i}	density of air in i-th eddy
$\bar{\bar{\tau}}$	stress tensor due to molecular transport of momentum
$\bar{\bar{\tau}}_S$	shear part of stress tensor

GREEK SYMBOLS (Contd)

$\bar{\bar{\tau}}_{..}$	turbulent stress tensor
$\bar{\bar{\tau}}_{rs}$	shear part of turbulent stress tensor
$\bar{\bar{\tau}}'_{s}$	shear stress tensor of turbulent velocity fluctuation
ϕ	nondimensional enthalpy
ϕ	represents any variable
ψ	transformed radial coordinate in Von Mises plane

PREFACE

The prediction of turbulent mixing rates has always been one of the darkest secrets in the black art of propulsion. Because of its importance and lack of understanding of its mechanism,this phenomenon has been restudied. A new formulation is developed in this dissertation based on new data obtained from a simple turbulent shear flow, the supersonic free jet. This formulation grew from the need to explain the static pressure defect, measured on the centerline of the free jet extending from the end of the potential core downstream to the last measurement station. This defect was measured for all initial Mach numbers, total pressures, and total temperatures tested in the laboratory. This pressure defect is so large, in the high Mach number region of the jet, that it must be included in the dynamic of the flow. This static pressure defect is now believed to be a direct measurement of the radial component of the Reynolds stresses at that point in the flow.

I wish to express my appreciation to Professor Rudolf Edse for the friendship, guidance, and understanding he has given me as my advisor since the start of my academic work at The Ohio State University.

This work was accomplished at the Air Force Aero Propulsion Laboratory as part of Project 3012, Special Ramjets. I also wish to express appreciation to the following men of the Ramjet Division for their contributions to this work: To Mr. John T. Hojnacki, friend and confidant, who taught me much about modern electronic instrumentation systems and was always there when extra help was needed. To Mr. Wayne A. Zwart, formerly of the Ramjet Division, who did a competent job of mechanical design of the water cooled free jet combustor and nozzle.

To Mr. Kenneth G. Schwartzkopf who programmed the transformation of the data acquisition system tapes into dimensional flow variables; a program that I wanted changed constantly. To the technicians of the Laboratory, Mr. Robert A. Schelenz, Mr. Dante Cincerelli, and Mr. Ashton Sayre who cooperated fully with me to put forth our best efforts on the successful experiments and also the many frustrating and unsuccessful experiments not reported.

I also want to express my appreciation to Dr. Harold Wright of the Air Force Institute of Technology who supported some preliminary hot wire anemometer experiments in the Mechanical Engineering Lab.

Finally, I want to thank Susan, for giving me five beautiful babies, our most important contribution to this world.

SECTION I

INTRODUCTION

1.1 BACKGROUND

The development of the supersonic combustion ramjet engine for hypersonic flight propulsion has necessitated much research on the processes of fuel injection and mixing because of their great influence on engine performance and design. Incomplete mixing is obviously undesirable since unmixed fuel cannot be burned. Long mixing lengths not only increase engine weight and cooling requirements but also drag. Therefore, rapid mixing is desirable. The fuel injection mode strongly governs total pressure losses due to mixing so that total engine performance may be reduced greatly by mixing. The mixing flow field in the supersonic combustion ramjet is highly turbulent and thus mixing rates are determined by the turbulent transport of mass and momentum rather than molecular transport. Turbulent transport results from the time correlation of the unsteady velocity and concentration fluctuations in the flow field. The turbulence kinetic energy produced by mixing can be a large fraction of the stream total energy. In recent publications (References 1 and 2), Swithenbank has calculated the turbulence generated by coaxial injection of fuel in the combustor. His analysis shows that large losses may be incurred by the turbulence energy production due to mixing. He also shows that this loss increases with flight speed, and that it ultimately becomes the primary factor limiting the top speed of the supersonic combination ramjet. The validity of Swithenbank's results are open to criticism since his analysis is based mainly on intuitive formula rather than rigorous theoretical development. Both experimental and analytical studies of gaseous mixing have been used for engine design. The most extensive work has been directed at the coaxial jet. Analytical models employing many eddy viscosity models have been developed.

The correct formulation of an eddy viscosity has been of prime importance in many researches. The eddy viscosity models developed in this country are generally minor modifications of the Prandtl velocity defect formula. These formulas relate the eddy viscosity to the mean flow velocity, however, rather than to the turbulence velocities. This appears to be a basic limitation to

these formulations and the number of models developed attests to the lack of confidence in their general applicability. This lack of confidence stems from the fact that no fundamental theory exists to explain these models; however, an attempt to formulate a uniform model has been proposed by Shetz (Reference 3). Recently, a new approach has been proposed by Bradshaw and Ferriss (Reference 4) which does away with the eddy viscosity concept and relates the turbulent shear stress directly to the turbulent kinetic energy. This method has been extended to coaxial mixing at low subsonic Mach numbers by Lee and Harsha (Reference 5). This method has the disadvantage that turbulent shear stress can only be zero when the turbulent kinetic energy is zero unless ad hoc assumptions are used to avoid this difficulty. In addition this model appears to reverse the roles of shear stress and energy in the dynamics of the generation of turbulence.

Normal fuel injection has also been investigated extensively and mathematical models for penetration have been developed (Reference 6); however, no analytical solutions of the mixing problem have been obtained due to the mathematical complexity of the three dimensional flow field. An important correlation of mixing rate for normal jets at various initial conditions has been obtained by Henry (Reference 7). Development of practical mixing systems depends primarily on empirical results for both coaxial and normal injection. These two modes of injection involve very different mixing characteristics and pressure losses. Figure 1 in the appendix shows the structure of turbulence obtained by a spark Schlieren photograph. The highly turbulent region in the center of the photograph is the turbulence generated by the shear flow of a supersonic free jet. It is evident that any theoretical calculation of turbulent flows should include a calculation of the turbulent energy field also; this will be the main effort of this dissertation.

1.2 PURPOSE

The purpose of this dissertation is to investigate the influence of the initial conditions in supersonic combustors on total pressure loss, the production of turbulence and performance loss, and then to determine the basic relationship between turbulent kinetic energy and turbulent transport rates.

SECTION II

THEORETICAL RELATIONSHIPS FOR TURBULENCE PRODUCTION AND PERFORMANCE LOSSES

2.1 DISCUSSION

The purpose of this section is to rigorously formulate the mathematical analysis in order to first, calculate the maximum turbulent kinetic energy produced in a given mixing flow, and, second, to calculate the effect of this turbulence on the performance of the supersonic ramjet engine.

This analysis is formulated for both the coaxial and normal fuel injection mode so that the importance of geometric boundary conditions can be assessed. The calculations are also done for incompressible and compressible flow so that the effects of compressibility can be determined as well as the effects of the dynamic initial conditions; Mach number, molecular weight, total temperature, and total pressure. The total pressure losses will be studied to determine if turbulence intensity can be varied independently of total pressure loss. The theoretical results of this section are then used to determine the single element injector design with the highest turbulence intensity.

2.2 ANALYSIS OF INTERNAL FLOW

The production entropy can occur by reversible and irreversible processes. The irreversible processes are caused by gradients of concentration and velocity driving the molecular transport of mass, energy, and momentum. We will assume that this entropy production is the result of mixing and the dissipation of turbulent energy. Thus we can calculate the total turbulence intensity produced in a given flow by considering flows without entropy change.

The one-dimensional or integral equations of motion for turbulent flow can be easily developed by following the procedure of defining the instantaneous field variables to be the sum of the time mean and fluctuating part and integrating the equations of motion. This integration defines the appropriate average value at any streamwise location.

Since this integration is both a time and space integration, the equations are mean conservation equations and they include the Reynolds stresses.

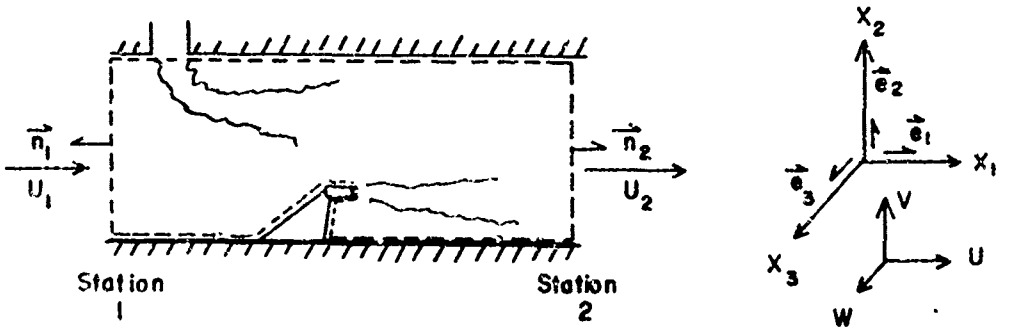

Sketch 1. Control Volume for Constant Area Mixing

The continuity equation is

$$\int_V \frac{\partial \rho}{\partial t}\, dV + \int_S \rho \vec{U} \cdot \vec{n}\, dS = 0 \tag{1}$$

The first term represents the accumulation in volume V bounded by surface S. The second term is the net mass flux through the boundary surface. Time averaging the above equation yields:

$$\int_V \frac{\partial}{\partial t}\left[\frac{1}{T}\int_T \rho\, dt\right] dV + \int_S \left[\frac{1}{T}\int_T \rho \vec{U}\, dt\right] \cdot \vec{n}\, dS = 0 \tag{2}$$

Since we have specified a flow which is statistically steady in time,

$$\frac{\partial}{\partial t}\left(\frac{1}{T}\int_T \rho\, dt\right) = 0 \tag{3}$$

by definition and this result can be generalized to any function ϕ as well as ρ. The mass flux term can be used to define a new integration variable

$$\left(\frac{1}{T}\int_T \rho \vec{U}\, dt\right) \cdot \vec{n} \equiv \frac{d\dot{m}}{dS} \tag{4}$$

The sign is determined by the product $\vec{U} \cdot \vec{n}$ where $\vec{n}$ is the outer normal to the boundary surface S. The continuity equation then becomes

$$\int_S d\dot{m} = 0 \tag{5}$$

For a mixing problem as shown in Sketch 1, the equation reduces to

$$\dot{m}_2 = \dot{m}_1 + \dot{m}_f \tag{6}$$

Note that continuity has not defined an average velocity.

The momentum integral equation is

$$\int_V \frac{\partial}{\partial t} \rho U \, dV + \int_S (\rho \vec{U} \vec{U} - \bar{\bar{\tau}} \cdot \vec{n}) \, dS = 0 \tag{7}$$

where $\bar{\bar{\tau}}$ is the stress tensor defined such that $\bar{\bar{\tau}} \cdot \vec{n}$ is the force per unit area acting externally on the boundary surface S and the sign is determined by the coordinate system positive direction; thus the normal force in the boundary at station 1 is positive and at station 2 is negative. Normally $\bar{\bar{\tau}}$ is written as the sum of a normal stress and shear stress

$$\bar{\bar{\tau}} = - p \bar{\bar{I}} + \bar{\bar{\tau}}_S \tag{8}$$

Proceeding to time average the momentum equation, the first term of Equation 7 vanishes if we define

$$\phi = (\rho \vec{U}) \tag{9}$$

in Equation 3. From this point we will consider the X_1 (streamwise) coordinate only, noting that according to Sketch 1 the outer normal $\vec{n}_1$ is negative and $\vec{n}_2$ is positive. Consider the momentum flux.

$$\left(\frac{1}{T} \int_T \rho \vec{U} \vec{U} \, dt \, \vec{n} \right)_{X_1} = \left(\frac{1}{T} \int_T \vec{U} (\rho \vec{U} \cdot \vec{n}) \, dt \right)_{X_1} \tag{10}$$

Equation 10 can be written as the sum of two terms, the mean momentum flux and the negative of the normal Reynolds stress

$$\left(\frac{1}{T} \int_T \rho \hat{U} \hat{U} \hat{n} \, dt \right)_{X_1} = \bar{U} \frac{d\dot{m}}{dS} - (\bar{\bar{\tau}}_T \cdot \vec{n})_{X_1} \tag{11}$$

Since by definition

$$\bar{\bar{\tau}}_T \equiv - \frac{1}{T} \int_T (\rho \vec{U})' \vec{U}' \, dt \tag{12}$$

The time average velocity $\bar{U}$ at a point has been defined by the momentum flux. The fluid particle has only three degrees of freedom at a given point. However, by time averaging the equation of motion, there are also effectively 3 internal degrees of freedom. These degrees of freedom, if excited, contribute to the

mean flow momentum and energy. The mean density at a point is defined as follows:

$$\bar{\rho} = \frac{\overline{\rho U}}{\bar{U}}$$

thus the average transverse velocity becomes

$$\bar{V} = \frac{\overline{\rho V}}{\bar{\rho}} = \frac{1}{T} \int_T V \, dt$$

Averaging Equation 7 yields

$$\left[\int_S \frac{1}{T} \int_T (\rho \vec{U} \vec{U} - \bar{\bar{\tau}}) \vec{n} \, dt \, dS \right]_{X_1} = \int_m \bar{U} \, d\dot{m} - \int_S \left[(\bar{\bar{\tau}}_T + \bar{\bar{\tau}}) \vec{n} \right]_{X_1} dS \qquad (13)$$

Equation 13 can now be integrated using the boundary condition that $\bar{\bar{\tau}}_T = 0$ on a solid boundary. There may also be area changes between station 1 and station 2 on which the normal stresses will produce either a thrust or drag (T-D).

The integrated shear stresses will be expressed by a friction coefficient and an effective $L/_D$. The result is

$$\begin{aligned} \dot{m}_2 \bar{U}_2 + (\bar{P}_2 + (\overline{\rho U})' U')_2 A_2 = {} & \dot{m}_1 \bar{U}_1 + (\bar{P} + (\overline{\rho U})' U')_1 A_1 \\ & + \dot{m}_f \bar{U}_f + (\bar{P} + (\overline{\rho U})' U')_f A_f \\ & + (T-D) - 4 C_f \frac{L}{D} A_1 \left(\frac{1}{2} \bar{\rho}_1 \bar{U}_1^2 \right) \end{aligned} \qquad (14)$$

The velocity in this equation has been time averaged and then mass flux averaged and thereby the mean total momentum flux has been defined. The pressure and normal Reynolds stress have been averaged over the cross sectional area normal to the X_1 coordinate.

Note that turbulence shows up in the momentum equation and contributes to the stream thrust. Finally the energy equation in integral form must be time averaged

$$\int_V \frac{\partial}{\partial t}(\rho H)\,dV + \int_S \rho \vec{U} H \cdot \vec{n}\,dS = \int_S (\vec{U}\cdot\bar{\bar{\tau}}_S)\cdot\vec{n}\,dS + \int_S \vec{q}\cdot\vec{n}\,dS + \int_V \frac{\partial P}{\partial t}\,dV \qquad (15)$$

Now by time averaging, terms 1 and 5 of Equation 15 will vanish and the viscous work term 3 is negligible. The fourth term is the net heat flux which is assumed to be due to conduction at the wall. The second term will need expansion.

By definition of mean and fluctuating quantities

$$H = \bar{h} + h' + \frac{\bar{\vec{U}}\cdot\bar{\vec{U}}}{2} + \bar{U}U' + \bar{V}V' + \bar{W}W' + \left(\frac{U'^2+V'^2+W'^2}{2}\right) \qquad (16)$$

and

(17)

then the integrand of term 2 becomes

$$\begin{aligned}\rho\vec{U}H = {} & (\overline{\rho\vec{U}})\bar{h} + (\overline{\rho\vec{U}})h' + (\overline{\rho\vec{U}})\frac{\bar{\vec{U}}\cdot\bar{\vec{U}}}{2} + (\overline{\rho\vec{U}})\bar{U}U' \\ & + (\overline{\rho\vec{U}})\bar{V}V' + (\overline{\rho\vec{U}})\bar{W}W' + (\overline{\rho\vec{U}})\left(\frac{U'^2+V'^2+W'^2}{2}\right) \\ & + (\rho\vec{U})'\bar{h} + (\rho\vec{U})'h' + (\rho\vec{U})'\frac{\bar{\vec{U}}\cdot\bar{\vec{U}}}{2} + (\rho\vec{U})'U'\bar{U} \\ & + (\rho\vec{U})'V'\bar{V} + (\rho\vec{U})'W'\bar{W} + (\rho\vec{U})'\left(\frac{U'^2+V'^2+W'^2}{2}\right)\end{aligned} \qquad (18)$$

time averaging the above expression gives

$$\overline{\rho\vec{U}H} = \overline{\rho\vec{U}}\,\bar{h} + \overline{\rho\vec{U}}\,\frac{\vec{\bar{U}}\cdot\vec{\bar{U}}}{2}$$

$$\text{I} \qquad + \vec{\bar{U}}\cdot\bar{\bar{\tau}}_T$$

$$\text{II} \qquad + \overline{\rho\vec{U}}\left(\frac{U'^2+V'^2+W'^2}{2}\right) \qquad (19)$$

$$\text{III} \qquad + \overline{(\rho\vec{U})'h'}$$

$$\text{IV} \qquad + \overline{(\rho\vec{U})'\left(\frac{U'^2+V'^2+W'^2}{2}\right)}$$

The turbulence terms in the equation have the following significance:

I. The work of the Reynolds stresses on the mean flow
II. The convection of the turbulence kinetic energy
III. The diffusion of specific enthalpy
IV. Diffusion of the turbulence kinetic energy

The equation can be simplified by defining the turbulent stress tensor to be the sum of a hydrostatic part and a shear stress. The turbulence pressure is defined to be (for incompressible flow)

$$P_T = \frac{\bar{\rho}}{3}\,\overline{(U'^2+V'^2+W'^2)} \qquad (20)$$

Equation 19 can be simplified to read

$$\overline{\rho\vec{U}H} = \overline{\rho\vec{U}}\,\bar{H} + \dot{\vec{q}}_T - \vec{\bar{U}}\cdot\bar{\bar{\tau}}_{T_S} \qquad (21)$$

where $\bar{H}$ and $\dot{\vec{q}}$ are defined to be

$$\bar{H} = \bar{h} + \frac{\overline{\vec{U}\cdot\vec{U}}}{2} + \frac{P_T}{\bar{\rho}} + \frac{\overline{U'^2+V'^2+W'^2}}{2} \qquad (22)$$

and

$$\dot{\vec{q}}_T = \overline{(\rho\vec{U})'h'} + \overline{(\rho\vec{U})'\left(\frac{U'^2+V'^2+W'^2}{2}\right)} \qquad (23)$$

The time average of Equation 15 now reads

$$\int_S \overline{\rho \vec{U} H} \cdot \vec{n}\, dS = \int_S \vec{\bar{U}} \cdot (\bar{\bar{\tau}}_{T_S} + \bar{\bar{\tau}}_S) \cdot \vec{n}\, dS + \int_S -(\dot{\vec{q}}_T + \dot{\vec{q}}) \cdot \vec{n}\, dS \qquad (24)$$

This equation is now integrated over the control volume to give the energy equation

$$\dot{m}_2 \left(\bar{h}_2 + \frac{\vec{\bar{U}}_2 \cdot \vec{\bar{U}}_2}{2} + \frac{P_{T_2}}{\rho_2} + \left(\frac{\overline{U'^2+V'^2+W'^2}}{2}\right)\right) = \dot{m}_1 \left(\bar{h}_1 + \frac{\vec{\bar{U}}_1 \cdot \vec{\bar{U}}_1}{2} + \frac{P_{T_1}}{\rho_1} + \frac{\overline{U'^2+V'^2+W'^2}}{2}\right) + \dot{m}_f \left(\bar{h}_f + \frac{\vec{\bar{U}}_f \cdot \vec{\bar{U}}_f}{2} + \frac{P_{T_f}}{\rho_f} + \frac{\overline{U'^2+V'^2+W'^2}}{2}\right) + C_h \bar{\rho} \bar{U}_1 (H_W - H_{AW}) 4 \frac{L}{D} A_1 \qquad (25)$$

From Equation 22 a turbulence enthalpy can be defined

$$h_T = \frac{P_T}{\rho} + \frac{\overline{U'^2+V'^2+W'^2}}{2} \qquad (26)$$

It is also useful at this point to introduce the concept of a turbulence temperature such that an equation of state exists for turbulence

$$P_T = \bar{\rho} R T_T \qquad (27)$$

Thus a useful expression for the turbulence enthalpy is

$$h_T = \frac{5}{2} R T_T \qquad (28)$$

These equations reinforce the idea that turbulence is an extra internal degree of freedom for the fluid. For this degree of freedom the thermodynamic properties correspond to those of a monatomic gas. Turbulence contributes to the thermodynamics of the flow but with a separate temperature from the gas.

This analysis is completely general at this point. To proceed several assumptions are needed. For incompressible flow the conservation of volume flow rate is assumed. First let us calculate the turbulence produced by a baffle or flame holder in a constant area pipe. The details are given to present the method of solution and explore this basic mechanism of producing turbulence.

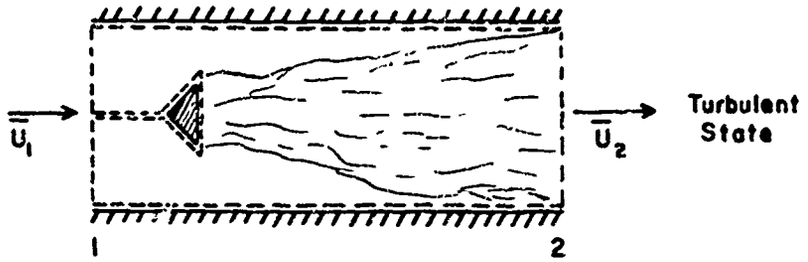

Sketch 2. Control Volume for Flow Over Flame Holder

The conservation equations are:

Incompressibility

$$\bar{U}_2 A_2 = \bar{U}_1 A_1 \tag{29}$$

Momentum

$$\dot{m}\,\bar{U}_2 + (\bar{P}_2 + P_{T_2})A_2 = \dot{m}\,\bar{U}_1 + \bar{P}_1 A_1 - D \tag{30}$$

Energy

$$\dot{m}\,\bar{H}_2 = \dot{m}\,\bar{H}_1 \tag{31}$$

where

$$\bar{H} = \bar{e} + \frac{\bar{P}}{\rho} + h_T + \frac{U^2}{2} \tag{32}$$

Assuming that no dissipation of turbulent kinetic energy has occurred, the internal energy is constant, Thus with Equation 29 the energy equation yields

$$h_T = \bar{P}_1 - \bar{P}_2 \tag{33}$$

The pressure drop can be found from the momentum equation. Following Swithenbank (Reference 2) we let

$$B_g = \frac{A_B}{A} \tag{34}$$

and

$$D = \frac{1}{2} \rho U_{max}^2 C_D A_B \tag{35}$$

where

$$U_{max} = \frac{U_1}{1 - B_g} \tag{36}$$

Then Equation 30 becomes upon substitution of Equation 29, 34, 35, and 36

$$P_{T_2} = \bar{P}_1 - \bar{P}_2 - \frac{C_D}{B_g} \frac{1}{2} \rho \bar{U}_1^2 \frac{B_g^2}{(1-B_g)^2} \tag{37}$$

Thus combining Equation 37 and 33 we find

$$P_T = \frac{1}{3} \rho \bar{U}_1^2 \frac{C_D}{B_g} \left(\frac{U_{max}}{U_1} - 1 \right)^2 \tag{38}$$

or we can write the turbulence intensity as

$$\frac{U'}{\bar{U}} = \left(\frac{1}{3} \frac{C_D B_g}{(1-B_g)^2} \right)^{1/2} \tag{39}$$

We can also determine the mean static pressure drop

$$\bar{P}_1 - \bar{P}_2 = \frac{5}{3} \left(\frac{1}{2} \rho \bar{U}^2 \right) \frac{C_D B_g}{(1-B_g)^2} \tag{40}$$

These formulas Equations 39 and 40 are not the same as Swithenbank (Reference 2) presents for this problem. Comparing specific cases we find for $B_g = 0.25$ and $C_D = 0.4$ that Swithenbank's formulas overestimate the turbulence kinetic energy by nearly a factor of three. This analysis shows that turbulence is produced by a velocity difference squared while it might be thought that turbulence would be a function of the differences of kinetic energy.

2.3 COMPARISON OF NORMAL AND COAXIAL FUEL INJECTION

Next we will look at two mixing problems (Sketches 3 and 4).

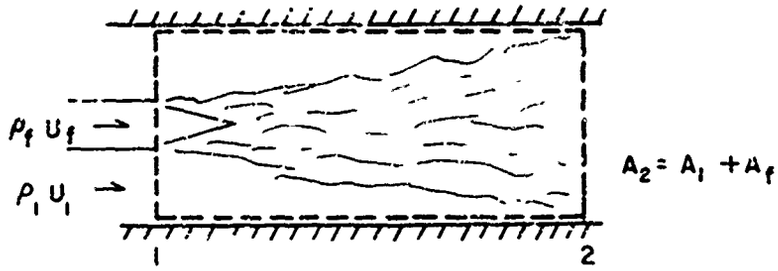

Sketch 3. Control Volume for Coaxial Mixing

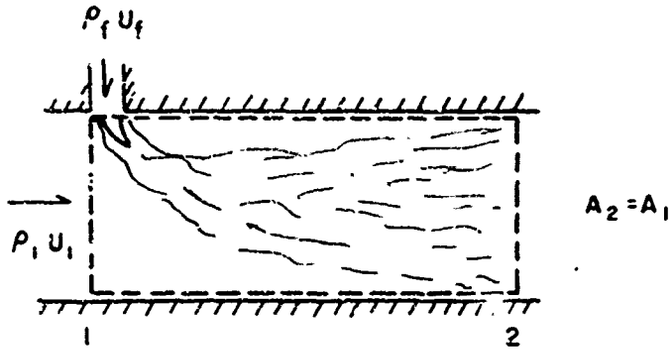

Sketch 4. Control Volume for Normal Jet Mixing

These are two practical configurations for supersonic mixing as well as the subsonic incompressible case. It is of interest to compare these two to determine the effects of geometry and jet velocity on the turbulence intensity and total pressure.

2.3.a. Coaxial Injection

Assuming the fluids are incompressible yields

$$\bar{U}_2 A_2 = \bar{U}_1 A_1 + \bar{U}_f A_f \tag{41}$$

Assuming no dissipation of turbulent energy

$$\bar{e}_2 = Y_1 \bar{e}_1 + Y_f \bar{e}_f \tag{42}$$

where

$$Y_1 = \frac{\dot{m}_1}{\dot{m}_2} \quad , \quad Y_f = \frac{\dot{m}_f}{\dot{m}_2} \tag{43}$$

and

$$\frac{f}{c} = \frac{\dot{m}_f}{\dot{m}_1}$$

the momentum equation for coaxial mixing is

$$\dot{m}_2 \overline{U}_2 + (\overline{P}_2 + P_T)A_2 = \dot{m}_1 \overline{U}_1 + \dot{m}_f \overline{U}_f + \overline{P}_1 (A_1 + A_2) \tag{44}$$

The energy equation becomes

$$\overline{H}_2 = Y_1 \overline{H}_1 + Y_f \overline{H}_f \tag{45}$$

where

$$\overline{H} = \overline{e} + \frac{\overline{P}}{\overline{\rho}} + \frac{\overline{U}^2}{2} + h_T \tag{46}$$

With a little algebra these equations can be solved to give

$$\frac{U_2'}{\overline{U}_2} = \left(\frac{1}{3} \left[Y_1 \left(\frac{\overline{U}_1}{\overline{U}_2} - 1 \right)^2 + Y_f \left(\frac{\overline{U}_f}{\overline{U}_2} - 1 \right)^2 \right] \right)^{1/2} \tag{47}$$

where

$$\overline{U}_2 = \overline{U}_1 \frac{\left(1 + \frac{f}{a} \frac{\rho_1}{\rho_f}\right)}{\left(1 + \frac{A_f}{A_1}\right)} \tag{48}$$

From continuity of mass flow rate, the mean density is

$$\overline{\rho}_2 = \rho_1 \frac{\left(1 + \frac{f}{a}\right)}{\left(1 + \frac{f}{a} \frac{\rho_1}{\rho_f}\right)} \tag{49}$$

The pressure change across the mixing zone is

$$\overline{P}_1 - P_2 = P_T + \frac{\rho_1 \overline{U}_1^2}{\left(1 + \frac{A_f}{A_1}\right)} \left[\frac{\left(1 + \frac{f}{a}\right)\left(1 + \frac{f}{a} \frac{\rho_1}{\rho_f}\right)}{\left(1 + \frac{A_f}{A_1}\right)} - \left(1 + \left(\frac{f}{a}\right)^2 \frac{A_1}{A_f} \frac{\rho_1}{\rho_f}\right) \right] \tag{50}$$

2.3.b. Normal Injection

For the problem of Sketch 4, the area is constant and there is no fuel momentum in the streamwise direction. The solution is

$$\frac{U_2'}{\bar{U}_2} = \left(\frac{1}{3}\left[\gamma_1\left(\frac{\bar{U}_1}{\bar{U}_2}-1\right)^2+\gamma_f\left(\frac{\bar{U}_f^2}{\bar{U}_2^2}-1\right)\right]\right)^{1/2} \tag{51}$$

where

$$\bar{U}_2 = \bar{U}_1\left(1+\frac{f}{a}\right)\frac{\rho_1}{\rho_f} \tag{52}$$

and

$$\bar{\rho}_2 = \rho_1\frac{\left(1+\frac{f}{a}\right)}{\left(1+\frac{f}{a}\frac{\rho_1}{\rho_f}\right)} \tag{53}$$

Equation 51 can also be written in terms of the known inputs and solved for turbulence intensity

$$\frac{U'}{\bar{U}_2} = \left(\frac{1}{3}\frac{1}{\left(1+\frac{f}{a}\right)}\left[\left(\frac{f}{a}\frac{\rho_1}{\rho_f}\right)^2\left(1+\frac{f}{a}\right)+\frac{f}{a}\left(1+2\frac{f}{a}\frac{\rho_1}{\rho_f}+\left(\frac{f}{a}\right)^2\left(\frac{\rho_1}{\rho_f}\right)^2\left(\frac{A_1}{A_f}\right)^2\right]\right)^{1/2} \tag{54}$$

For the normal jet there is always a pressure drop.

$$\bar{P}_1 - \bar{P}_2 = P_{T_2} + \rho_1 U_1^2\left[\left(1+\frac{f}{a}\right)\left(1+\frac{f}{a}\frac{\rho_1}{\rho_f}\right)-1\right] \tag{55}$$

Note that the last term in this equation is constant for a given fuel air ratio.

2.3.c. Total Pressure Losses

In the high speed case the losses or gains of total pressure from fuel injection will have an important effect on the total performance of an engine. It is, therefore, useful to examine the total pressure losses for the simpler incompressible case.

The final period in which the energy decays will be investigated by a similar analysis with the assumption that the final state will be free of turbulence.

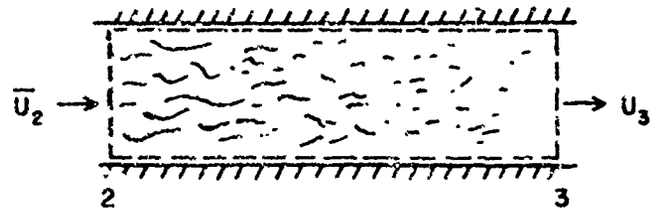

Sketch 5. Control Volume for Turbulence Decay

According to Sketch 5 which represents a constant area section in which the turbulence decays with no wall friction or heat transfer, the equations are:

Incompressibility

$$\bar{U}_3 A = \bar{U}_2 A \tag{56}$$

Momentum

$$\dot{m} \bar{U}_3 + \bar{P}_3 A = \dot{m} \bar{U}_2 + (\bar{P}_2 + P_T) A \tag{57}$$

Energy (including internal energy changes)

$$e_3 + \frac{P_3}{\rho} + \frac{\bar{U}_3^2}{2} = \bar{e}_2 + \frac{\bar{P}_2}{\rho} + \frac{\bar{U}_2^2}{2} + h_T \tag{58}$$

Solving Equations 56 and 57 for the static pressure, we find a pressure recovery:

$$P_3 = \bar{P}_2 + P_T \tag{59}$$

From Equation 58 the dissipation is found to be

$$e_3 = e_2 + \frac{3}{2} RT_T \tag{60}$$

Equation 59 shows that it is the sum of the mean static pressure and the turbulence pressure that should be considered the true hydrostatic normal stress in a fluid.

For a real flow the processes are not discrete nor one-dimensional, and production, convection, and dissipation of turbulent kinetic energy is a continuous process. The above analysis is correct for state 3, however, and is useful for comparing the performance of real systems.

Let us now compare the concurrent and normal fuel injectors relative to their abilities to produce turbulence and their associated pressure losses for a given fuel-to-air ratio as the jet velocity is varied while holding the inlet air conditions fixed. Pressure losses are taken to be the difference between the inlet total pressure and the outlet static and dynamic pressure plus turbulence pressure.

While these results are essentially only applicable to incompressible mixing, they do also provide some insight to the problem of supersonic mixing since the velocity ratio will be of the order of unity and thus density changes would be small. It is interesting that the mixing generates turbulence in the same way as a baffle by velocity difference squared. In this regard the normal jet is slightly different in that the jet kinetic energy is not controlled this way and it is easier to transform jet energy into turbulence.

These results indicate the presence of influences due to geometry and dynamic conditions. For the coaxial jet velocity, ratios between 0.5 and 2 produce relatively little turbulence. The normal jet produces larger turbulence intensities with smaller variation as velocity ratio changes; however, no thrust is produced by normal injection. There is another feature of the normal injector that merits note, the total pressure loss is constant for a given fuel-to-air ratio; that is, it is independent of turbulence intensity. Thus the designer can control mixing rate and losses for this type of injection. It further points out that losses are determined ultimately by the boundary conditions and not by "turbulence." The turbulence is the intermediate state which is dependent on the total dissipation necessary to arrive at the final equilibrium state from the initial conditions. Turbulence should be considered the mechanism of the transition processes from an initial unmixed state to a final equilibrium state. The analysis for these two cases will be extended to the case of supersonic mixing by including compressibility effects. This extension is necessary since "flow work" can indeed modify the results.

2.4 COMPRESSIBLE HOMOGENEOUS TURBULENCE

We will consider the ideal situation in which no transformation of turbulent kinetic energy into thermal energy has taken place; further let us assume an

absence of molecular mixing or heat conduction which is consistent with the first assumption. These conditions represent the limiting case of an infinite Reynolds number. In order to evaluate the integral equations of motion, we will have to specify the spectrum and scale of turbulence. However, it appears that this scale is arbitrary as long as the turbulence is homogeneous and no gradients exist. We will assume that a definite scale for the "eddies" exists and that the turbulent velocity spectrum of these is single valued at U'. Consider the following sketch of a set of cubical cells of length L' which represent the turbulent eddy flux.

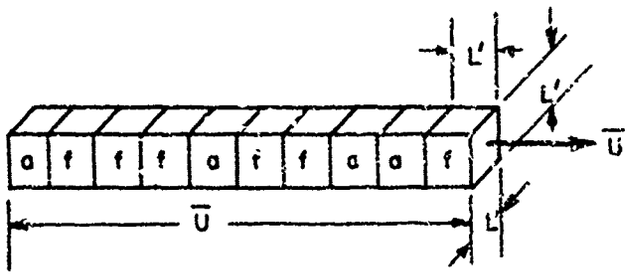

Sketch 6. Compressible Mixing Model

Some of these eddies are fuel eddies and some are air eddies. For the i-th fuel cell, the density is

$$\rho_{fi} = \bar{\rho}_f + \rho'_{fi} \tag{61}$$

The velocity can be written

$$\vec{U}_i = (\bar{U} + U'_i)\vec{e}_1 + V'_i \vec{e}_2 + W'_i \vec{e}_3 \tag{62}$$

where by assumption

$$|U'_i| = |V'_i| = |W'_i| = U' \tag{63}$$

Similarly for air the density and velocity are

$$\rho_{aj} = \bar{\rho}_a + \rho'_{aj} \tag{64}$$

$$\vec{U}_j = (\bar{U} + U'_j)\vec{e}_1 + V'_j \vec{e}_2 + W'_j \vec{e}_3 \tag{65}$$

Now the total number of cells which cross the area L'^2 per unit time are

$$n = \frac{\bar{U}}{L'} \tag{66}$$

where total number is the sum of air and fuel cells

$$n = n_a + n_f$$

From the known mixture ratio

$$\frac{\sum_{i=1}^{n_f} \rho_{fi} L'^3}{\sum_{j=1}^{n_a} \rho_{aj} L'^3} = \frac{f}{a} \tag{67}$$

which can be reduced to

$$\frac{n_f}{n_a} = \frac{f}{a} \frac{\bar{\rho}_a}{\bar{\rho}_f} \tag{68}$$

The mass flux per unit area per unit time is

$$\overline{\rho \vec{U}} = \frac{1}{T} \int_T \rho \vec{U} \, dt \tag{69}$$

or considering the air and fuel cells separately yields

$$\overline{\rho \vec{U}} = \frac{1}{T} \sum_{i=1}^{n_f} \int_{t_i} (\bar{\rho}_f + \rho'_{fi})(\bar{U} + U'_i) dt + \frac{1}{T} \sum_{j=1}^{n_a} \int_{t_j} (\bar{\rho}_a + \rho'_{aj})(U + U'_j) dt \tag{70}$$

Now we assume there is no correlation between ρ' and U' then

$$\overline{\rho \vec{U}} = \bar{\rho}_f \bar{U} \sum_i^{n_f} t_i + \bar{\rho}_a \bar{U} \sum_j^{n_a} t_j \tag{71}$$

Substituting for t_i yields

$$\overline{\rho \vec{U}} = \bar{\rho}_f \bar{U} \frac{n_f L'}{\bar{U}} + \bar{\rho}_a \bar{U} \frac{n_a L'}{\bar{U}} \tag{72}$$

Now in order to eliminate n_f and n_a, the following relations are used

$$\frac{n_f L'}{\bar{U}} = \frac{n_f / n_a}{1 + n_f / n_a} \tag{73}$$

which can be reduced to

$$\frac{n_f L'}{\overline{U}} = \frac{\frac{f}{a}\frac{\rho_a}{\rho_f}}{1+\frac{f}{a}\frac{\rho_a}{\rho_f}} \tag{74}$$

and similarly for the air eddies

$$\frac{n_a L'}{\overline{U}} = \frac{1}{1+\frac{f}{a}\frac{\rho_a}{\rho_f}} \tag{75}$$

Upon substitution into Equation 72 the mass flux becomes

$$\frac{\dot{m}}{A} = \frac{\left(1+\frac{f}{a}\right)\overline{\rho}_a\overline{U}}{\left(1+\frac{f}{a}\frac{\rho_a}{\rho_f}\right)} \tag{76}$$

The stream thrust can be treated in a similar manner. The expression for stream thrust is

$$F_x = \left(\overline{\rho \vec{U}\vec{U}}\right)_x A + \bar{P}A \tag{77}$$

where

$$\left(\overline{\rho \vec{U}\vec{U}}\right) = \frac{1}{T}\int_T \rho \vec{U}\vec{U}\, dt \tag{78}$$

Considering the flux of eddies, Equation 78 can be written

$$\left(\overline{\rho \vec{U}\vec{U}}\right)_x = \frac{1}{T}\sum_{i=1}^{n_f}\int_{t_i}(\overline{\rho}_f+\rho'_{fi})(\overline{U}+U'_i)(\overline{U}+U'_i)\,dt + \frac{1}{T}\sum_{j=1}^{n_a}\int_{t_j}(\overline{\rho}_a+\rho'_{aj})(\overline{U}+U'_j)(\overline{U}+U'_j)\,dt \tag{79}$$

which becomes

$$\left(\overline{\rho \vec{U}\vec{U}}\right) = \overline{\rho}_f\overline{U}^2\sum_{i=1}^{n_f}t_i + \overline{\rho}_f\sum_{i=1}^{n_f}U_i'^2 t_i + \overline{\rho}_a\overline{U}^2\sum_{j=1}^{n_a}t_j + \overline{\rho}_a\sum_{j=1}^{n_a}U_j'^2 t_j \tag{80}$$

Now since $U_1'^2 = U'^2$ this equation reduces to

$$\overline{(\rho \vec{U} \vec{U})} = \bar{\rho}_f \bar{U}^2 \frac{n_f}{n} + \bar{\rho}_f \overline{U'^2} \frac{n_f}{n} + \bar{\rho}_a \bar{U}^2 \frac{n_a}{n} + \bar{\rho}_a \overline{U'^2} \frac{n_a}{n} \tag{81}$$

Now Equation 81 becomes by substitution of Equations 74 and 75

$$\overline{(\rho \vec{U} \vec{U})} = \frac{\bar{\rho}_a \bar{U} (1 + \frac{f}{a})}{(1 + \frac{f}{a} \frac{\bar{\rho}_a}{\bar{\rho}_f})} \bar{U} + \frac{\bar{\rho}_a \overline{U'^2} (1 + \frac{f}{a})}{(1 + \frac{f}{a} \frac{\bar{\rho}_a}{\bar{\rho}_f})} \tag{82}$$

The stream thrust Equation (77) becomes

$$F_x = (\bar{P} + P_T) A + \dot{m} \bar{U} \tag{83}$$

Again the turbulence contributes to the stream thrust. Finally the energy flux will be obtained by the same method.

The energy equation requires an average enthalpy flux

$$\overline{\rho \vec{U} H} = \frac{1}{T} \int_T \rho \vec{U} H \, dt \tag{84}$$

where

$$H = \bar{h} + h' + \frac{\bar{U}^2}{2} + \bar{U} U' + \frac{U'^2 + V'^2 + W'^2}{2} \tag{85}$$

Substituting Equation 85 into Equation 84 and separating the air eddies from the fuel eddies yields

$$\overline{(\rho \vec{U} H)}_x = \frac{1}{T} \sum_{i=1}^{n_f} \int_{t_i} (\bar{\rho}_f + \rho'_{fi})(\bar{U} + U'_i)(\bar{h}_f + h'_{fi} + \frac{\bar{U}^2}{2} + \bar{U} U'_i + \frac{3}{2} U_i'^2) \, dt$$

$$+ \frac{1}{T} \sum_{j=1}^{n_a} \int_{t_j} (\bar{\rho}_a + \rho'_{aj})(\bar{U} + U'_j)(\bar{h}_a + h'_{aj} + \frac{\bar{U}^2}{2} + \bar{U} U'_j + \frac{3}{2} U_j'^2) \, dt \tag{86}$$

This equation becomes

$$\overline{(\rho \hat{U} H)}_x = \frac{n_f}{n}\left(\bar{\rho}_f \bar{U}\left(\bar{h}_f + \frac{\bar{U}^2}{2} + \frac{5}{2}\overline{u'^2}_f\right)\right) + \frac{n_a}{n}\left(\bar{\rho}_a \bar{U}\left(\bar{h}_a + \frac{\bar{U}^2}{2} + \frac{5}{2}\overline{u'^2}\right)\right) \tag{87}$$

where summations of the following form are assumed zero:

$$\sum \rho'_j h'_j t_j = \sum \rho'_j u'_j t_j = \sum \rho'_j u'^2_j t_j = \sum \rho'_j u'_j h'_j t_j$$
$$= \sum h'_j t_j = \sum u'_j t_j = \sum \rho'_j t_j = 0 \tag{88}$$

Again substituting from Equations 74 and 75 yields

$$\overline{(\rho \hat{U} H)}_x = \frac{\bar{\rho}_a \bar{U} \bar{H}_a}{1 + \frac{f}{a}\frac{\bar{\rho}_a}{\bar{\rho}_f}} + \frac{\frac{f}{a}\bar{\rho}_a \bar{U} \bar{H}_f}{1 + \frac{f}{a}\frac{\bar{\rho}_a}{\bar{\rho}_f}} \tag{89}$$

Finally the energy equation becomes

$$\overline{(\rho \hat{U} H)}_x = \frac{\dot{m}}{A}\left(\bar{H}_a + \frac{f}{a}\bar{H}_f\right) \tag{90}$$

where

$$\bar{H} = \bar{h} + \frac{\bar{U}^2}{2} + h_T \tag{91}$$

Summarizing the equations for the compressible case, we arrive at

Continuity

$$\frac{\bar{\rho}_{a_2} \bar{U}_2 A_2 \left(1 + \frac{f}{a}\right)}{1 + \frac{f}{a}\frac{\bar{\rho}_{a2}}{\bar{\rho}_{f2}}} = \dot{m}_2 \tag{92}$$

Momentum

$$\left(\bar{P}_2 + P_{T_2}\right) A_2 + \dot{m}_2 \bar{U}_2 = F_2 \tag{93}$$

Energy

$$\bar{h}_{a_2} + \frac{f}{a}\bar{h}_{f_2} + (1+\frac{f}{a})(\frac{5}{2}RT_T + \frac{\bar{U}_2^2}{2}) = \bar{H}_2 \qquad (94)$$

Nondissipative flow

$$\frac{\bar{P}_2}{\bar{P}_1} = \left(\frac{\bar{\rho}_{a_2}}{\bar{\rho}_{a_1}}\right)^{\gamma_a} \quad , \quad \frac{\bar{P}_2}{\bar{P}_{1_f}} = \left(\frac{\bar{\rho}_{f_2}}{\bar{\rho}_{f_1}}\right)^{\gamma_f} \qquad (95)$$

2.5 SOLUTION OF THE COMPRESSIBLE EQUATIONS OF MOTION FOR COAXIAL AND NORMAL INJECTION

We will consider gaseous injection for the coaxial and normal fuel injector. Then let us further assume the fuel is a diatonic gas. Thus

$$\gamma_a = \gamma_f = 1.4 \qquad (96)$$

We further assume that the fuel is injected at the same static pressure as the air without creating shock waves

$$\bar{P}_{1_f} = \bar{P}_1 \qquad (97)$$

Let us introduce the following nondimensional variables

$$\eta = \frac{f}{a}\frac{\bar{\rho}_{a_1}}{\bar{\rho}_{a_1}} \qquad (98)$$

$$\tilde{U} = \frac{\bar{U}}{\bar{U}_1} \qquad (99)$$

$$\tilde{P} = \frac{\bar{P}}{P_1} \qquad (100)$$

$$\tilde{A}_2 = \frac{A_2}{A_1} \qquad (101)$$

$$\tilde{F} = \frac{F}{P_1 A_1} \qquad (102)$$

$$\tilde{U}' = \frac{U'}{\bar{U}} \qquad (103)$$

$$\theta = \frac{\bar{H}}{\bar{h}_{a_1}} \qquad (104)$$

Then the equations become for a unit mass flow of air

$$(1+\eta)\,\tilde{U}^{-1}\,\tilde{P}^{-\frac{1}{\gamma}} = \tilde{A}_2 \tag{105}$$

$$\tilde{P}\,A + (1+\tfrac{f}{a})(\tilde{F}_1 - 1)\,\tilde{U}\,(1+\tilde{U}'^2) = \tilde{F}_2 \tag{106}$$

$$\frac{(1+\eta)}{(1+\frac{f}{a})}\,\tilde{P}^{\gamma-1/\gamma} + (\theta_1 - 1)\,\tilde{U}^2\,(1+5\tilde{U}'^2) - \theta = 0 \tag{107}$$

If we introduce a new variable,

$$X^7 = \tilde{P} \tag{108}$$

We can reduce Equations 102, 103, and (104) to a single equation in X

$$A_{12}\,X^{12} + A_{10}\,X^{10} + A_5\,X^5 + A_0 = 0 \tag{109}$$

where

$$A_{12} = \frac{(1+\eta)}{(1+\frac{f}{a})}\left(1 - 5\,\frac{\theta_1 - 1}{\tilde{F}_1 - 1}\right) \tag{110}$$

$$A_{10} = -\theta_2 \tag{111}$$

$$A_5 = 5\,\frac{(\theta_1 - 1)}{(\tilde{F}_1 - 1)}\,\frac{(1+\eta)}{(1+\frac{f}{a})}\,\frac{\tilde{F}_2}{\tilde{A}_2} \tag{112}$$

$$A_0 = -4\,(\theta_1 - 1)\,(1+\eta)^2\,\tilde{A}_2^2 \tag{113}$$

$$\tilde{F}_1 = 1 + \gamma M_1^2 \tag{114}$$

$$\theta_1 = 1 + \frac{\gamma - 1}{2} M_1^2 \tag{115}$$

$$\tilde{A}_2 = 1 + \epsilon\,\frac{i}{a}\left(\frac{m_a}{m_f}\,\frac{T_{0_f}}{T_{0_i}}\right)\left(\frac{P_{0_i}}{P_{0_f}}\right)\frac{D_i}{D_f} \tag{116}$$

[1]See list of symbols for definition of D_1, D_2.

$$\tilde{F}_2 = \tilde{F}_1 + (\tilde{A}_2 - 1)\ (1 + \gamma M_f^2) \tag{117}$$

$$\theta_2 = \theta_1 \left[1 + \frac{f}{a}\left(\frac{\dot{m}_a}{\dot{m}_f}\frac{T_{0_f}}{T_{0_1}}\right)\right] \frac{1}{\left(1 + \frac{f}{a}\right)} \tag{118}$$

$$M_f^2 = 2\left[\left(\frac{P_{0_f}}{P_{0_1}}\right)^{\frac{\gamma-1}{\gamma}} \theta_1 - 1\right]\frac{1}{\gamma - 1} \tag{119}$$

and

$$M_1\ ,\ \frac{P_{0_f}}{P_{0_1}}\ ,\ \frac{T_{0_f}}{T_{0_1}}\ ,\ \frac{f}{a}\ ,\ \epsilon$$

are considered given.

Typical conditions for mixing in a supersonic combustor would be

$$\frac{P_{0_f}}{P_{0_1}} = 0.5$$

$$\frac{T_{0_f}}{T_{0_1}} = 0.35$$

$$\frac{f}{a} = 0.03$$

$$M_1 = 4.0$$

These conditions apply to a hypothetical engine flying at M = 8.0 at an altitude of 100,000 feet with a regeneratively cooled combustor.

These conditions result in a velocity ratio

$$\frac{\bar{U}_f}{\bar{U}_a} = 2.24$$

Comparing this result with that obtained for incompressible flow (see Figure 2), we find a significant effect of compressibility which reduces the amount of energy transformed into turbulence. However, it appears that there is still a sufficient supply of energy for turbulent mixing to predominate over molecular diffusion. This reduction in the maximum energy of turbulence can be one reason to explain the observed slower mixing rates in compressible flows.

The effect of the parameters M_1, $\frac{P_{0f}}{P_{01}}$, and $\frac{f}{a}$ are shown in the Figure 3. The effects of M_1 and $\frac{P_{0f}}{P_{01}}$ are minor. Thus we find that $\frac{\bar{U}_f}{\bar{U}_a}$ is the most important dynamic parameter for the compressible case; however, it is controlled by the temperature and molecular weight of the fuel entering the combustor. Thus we find it is important to simulate correctly the fuel total temperatures in combustor development work with boilerplate engine hardware in order to obtain the correct mixing rates and heat release rates which may interact with each other.

2.6 FROZEN FLOW

It is of fundamental interest to calculate the thrust loss in a supersonic nozzle due to a frozen pattern of turbulence. We will assume that the gases mix on a molecular scale so that thermal equilibrium prevails but let the turbulence kinetic energy be frozen. Further we will assume that this molecular mixing takes place in a constant area section; heat is added downstream and then expanded in the nozzle. The process is depicted in the following sketch.

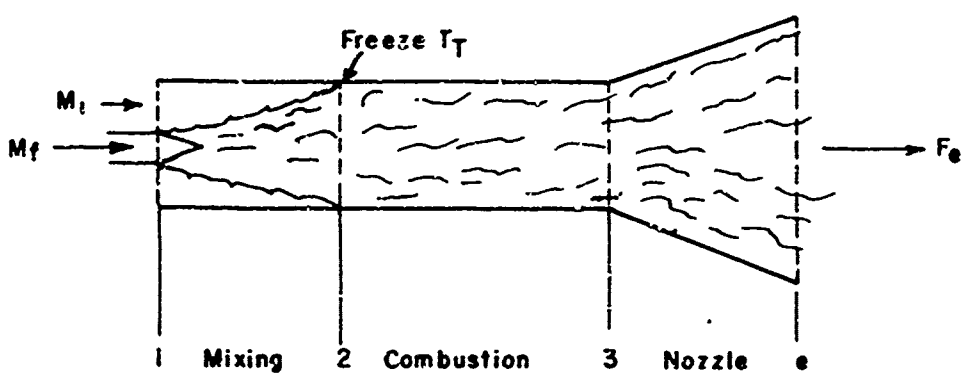

Sketch 7. Control Volume for Turbulent Combistion and Expansion

The energy equation can be written as

$$\bar{H} = \bar{h} + h_T + \frac{\bar{U}^2}{2} \qquad (120)$$

Since for a perfect gas $\gamma = 1.4$, this equation can be reduced to

$$T_0 = \overline{T}\left(1 + \frac{\gamma-1}{2} M^2\right) + \frac{1}{\gamma} T_T \tag{121}$$

Let us define an effective total temperature

$$T_{0_T} = T_0 - \frac{1}{\gamma} T_T \tag{122}$$

or

$$\overline{T}_{0_T} = \overline{T}\left(1 + \frac{\gamma-1}{2} M^2\right) \tag{123}$$

If the gas is brought to rest isentropically while the turbulent motion remains the same, we have

$$\overline{P}_{0_T} = \overline{P}\left(1 + \frac{\gamma-1}{2} M^2\right)^{\frac{\gamma}{\gamma-1}} \tag{124}$$

To simplify the formulation of the problem, let us assume that the properties of the combustion products at station 3 do not differ from those of air. Then conservation of mass and momentum yield the following equations for Mach number at station 3

$$\frac{M_3\left(1 + \frac{\gamma-1}{2} M_3^2\right)^{1/2}}{\left(1 + \frac{T_T}{T_{0_{T_3}}}\left(1 + \frac{\gamma-1}{2} M_3^2\right) + \gamma M_3^2\right)} = \frac{\left(1 + \frac{f}{a}\right)\left(T_{0_{T_3}}\right)^{1/2}}{F_2\left(\frac{\gamma}{R}\right)^{1/2}} \tag{125}$$

where

$$\overline{P}_3 = \frac{F_2}{A_3}\left(1 + \frac{T_T}{T_{0_{T_3}}}\left(1 + \frac{\gamma-1}{2} M_3^2\right) + \gamma M_3^2\right)^{-1} \tag{126}$$

and

$$T_{0_3} = \left(T_{0_1} + \frac{\Delta Q}{C_p}\right) \Big/ \left(1 + \frac{f}{a}\right) \tag{127}$$

Now there is also no loss of generality in assuming that the expansion is isentropic when the turbulence is frozen. The equation for M_e is

$$M_e \left(1 + \frac{\gamma-1}{2} M_e^2\right)^{-\frac{(\gamma+1)}{2(\gamma-1)}} = \frac{\left(1+\frac{f}{a}\right)\left(T_{o_{T_3}}\right)^{1/2}}{\bar{P}_{o_{T_3}} A_e \left(\frac{\gamma}{R}\right)^{1/2}} \tag{128}$$

Now since the stream thrust is

$$F_e = \bar{P}_e \left(1 + \frac{T_T}{T_{o_{T_3}}} \left(1 + \frac{\gamma-1}{2} M_e^2\right) + \gamma M_e^2\right) A_e \tag{129}$$

we can write for specific impulse

$$I_{SP} = \frac{1}{\frac{f}{a}} \sqrt{\frac{R}{\gamma G}} \sqrt{T_{o_3} - \frac{T_T}{\gamma}} \frac{\left[1+\left(\frac{T_T}{T_{o_3} - \frac{T_T}{\gamma}}\right)\left(1+\frac{\gamma-1}{2} M_e^2\right) + \gamma M_e^2\right]}{M_e \left(1+\frac{\gamma-1}{2} M_e^2\right)^{1/2}} \tag{130}$$

This analysis allows us to compare "equilibrium" performance and "frozen" performance. Frozen expansion losses are depicted in Figure 4. When the results are plotted in this manner, there is no difference between coaxial and normal injection. A small effect was observed when heat was added; the results presented are for the limiting case of constant total temperature.

These losses seem small enough for the large turbulence temperatures involved. First, the turbulence pressure contributes to the stream thrust and contributes to the flow work in the nozzle; second, a large part of this energy is unavailable in any case since it will generate entropy when dissipated. In fact, the total pressure decreases when the turbulence is relaxed in the constant area process. These performance losses are nearly one order of magnitude smaller than presented in Reference 1. Thus this fundamental limitation to performance of supersonic combustion ramjets is not as severely restrictive as previously thought.

2.7 RELATIVE PERFORMANCE

Finally, let us compare the effects of fuel injection mode on performance of the engine when the air and fuel initial conditions are identical except for geometry. For the coaxial mode the fuel momentum contributes directly to the engine thrust. The normal jet contributes no momentum and the air must

transfer momentum to the fuel stream; this behavior results in an overall Mach number reduction and total pressure loss. However, the heat addition losses will be reduced at this higher pressure but lower Mach number condition. A larger expansion ratio is also available from the combustor to nozzle exit since there is no area change in the mixing region as in the coaxial mode. The relative effects depend on the fuel total temperature, total pressure, and molecular weight.

Results presented in Figures 5 and 6 show that very large mixing losses occur for the normal jet as compared to the coaxial jet. However, total pressure losses with heat addition are comparable and the loss of engine performance is small.

2.8 SUMMARY OF DESIGN CONSIDERATIONS

This analysis comparing the characteristics of supersonic mixing has yielded the following results which are important design considerations.

1. Fuel injection mode is the biggest single factor affecting turbulence intensity, normal jets produce much more turbulent energy than coaxial jets. Thus normal jets should have faster mixing rates.

2. Normal jets produce nearly constant turbulence intensity for a given fuel-air ratio independent of other initial conditions while the energy produced by coaxial jets varies widely with jet velocity ratio. Thus normal jets should have more constant mixing lengths as flight speed varies.

3. Frozen turbulence performance losses are not large but do increase with flight speed. Thus large turbulence intensities can be generated to achieve rapid mixing at all but extreme hypersonic speed.

4. Normal jets do not produce large performance losses compared with coaxial mixing; however, a constant area burner will choke at a lower flight speed when normal injection is used. Thus coaxial jets may be very advantageous for low flight velocity.

It is concluded that normal jet fuel injection that maximizes turbulence intensity should be developed in order to minimize and stabilize mixing length.

SECTION III

TURBULENT FIELD EQUATIONS FOR COAXIAL MIXING

3.1 COMPRESSIBLE MIXING

In the mixing field, turbulence is produced and dissipated continuously. There is a strong coupling between the mean flow and turbulence. The mean flow determines the scale of turbulence. The scale and the mean profile determine both the rate of production and the dissipation rate of the turbulent kinetic energy. The coupling is complete since this turbulence intensity directly determines the mean velocity field through the Reynolds stresses. In the approach that follows a unique relation between turbulence intensity (turbulent kinetic energy) and "eddy" viscosity is assumed to exist. Further a unique relation between the intensity and scale of turbulence and the dissipation rate is also assumed to exist.

In this regard the turbulence must be fully developed such that an equilibrium spectrum function exists or nearly exists. Thus these assumptions and formulation which follow are valid for this "equilibrium" turbulent flow field. Thus the question of intermittency is raised. No direct account of intermittency is taken in the present formulation since, where intermittency is large, the turbulent transport is small and the overall effect on the flow field is small.

Heat transfer, diffusion, and momentum transport are all assumed to be similar. It is further assumed that the eddy viscosity, Prandtl number relation, etc., found in any turbulent flow will be valid in all turbulent flows as long as the above restrictions are true.

3.2 TURBULENT STRESS TENSOR

The Reynolds stresses are defined by the following expression

$$\bar{\tau}_T = -\overline{(\rho \vec{U})' \vec{U}'} \qquad (131)$$

which for cylindrical coordinates has the following components:

$$\tau_{rr} = -\overline{(\rho U)' U'} \tag{132}$$

$$\tau_{rz} = -\overline{(\rho U)' W'} = \tau_{zr} \qquad \text{"from dynamic"} \tag{133}$$

$$\tau_{r\theta} = \overline{(\rho V)' U'} = \tau_{\theta r} \qquad \text{"equilibrium"} \tag{134}$$

$$\tau_{\theta z} = -\overline{(\rho V)' W'} = \tau_{z\theta} \tag{135}$$

$$\tau_{\theta\theta} = -\overline{(\rho V)' V'} \tag{136}$$

$$\tau_{zz} = -\overline{(\rho W)' W'} \tag{137}$$

Let us introduce the eddy viscosity so that we can write the turbulent stresses as the sum of a normal "hydrostatic" part and a shear stress[2]

$$\overline{\overline{\tau}}_T = -P_T \overline{\overline{I}} + \mu_T \, \mathrm{def}\vec{U} \tag{138}$$

where

$$\mu_T = \bar{\rho}\epsilon \tag{139}$$

such that ϵ is a kinematic eddy viscosity.

The expression for turbulence pressure is

$$P_T = \bar{\rho} \frac{2}{3} K \tag{140}$$

where

$$K = \frac{1}{2} (\tau_{rr} + \tau_{\theta\theta} + \tau_{zz}) / \bar{\rho} \tag{141}$$

is the turbulent kinetic energy.

---

[2]The deformation tensor $\mathrm{def}\vec{U}$ is formed from the $\vec{\nabla}$ operator: $\mathrm{def}\vec{U} = \vec{\nabla}\vec{U} + (\vec{\nabla}\vec{U})^*$ where $(\vec{\nabla}\vec{U})^*$ is transpose of $(\vec{\nabla}\vec{U})$.

Then the components can be written as:

$$\tau_{rr} = 2\bar{\rho}\left[-\frac{K}{3} + \epsilon\frac{\partial\bar{U}}{\partial r}\right] \tag{142}$$

$$\tau_{\theta\theta} = 2\bar{\rho}\left[-\frac{K}{3} + \epsilon\left(\frac{1}{r}\frac{\partial\bar{V}}{\partial\theta} + \frac{\bar{U}}{r}\right)\right] \tag{143}$$

$$\tau_{zz} = 2\bar{\rho}\left[-\frac{K}{3} + \epsilon\frac{\partial\bar{W}}{\partial z}\right] \tag{144}$$

$$\tau_{rz} = \bar{\rho}\epsilon\left(\frac{\partial\bar{W}}{\partial r} + \frac{\partial\bar{U}}{\partial z}\right) \tag{145}$$

$$\tau_{r\theta} = \bar{\rho}\epsilon\left(r\frac{\partial}{\partial r}\left(\frac{\bar{V}}{r}\right) + \frac{1}{r}\frac{\partial\bar{U}}{\partial\theta}\right) \tag{146}$$

$$\tau_{\theta z} = \rho\epsilon\left(\frac{\partial\bar{V}}{\partial z} + \frac{1}{r}\frac{\partial\bar{W}}{\partial\theta}\right) \tag{147}$$

It can be argued that the eddy viscosity should be a function of both the mean flow scale and the turbulence intensity. Obviously the eddy sizes are much larger in ocean currents than in laboratory flows and thus the cross velocity products should be correlated for much longer periods of time, while, if the turbulence intensity vanishes, the cross correlations also vanish. It will be necessary to determine this relationship experimentally.

3.3 DYNAMIC EQUATIONS FOR MEAN MOTION

The differential equations for the time mean flow are well known. We present them here without derivation in cylindrical coordinates for flow with axial symmetry in the usual boundary layer approximation.

Continuity

$$\frac{1}{r}\frac{\partial}{\partial r}(r\,\rho\bar{U}) + \frac{\partial}{\partial z}(\rho\bar{W}) = 0 \tag{148}$$

Diffusion

$$\frac{1}{r}\frac{\partial}{\partial r}(r\bar{\rho}\bar{U}Y_i) + \frac{\partial}{\partial z}(\bar{\rho}\bar{W}Y_i) = \frac{1}{r}\frac{\partial}{\partial r}\left[r\bar{\rho}(D_i + \epsilon_D)\frac{\partial Y_i}{\partial r}\right] \tag{149}$$

where

$$\epsilon_D = \frac{\overline{(\rho U)' Y_i'}}{\bar{\rho} \frac{\partial \bar{Y}_i}{\partial r}} \tag{150}$$

Radial Momentum

$$\bar{F} + \overline{(\rho U)' U'} = P_\infty \tag{151}$$

Streamwise Momentum

$$\frac{1}{r} \frac{\partial}{\partial r} (r \overline{\rho U} \bar{W}) + \frac{\partial}{\partial z} (\overline{\rho W} \bar{W}) = - \frac{\partial P_\infty}{\partial z} + \frac{1}{r} \frac{\partial}{\partial} \left(r (\bar{\mu} + \bar{\mu}_T) \frac{\partial \bar{W}}{\partial r} \right) \tag{152}$$

where we have assumed

$$P_T = \overline{(\rho U)' U'} = \overline{(\rho W)' W} \tag{153}$$

Total Enthalpy

$$\begin{aligned} \frac{1}{r} \frac{\partial}{\partial r} (r \overline{\rho U} \bar{H}) + \frac{\partial}{\partial z} (\overline{\rho W} \bar{H}) = {} & \frac{1}{r} \frac{\partial}{\partial r} \left(r \bar{k} \frac{\partial \bar{T}}{\partial r} \right) \\ & + \frac{1}{r} \frac{\partial}{\partial r} \left(r \sum_i \bar{\rho} \bar{h}_i D_i \frac{\partial Y_i}{\partial r} \right) \\ & + \frac{1}{r} \frac{\partial}{\partial r} \left(r \bar{\vec{U}} \cdot (\bar{\bar{\tau}} + \bar{\bar{\tau}}) \right) + \frac{1}{r} \frac{\partial}{\partial r} \left(r \overline{\vec{U} \cdot \bar{\bar{\tau}}'} \right) \\ & - \frac{1}{r} \frac{\partial}{\partial r} \left(r \overline{(\rho U)' h'} \right) - \frac{1}{r} \left(r \overline{(\rho U)' K'} \right) \end{aligned} \tag{154}$$

where

$$\overline{(\rho U)' h'} = \bar{C}_p \overline{(\rho U)' T'} + \sum_i \bar{h}_i \overline{(\rho U)' Y_i'} \tag{155}$$

With the definitions of the turbulent diffusion coefficients for heat and mass transfer, we obtain

$$\overline{(\rho U)' h'} = - \bar{\rho} \bar{C}_p \epsilon_T \frac{\partial \bar{T}}{\partial r} - \bar{\rho} \epsilon_D \sum_i \bar{h}_i \frac{\partial \bar{Y}_i}{\partial r} \tag{156}$$

Also the total enthalpy is defined as before as

$$\bar{H} = \tilde{h} + h_T + \frac{\bar{W}^2}{2} \tag{157}$$

where

$$h_T = \frac{5}{3} K \tag{158}$$

Finally we introduce the term

$$\epsilon_K = \frac{\overline{(\rho U)' K'}}{\bar{\rho} \frac{\partial K}{\partial r}} \tag{159}$$

Let us now define the effective transport coefficients

$$\mu_e = \bar{\mu} + \bar{\rho}\epsilon \tag{160}$$

$$R_e = \bar{k} + \bar{\rho}\epsilon_k \bar{C}_p \tag{161}$$

$$D_e = D_i + \epsilon_D \tag{162}$$

In terms of these coefficients, the energy equation can be written as

$$\begin{aligned} \frac{1}{r}\frac{\partial}{\partial r}(r\,\overline{\rho U}\,\bar{H}) + \frac{\partial}{\partial z}(\overline{\rho W}\,\bar{H}) = {} & \frac{1}{r}\frac{\partial}{\partial r}\left(r k_e \frac{\partial \bar{T}}{\partial r}\right) \\ & + \frac{1}{r}\frac{\partial}{\partial r}\left(r \sum_i \bar{\rho} D_e \frac{\partial \bar{Y}_i}{\partial r}\right) \\ & + \frac{1}{r}\frac{\partial}{\partial r}\left(r \mu_e \frac{\partial \frac{\bar{W}^2}{2}}{\partial r}\right) \\ & + \frac{1}{r}\frac{\partial}{\partial r}\left(r \bar{\rho}\epsilon_k \frac{\partial K}{\partial r}\right) \end{aligned} \tag{163}$$

Further let us introduce the effective Schmidt, Lewis, and Prandtl numbers:

$$S_c = \frac{\mu_e}{\bar{\rho} D_e} \tag{164}$$

$$L_e = \frac{\bar{\rho}\,\bar{C}_p D_e}{k_e} \tag{165}$$

$$P_r = \frac{\bar{C}_p\,\mu_e}{k_e} \tag{166}$$

Then the energy equation can be written as:

$$\frac{1}{r}\frac{\partial}{\partial r}\left(r\,\overline{\rho U}\,\overline{H}\right)+\frac{\partial}{\partial z}\left(\overline{\rho W}\,\overline{H}\right)=\frac{1}{r}\frac{\partial}{\partial r}\left[r\left(\frac{\mu_e}{P_r}\right)\frac{\partial \overline{H}}{\partial r}\right]$$

$$+\frac{1}{r}\frac{\partial}{\partial r}\left[r\left(\frac{\mu_e}{P_r}\right)(L_e-1)\sum_i \overline{h}_i\frac{\partial Y_i}{\partial r}\right]$$

$$+\frac{1}{r}\frac{\partial}{\partial r}\left[r\left(\frac{\mu_e}{P_r}\right)(P_r-1)\frac{\partial \overline{W}^2/2}{\partial r}\right]$$

$$+\frac{1}{r}\frac{\partial}{\partial r}\left[r\left(\frac{\mu_e}{P_r}\right)\left(\frac{3}{5}\frac{\epsilon_k}{\epsilon_T}-1\right)\frac{\partial h_T}{\partial r}\right] \qquad (167)$$

Turbulent Energy Field

The turbulent kinetic energy equation becomes

$$\frac{1}{r}\frac{\partial}{\partial r}\left(r\,\overline{\rho U}K\right)+\frac{\partial}{\partial z}\left(\overline{\rho W}\,K\right)=\mu_T\left(\frac{\partial \overline{W}}{\partial r}\right)^2-P_T\frac{\partial \overline{W}}{\partial z}$$

$$+\frac{1}{r}\frac{\partial}{\partial r}\left(r\,\overline{P}\,\epsilon_k\frac{\partial K}{\partial r}\right)$$

$$-d_k$$

where

$$d_k = d+\overline{U'\cdot\vec{\nabla}P'}$$

The terms are explained as follows:

d dissipation of turbulent kinetic energy

$\overline{U'\nabla P'}$ acoustic coupling; this term is assumed to be a small loss unless an interaction with a sound source is introduced. Such effects have been observed and can be large.

An assumption has been made regarding the role of viscosity on the generation of turbulence. We have assumed that this action on turbulence is purely dissipative. Thus the viscous production term in the equation is replaced by the turbulence dissipation rate

$$\overline{\left(\vec{U}'\cdot\vec{\nabla}\,\overline{\overline{\tau}}'_s\right)}=-d \qquad (168)$$

and in the total enthalpy equation the turbulent viscous work becomes

$$\vec{\nabla}\cdot\overline{\left(\vec{U}'\cdot\overline{\overline{\tau}}'_s\right)}=0$$

The arguments for this assumption are discussed below.

Dissipation

The dissipation of turbulent kinetic energy in isotropic incompressible turbulence has been shown to obey the law (Reference 8),

$$d_k = -\frac{3}{2}\,\bar{\rho}\,\frac{u'^3}{L_D} \tag{170}$$

where

L_D = the dissipation scale which is approximately equal to the integral scale (or scale of large "eddies")

This law determined by dimensional reasoning and verified by experiment can be explained by existence of an equilibrium turbulence velocity distribution function. The dissipation occurs at the smallest scale while the energy of the smallest scale is directly related through the distribution function to the large scale eddies which contain most of the energy. This dynamic equilibrium determined by the energy transfer process from one scale to another is essentially viscosity independent since the energy flows from large scale to small scale and is finally terminated by viscous dissipation into heat at the end of this process. Since data are available for incompressible flow only, the dependence of dissipation on turbulence intensity will be determined experimentally.

Static Enthalpy

The equation for static enthalpy is somewhat simpler to use for solutions by numerical integration and can be written

$$\begin{aligned}\overline{\rho u}\,\frac{\partial \bar{h}}{\partial r} + \overline{\rho w}\,\frac{\partial \bar{h}}{\partial z} = \overline{w}\,\frac{\partial \bar{P}}{\partial z} + d_e \\ + \frac{1}{r}\,\frac{\partial}{\partial r}\left(r\,\frac{\mu_e}{P_r}\,\bar{C}_p\,\frac{\partial \bar{T}}{\partial r}\right) \\ + \frac{1}{r}\,\frac{\partial}{\partial r}\left(r\,\frac{\mu_e}{Sc}\,\sum_i \bar{h}_i\,\frac{\partial \bar{Y}_i}{\partial r}\right)\end{aligned} \tag{171}$$

where

$$d_\epsilon = d_k + \bar{\mu}\left(\frac{\partial \bar{W}}{\partial r}\right)^2 \tag{172}$$

The form of these equations makes them applicable to laminar as well as turbulent flows when $K \to 0$. Since the boundary layer equations are parabolic, we must specify the pressure gradient in order to obtain a solution.

3.4 TRANSFORMATION OF EQUATIONS

The equations will be solved in the Von Mises plane by using the transformation

$$Z = z$$

$$\psi_r = \overline{\rho W}\, r \tag{173}$$

$$\psi_z = -\overline{\rho U}\, r \tag{174}$$

The equations of conservation then become

Momentum

$$\frac{\partial \bar{W}}{\partial Z} = \frac{1}{\rho \bar{W}} \frac{\partial P_e}{\partial Z} + \frac{1}{\psi} \frac{\partial}{\partial \psi}\left(a \frac{\partial \bar{W}}{\partial \psi}\right) \tag{175}$$

Mean flow energy

$$\frac{\partial \bar{h}}{\partial Z} = \frac{1}{\bar{\rho}} \frac{\partial \bar{P}}{\partial Z} + \frac{1}{\psi} \frac{\partial}{\partial \psi}\left(\frac{\bar{C}_p a}{P_r} \frac{\partial \bar{T}}{\partial \psi}\right)$$

$$+ \frac{1}{\psi} \frac{\partial}{\partial \psi}\left(\frac{a}{S_c} \sum_i \bar{h}_i \frac{\partial \bar{Y}_i}{\partial \psi}\right) + \frac{d_\epsilon}{\rho W} \tag{176}$$

Turbulence energy

$$\frac{\partial K}{\partial Z} = -\frac{d_k}{\overline{\rho W}} + \frac{1}{\psi} \frac{\partial}{\partial \psi}\left(\frac{a \bar{\rho} \epsilon_k}{\mu_e} \frac{\partial K}{\partial \psi}\right)$$

$$+ \frac{c}{\psi}\left(\frac{\partial \bar{W}}{\partial \psi}\right)^2 - \frac{P_T}{\overline{\rho W}} \frac{\partial \bar{W}}{\partial z} \tag{177}$$

Diffusion

$$\frac{\partial \overline{Y_i}}{\partial Z} = \frac{1}{\psi} \frac{\partial}{\partial \psi} \left(\frac{a}{Sc} \frac{\partial \overline{Y_i}}{\partial \psi} \right) \tag{178}$$

where

$$a = \mu_e \frac{\overline{\rho W} r}{\psi} \tag{179}$$

3.5 NUMERICAL TREATMENT OF DIFFERENTIAL EQUATIONS

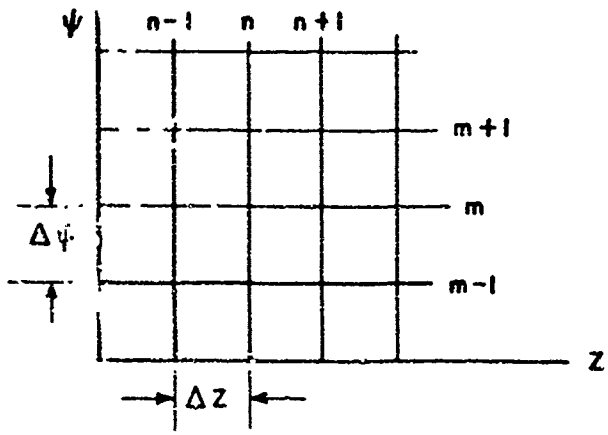

Sketch 8. Definition of Differences

This finite difference formulation for the solution of the turbulent equations of motion is a minor modification of the work of Edelman and Fortune (Reference 9). The definition of the finite difference analogues, for any variable ϕ of the differential operators in the equations of motion are defined according to Sketch 8, as follows. The difference between this formulation and that of Edelman is the inclusion of the variation of the eddy viscosity across the mixing layer in Equation 182. The first derivative in the Z direction is

$$\left.\frac{\partial \phi}{\partial Z}\right)_{n+1,m} = (\phi_{n+1,m} - \phi_{n,m}) / \Delta Z \tag{180}$$

The first derivative in the ψ direction is

$$\frac{\partial \phi}{\partial \psi}\Big)_{n,m} = \left(\phi_{n,m+1} - \phi_{n,m-1}\right)/ 2\Delta\psi \tag{181}$$

The second derivative in the ψ direction is

$$\frac{\partial}{\partial \psi}\left(a \frac{\partial \phi}{\partial \psi}\right)_{n,m} = \frac{a_{nm}}{\Delta\psi^2}\left(\phi_{n,m+1} - 2\phi_{n,m} + \phi_{n,m-1}\right)$$

$$+ \frac{1}{4\Delta\psi^2}\left(\phi_{n,m+1} - \phi_{n,m-1}\right)\left(a_{n,m+1} - a_{n,m-1}\right) \tag{182}$$

In difference form the Equations 175 and 176 become

Momentum

$$W_{n+1,m} = W_{n,m} + \frac{a_{n,m}}{\Delta\psi^2}\left(W_{n,m+1} 2W_{n,m} + W_{n,m-1}\right)\Delta Z$$

$$+ \frac{\Delta Z}{4\Delta\psi^2}\left(a_{n,m+1} - a_{n,m-1}\right)\left(W_{n,m+1} - W_{n,m-1}\right)$$

$$- \frac{\Delta Z}{(\rho W)_{n,m}}\left(\frac{\partial P_e}{\partial Z}\right)_{n+1} \tag{183}$$

Turbulent kinetic energy

$$K_{n+1,m} = K_{n,m} - \left(\frac{dk}{\rho W}\right)_{n,m}\Delta Z$$

$$+ \frac{\Delta Z}{4\Delta\psi^2}\,\frac{a_{nm}}{\psi}\left(W_{n,m+1} - W_{n,m-1}\right)^2$$

$$+ \frac{\Delta Z}{\psi\Delta\psi^2}\left(\frac{a\rho\epsilon_k}{\mu_e}\right)_{n,m}\left(K_{n,m+1} - 2K_{n,m} + K_{n,m-1}\right)$$

$$+ \frac{\Delta Z}{4\psi\Delta\psi^2}\left[\left(\frac{a\bar{\rho}\epsilon_k}{\mu_e}\right)_{n,m+1} - \left(\frac{a\rho\epsilon_k}{\mu_e}\right)_{n,m-1}\right]\left(K_{n,m+1} - K_{n,m-1}\right)$$

$$- \frac{2}{3}\left(\frac{K}{W}\right)_{n,m}\left(W_{n+1,m} - W_{n,m}\right) \tag{184}$$

Diffusion

$$Y_{i_{n+1,m}} = Y_{i_{n,m}} + \frac{\Delta Z}{\psi \Delta \psi^2} \left(\frac{a}{S_c}\right)_{n,m} \left(Y_{i_{n,m+1}} - 2Y_{i_{n,m}} + Y_{i_{n,m-1}}\right)$$

$$+ \frac{1}{4} \frac{\Delta Z}{\psi \Delta \psi^2} \left[\left(\frac{a}{S_c}\right)_{n,m+1} - \left(\frac{a}{S_c}\right)_{n,m-1}\right] \left(Y_{i_{n,m+1}} - Y_{i_{n,m-1}}\right) \qquad (185)$$

The static enthalpy equation written in terms of static temperature becomes

$$T_{n+1,m} = T_{n,m} + \left\{ \left(\frac{\partial \bar{P}}{\partial Z}\right)_{n+1} \frac{\Delta Z}{\rho_{n,m}} + \left(\frac{d_k}{\rho W}\right)_{n,m} \Delta Z \right.$$

$$+ \frac{\Delta Z}{\psi \Delta \psi^2} \left(\frac{\bar{C}_p a}{P_r}\right)_{n,m} \left(T_{n,m+1} - 2T_{n,m} + T_{n,m-1}\right)$$

$$+ \frac{1}{4} \frac{\Delta Z}{\psi \Delta \psi^2} \left[\left(\frac{C_p a}{P_r}\right)_{n,m+1} - \left(\frac{C_p a}{P_r}\right)_{n,m-1}\right] \left(T_{n,m+1} - T_{n,m-1}\right)$$

$$\left. + \frac{1}{4} \frac{\Delta Z}{\psi \Delta \psi^2} \sum_i \left(\frac{C_{p_i} a}{S_c}\right)_{n,m} \left(Y_{i_{n,m+1}} - Y_{i_{n,m-1}}\right) \left(T_{n,m+1} - T_{n,m-1}\right) \right] \Big/$$

$$\left(C_p - \frac{R P_T}{P_\infty}\right)_{n,m} \qquad (186)$$

where

$$\frac{1}{\rho_{n,m}} \left(\frac{\partial \bar{P}}{\partial Z}\right)_{n+1} = \left(\frac{dP_\infty}{dZ}\right)_{n+1} \frac{1}{\rho_{n,m}} \left(1 - \frac{P_T}{P_\infty}\right)_{n,m} - \frac{2}{3} \left(1 + \frac{P_T}{P_\infty}\right) \left(\frac{d_k}{dZ}\right)_{n+1,m}$$

$$+ \frac{2}{3} (K m)_{n,m} \sum_i \frac{1}{m_i} \left(\frac{dY_i}{dZ_i}\right)_{n+1,m} \qquad (187)$$

3.6 EQUATIONS OF MOTION ON THE AXIS

These equations have a singular point on the axis as $r \to 0$ or $\psi \to 0$ and their limiting form must be investigated. This limiting form is also useful for evaluating experimental data to deduce or determine inversely the turbulent transport coefficients.

Streamwise momentum

$$\bar{\rho} \bar{W} \frac{\partial \bar{W}}{\partial z} = 2 \mu_e \frac{\partial^2 \bar{W}}{\partial r^2} - \frac{\partial P_\infty}{\partial z} \qquad (188)$$

Static enthalpy

$$\overline{\rho W}\,\frac{\partial \bar{h}}{\partial z} = d_e + \bar{W}\,\frac{\partial \bar{P}}{\partial z} + 2\frac{\mu_e}{P_r}\bar{C}_p\,\frac{\partial^2 \bar{T}}{\partial r^2} + 2\frac{\mu_e}{S_c}\sum_i \bar{h}_i\,\frac{\partial^2 \bar{Y}_i}{\partial r^2} \tag{189}$$

Turbulence

$$\overline{\rho W}\,\frac{\partial K}{\partial z} = -\,d_k + 2\bar{\rho}\,\epsilon_k\,\frac{\partial^2 K}{\partial r^2} \tag{190}$$

Diffusion

$$\overline{\rho W}\,\frac{\partial \bar{Y}_i}{\partial z} = 2\,\frac{\mu_e}{S_c}\,\frac{\partial^2 \bar{Y}_i}{\partial r^2} \tag{191}$$

The equations in the Von Mises Plane are:

$$\frac{\partial \bar{W}}{\partial Z} = 2\mu_e\,\frac{\partial^2 \bar{W}}{\partial \psi^2} + \frac{1}{\overline{\rho W}}\,\frac{\partial P_e}{\partial Z}$$

$$\frac{\partial \bar{h}}{\partial Z} = \frac{1}{\bar{\rho}}\,\frac{\partial \bar{P}}{\partial z} + \frac{d_e}{\overline{\rho W}} + 2\,\frac{\bar{C}_p \mu_e}{P_r}\,\frac{\partial^2 \bar{T}}{\partial \psi^2} + 2\frac{\mu_e}{S_c}\sum_i \bar{h}_i\,\frac{\partial^2 \bar{Y}_i}{\partial \psi^2} \tag{192}$$

$$\frac{\partial K}{\partial Z} = -\frac{d_k}{\overline{\rho W}} + 2\bar{\rho}\epsilon_k\,\frac{\partial^2 K}{\partial \psi^2} \tag{193}$$

$$\frac{\partial Y_i}{\partial Z} = 2\,\frac{\mu_e}{S_c}\,\frac{\partial^2 \bar{Y}_i}{\partial \psi^2} \tag{194}$$

Finally the difference equations ar..

Momentum

$$W_{n+1,1} = W_{n,1} + \frac{4\mu_e \Delta Z}{\Delta \psi^2}\,(W_{n,2} - W_{n,1}) + \frac{\Delta Z}{(\rho W)_{n,1}}\left(\frac{\partial P}{\partial Z}\right)_{n+1} \tag{195}$$

Energy

$$h_{n+1,1} = h_{n,1} + \frac{\Delta Z}{\rho_{n,1}}\left(\frac{\partial \bar{P}}{\partial Z}\right)_n + \left(\frac{d_e}{\rho \bar{W}}\right)_{n,1} \Delta Z$$

$$+ \frac{\Delta Z}{\Delta \psi^2}\left[\left(\frac{4 \bar{C}_p \mu_e}{P_r}\right)_{n,1}\left(T_{n,2} - T_{n,1}\right) + \frac{4\mu_e}{S_c}\sum_i h_{i_{n,1}}\left(Y_{i_{n,2}} - Y_{i_{n,1}}\right)\right] \qquad (196)$$

Turbulence kinetic energy

$$K_{n+1,1} = K_{n,1} - \Delta Z \left(\frac{d_k}{\rho W}\right)_{n,1} \qquad (197)$$

Diffusion

$$Y_{i_{n+1,1}} = Y_{i_{n,1}} + \frac{\Delta Z 4 \mu_e}{\Delta \psi^2 S_c}\left(Y_{i_{n,2}} - Y_{i_{n,1}}\right) \qquad (198)$$

3.7 THE INVERSE TRANSFORMATION

The physical coordinates (r, z) can be found by the equations:

$$z = \xi \qquad (199)$$

$$r = \left(\int_0^{\psi} \frac{2\psi\, d\psi}{\rho W}\right) \qquad (200)$$

Equation 200 expressed in difference form can be written

$$r_{n+1,m} = \left[r^2_{n+1,m-1} + \Delta\psi\left(\frac{\psi_m}{(\rho W)_{n+1,m}} + \frac{\psi_{m-1}}{(\rho W)_{n+1,m-1}}\right)\right]^{1/2} \qquad (201)$$

3.8 SUMMARY OF THEORETICAL CONSIDERATIONS

In Section II it was shown that turbulence has an equation of state

$$P_T = \bar{\rho}\, R T_T \qquad (202)$$

and that associated with this turbulent state were the state functions of turbulent energy and turbulent enthalpy. In the present section, it was assumed that the transport properties of the turbulent flow are also functions of the turbulent state. Thus, it is assumed that an eddy viscosity exists; that is, that eddy viscosity is functionally related to the equation of state. This assumption implies that an

equilibrium turbulent velocity spectrum exists such that shear produces only a minor departure from this equilibrium structure.

The dissipation into thermal energy for turbulent shear flow must also be related to the turbulent state under these assumptions. Thus, the experimental determination of the relations between eddy viscosity and turbulent energy and between energy dissipation and turbulent energy are required to verify the present theoretical model.

SECTION IV

DESCRIPTION OF EXPERIMENTS

4.1 SUPERSONIC FREE JET

The objective of these experiments was to obtain basic data on mixing rates, dissipation, and turbulence intensity in a compressible flow. The jet Mach number and total temperature were varied independently by use of interchangeable nozzles fitted to a hydrogen fueled burner. The total temperature was restricted to 1500°R in order that the combustion products would not deviate appreciably from calorically perfect air.

4.1.a. Nozzles

The nozzle internal contours were computed by the method of characteristics for a $\gamma = 1.4$. The nominal design Mach numbers of 1.0, 1.5, 2.0, and 2.5 were chosen based on limitations of the available air supply. The nozzle exit diameters were all equal to 0.1 foot. Exit Mach number profiles are shown in Figure 7a through 7d. Typical total temperature profiles at the nozzle exit are shown in Figure 8a through 8d.

4.1.b. Instrumentation

The free jet combustor was instrumented for pressure and temperature. The jet was probed for impact pressure, static pressure, and total temperature. Consolidated Electrodynamics Corporation pressure transducers with bridge balancing networks were used to measure pressure for temperature measurements. Iron constantan thermocouples were used with Brown Instrument vertical scale potentiometers and a room-temperature reference junction. Probe position was determined by calibrated voltage drops from battery-powered variable resistors mounted on the probe positioning cart. All data were recorded on magnetic tape with a digital data acquisition system SRL-200 scanning at a rate of 200 channels/second. Schlieren photographs were taken with a spark light source of 0.2-microsecond time constant. Total pressure and temperature surveys of the jet were obtained with a combination probe shown

in Figure 9a. This probe was not explicitly compensated for radiation or conduction losses. Various size thermocouple wires were tested until temperature readings at identical conditions did not change. A 5-mil thermocouple wire was found to give good results. Radiation compensation was provided for by surrounding the thermocouple with a low conductivity material (LAVA) which minimized the radiation losses from the thermocouple. Probe bleed was maximized to provide as rapid a response to changing conditions while not degrading the total pressure measurement. A simple impact probe was used to verify the pressure measurement. Temperature measurements were also made with a conical recovery temperature probe, developed at the Naval Ordnance Laboratory, White Oak, Maryland (Figure 9b). These measurements were in agreement with those made with the combination probe (Figure 10).

Static pressure surveys were made with the probe shown in Figure 9c. Three static taps were positioned 120° apart at the same axial location. It was hoped this spacing would allow the true static pressure to be measured uninfluenced by the cross flows induced by the turbulent velocity fluctuations.

4.1.c. Procedure

Jet operating conditions were established and allowed to stabilize as near the design operating conditions for the nozzle as possible. Then radial impact pressure and total temperature surveys were made at three axial positions followed by a centerline survey of impact pressure and total pressure. Next, the static pressure probe was positioned on the jet centerline and a centerline survey of static pressure was recorded. Since the data system was of the analog to digital converter design which takes essentially instantaneous readings, 10 scans were taken at each position so that most of the noise could be averaged out of the pressure measurements.

4.1.d. Accuracy of the Measurements

Pressure transducers used to measure total pressure were rated at 1/2% of full scale accuracy and were changed, to give the largest possible voltage reading, for each Mach number nozzle. Thus good accuracy was obtained near the early part of the jet decay but it decreased as the decay increased. The

static pressure transducer had a 0-25 PSIA range and the accuracy should have been constant in the whole flow field. No attempt was made to determine any probe effects on the accuracy of the static pressure probe other than to introduce small amounts of deflection in the proble and compare results from different experiments. No trends were observed that could not be attributed to run variation in jet conditions. Another source of error was that of bridge unbalance which had various causes. This error had the effect of shifting the calibration a constant amount over the entire range. This effect was corrected by taking a reading with no flow and comparing it with the 1 atmosphere calibration values for each transducer.

As an overall system check, mass flows were computed from measured chambers conditions and were compared with integraded radial profile surveys taken at the nozzle exit. The results are shown in Figure 11. The agreement is good; the maximum deviation being about 15%. Shown in Figure 12 is the comparison of integrated with calculated exit stream momentum; the agreement is again quite good with the maximum deviation being about 6%. Integrated excess enthalpy and stream thrust from various experiments at downstream stations are shown in Figures 13 and 14. These integrals are theoretically constants of motion; however, some noticeable deviations from constancy are seen. The large deviations are believed to be caused by the reduced accuracy of the probe position measurement at large distances from the centerline where the signals are low but make significant contributions to the integrated values.

4.2 COAXIAL SUPERSONIC MIXING

The objective of these experiments was to determine the structure of the mixing field. A hot film anemometer was used to determine the extent of the turbulence field. Helium was injected coaxially from a Mach 4 conical nozzle into a Mach 3 air stream. The gas injection nozzle was attached to a half-inch diameter steel tubing which extended through the facility nozzle into the test section. The long length of the steel tubing gave rise to a thick turbulent boundary layer on the outside of the tubing. Since it was impossible to remove the boundary layer, its effect on mixing was not determined experimentally. The wind tunnel had a free jet test section and a Mach 3 nozzle of rectangular cross section, 4 in. x 7 in. The usable test section length was about 12 in.

Mixing of the gas of this jet with the surrounding air was found to be extremely slow. The jet was operated so that the jet exit pressure was equal to the air static pressure.

4.2.a. Instrumentation

Instrumentation for this experiment consisted of pressure transducers and thermocouples to measure upstream reservoir pressure and temperature of both air and helium. Impact pressure, static pressure. and output of a conical hot film anemometer probe were also measured. The hot film probe was used to make RMS measurements of the turbulent fluctuations. The anemometer used was a Thermo Systems Inc. Model 1050. This system had approximately a 200,000-Hertz frequency response which depended upon the operating temperature of the sensor. The RMS voltage was measured by a Hewlett Packard true RMS voltmeter. Autocorrelations of the fluctuating hot wire signal were made with a Honeywell Correlator Model 9410. Probe positioning was accomplished by a precision X-Y table controlled by a SloSyn digital stepping motor and indexer. All data except the autocorrelations were recorded on a Hewlett Packard Model 2412B Data System.

4.2.b. Procedure

Impact pressure, concentration, and static pressure were measured on the jet centerline. The jet decay was found to extend beyond the useful test section of the free jet wind tunnel. At an axial location of 10 jet diameters, radial profiles of impact pressure and concentration were measured. Turbulence RMS measurements and autocorrelations were obtained at the same locations in the radial direction with the conical hot film sensor. It was noticed that there was a coupling between the test cabin noise and the signal from hot film anemometer. Whenever the test cabin produced howling or screeching tones, the hot film output increased by a large amount. To overcome this difficulty a constant area nozzle extension was fabricated to provide a shield for the mixing region against noise emitted by the test cabin. After this modification the radial data at $\frac{Z}{D_j} = 10$ were determined once more.

4.2.c. Accuracy

The data signals were recorded at a low level without a signal conditioning. No amplifiers or bridge balances were used to keep errors introduced by these devices out of the measurements. Pressure transducers were rated at 0.10% full scale combined nonlinearity and hysteresis. The gas analyzer was found to be within 1% accurate as determined by repeated calibrations. The accuracy of the Hewlett Packard true RMS voltmeter was found to be within 1.2% by calibration with a precision signal generator. Accuracy of the hot film anemometer to indicate the random turbulent signals in conjunction with the Honeywell correlator could not be determined. However, steady state calibrations were reproducible within a few percent. Probe positioning was calibrated and found to be accurate to within .001 inch in 6 inches.

4.3 NORMAL JET PENETRATION AND MIXING

The objective of this experiment was to examine the performance of an injector designed to maximize turbulence. The injector was a Mach 4 contoured nozzle of the same exit area as the coaxial injector. This Mach number was chosen to maximize jet velocity at reasonable jet total pressure. The exit was rectangular with a ratio of width to height of 10, with the narrow edge facing the stream. This injector was tested in a Mach 2.5 and 3.0 air stream to determine the Mach number effects on penetration. Concentration measurements were taken in the Mach 3.0 stream only.

4.3.a Procedure

Initial penetration experiments were made with the injector mounted on a flat plate. Penetration was determined from Schlieren pictures at Mach 3.0 and 2.5. Then the injector was mounted on the same nozzle extension that was used in the coaxial test. The flow field at $\frac{Z}{D_{eff}} = 10$ was mapped using impact probes and gas analyzer. Downstream variation of the peak helium concentration was then determined.

Sketch 9. Schlieren Photograph of a Normal Sonic Jet

SECTION V

EXPERIMENTAL RESULTS

5.1 STRUCTURE OF FREE JET

5.1.a. Velocity Profiles

The Rayleigh Pitot formula was used to determine the local Mach number from measured pitot pressure and the barometric pressure. From the measured total temperature, the static temperature and speed of sound were determined and then the velocity calculated from the product of Mach number times speed of sound. For subsonic flow the Mach number was determined from the isentropic total pressure relation.

The absolute centerline velocity profile for Mach numbers 0.8, 1.4, 2.0, and 2.5 are shown in Figure 15. The similarity of the radial profiles is shown in Figure 16. These data show no effect of total temperature or Mach number. Also plotted is the exponential or Gaussian profile which seems to fit the data very well. Measured velocity half widths are shown in Figure 17 for flows with constant total enthalpy. Half widths for flows with excess total enthalpy are shown in Figure 18.

In summary we can state that Mach number and total temperature influenced the mixing rate on the basis of the centerline velocity graph and the half widths; however, the similarity profile seems to be unaffected.

5.1.b. Total Temperature

The decay of the total temperature is shown in Figure 19. Examination of this figure shows that the total temperature profiles do not exhibit a potential core of constant total temperature near the jet nozzle. The decay is continuous from the combustion chamber and shows that turbulence is not relaxed in the supersonic nozzle. The decay rate then increases as the shear generated turbulence reaches the centerline. The similarity profile of excess total enthalpy is shown in Figure 20. These profiles taken downstream in the similarity region can also be fitted by a Gaussian profile but with different

temperature half radius. The enthalpy half radius used to generate the similarity profile is shown in Figure 21. These figures reveal the strong effect of Mach number as increasing Mach number reduced the mixing rate.

5.1.c. Static Pressure Defect

The most striking observation of these experiments was the existence of a static pressure defect of considerable magnitude for each experiment (Figure 22). Again, we can see the strong effects of Mach number. While no absolute accuracy can be given for these data since no method was available to perform a check on this probe, internal consistency from one experiment to the next is evident. These data were reduced to turbulence normal stress through Equation 151, Section III. Assuming isotropy on the axis, these data were converted to turbulence kinetic energy K. These data are shown in Figure 23. The turbulence energy appears to be expressible as a function of the jet velocity rather than the Mach number.

5.1.d. Eddy Viscosity and Prandtl Number

The dynamic viscosity for the compressible jet was determined from the velocity decay, similarity radial profile, and velocity half width through the formula

$$\mu_T = \frac{\bar{\rho}\, r_{1/2}^2 \left(\frac{d\bar{W}}{dz}\right)}{4 \ln 2} \tag{203}$$

which can be derived from Equation 188 for Gaussian profiles. Data were obtained on the centerline from Mach numbers 0.2 to 1.7 for both the heated and unheated jets. Incompressible freejet data were obtained from Arseyeva (Reference 10) and treated the same way. These results are shown in Figure 24 and are seen to correlate very well with the radial turbulence pressure. Shown in the figure is a line drawn through the data having the slope 1/2. The apparent trend of the data deviates from this line for the higher intensity. This trend is attributed to compressibility effects beginning with the data points corresponding to M = 0.3 and above.

According to Figure 24 the incompressible eddy viscosity is well represented by the Prandtl formula

$$\epsilon_o = U' \ell_{mix} \tag{204}$$

where ℓ_{mix} is some fraction of the local velocity half radius and that the compressible viscosity is lower by an amount which is Mach number dependent.

Prandtl numbers were calculated by the formula

$$P_r = - \frac{\bar{\rho}\left(\frac{d\bar{W}}{dz}\right)\left(\bar{W}^2 - C_p(\bar{T}_o - T_\infty)\frac{r_{1/2}^2}{(r_{1/2})_T^2}\right)}{\bar{\rho}\,\bar{W}\frac{d\bar{h}}{dz} + \left(\bar{W}\frac{dP_T}{dz} - d_e\right)} \tag{205}$$

which was derived from Equation 189 for Gaussian profiles. Large scatter was found in all the experiments with heated jets, probably as a result of the lack of conservation of excess enthalpy as noted in Figure 14. The data from the constant total enthalpy runs were consistent and Prandtl numbers ranged from 0.73 to 0.80.

5.1.6. Dissipation

Dissipation of turbulent kinetic energy was determined from the formula

$$d_k = -\bar{\rho}\,\overline{W}\left(\frac{dK}{dz}\right) \tag{206}$$

which results from Equation 190 for negligible diffusion on the centerline. These data are shown in Figure 25, which reveals decay law is of the form of Equation 170. The dissipation length scale is very nearly equal to the velocity half radius. This scale is comparable with the results of isotropic incompressible turbulence for which the dissipation scale is of the order of the integral lateral scale of turbulence. Considerably more scatter was obtained from these data although most experiments did exhibit individually the 3/2 power dependence, the open squares are from experiment 5 and show this dependence quite well. No Mach number dependency was observed in these data although the large scatter of the data makes this result inconclusive.

5.2 COAXIAL MIXING

5.2.a Pitot Pressures and Static Pressure

Pitot pressure and static pressure radial profiles for one half the mixing region are shown in Figure 26 at a downstream distance $Z/D_j = 10$. The pitot pressure shows a maximum at $r/D_j = 0.2$ and then goes into a trough out to $r/D_j = 1.6$. This trough is a result of the initial boundary layer which still remains. The static pressure profile shows the existence of an expansion wave in the jet core which results from the shock expansion system of the conical nozzle used as the fuel injector. The initial boundary layer is nearly 1.1 times the jet exit diameter which is sufficient to drastically alter the effective boundary conditions for this problem.

5.2.b. Concentration

The concentration profile shown in Figure 27 is the average of both sides of the mixing profile. This profile shows that the jet spreading has moved less than one half jet diameter radially at a downstream distance of 10 jet diameters.

5.2.c. Velocity Profile

The pitot pressure, static pressure, and concentration profiles were reduced to Mach number, Figure 28. The velocity was calculated from the Mach number profiles by assuming that a constant total enthalpy profile existed, Figure 29. The velocity profile shows the same extent of spreading as the concentration profile. This figure, however, shows that a large part of the velocity defect has been removed in the boundary layer.

5.2.d. Turbulence

The Eulerian integral time scale was calculated from the autocorrelations. The time scale given by the integral to infinite time delay

$$T_E = \int_0^\infty R_\tau \, d\tau \qquad (207)$$

was modified by terminating integration when the correlation coefficient has fallen to 0.05. These time scales exhibit a strong variation across the mixing zone and then seem to level off (Figure 31).

5.2.e. Scale of Turbulence

It is of fundamental importance in the present theory to determine the variation of the scale of turbulence across the mixing zone. By using the "Taylor Hypothesis" that turbulence is locked into the flow locally; we can derive a longitudinal scale of turbulence from the formula

$$\Lambda = \bar{W} T_E \tag{208}$$

The results are shown in Figure 32. First, we see that the scale is of the same order of magnitude as the jet diameter. Secondly, we find that the scale is constant in the mixing layer and that a separate scale exists in the boundary layer. Thus, this flow contains two turbulent shear layers, a new shear layer due to mixing and an old shear layer from the injector boundary layer.

5.3 NORMAL INJECTION

5.3.a. Optical Measurement Penetration

Schlieren photographs of normal jet penetration into the air stream with varying jet total pressure are shown in Figures 33 and 34 for free stream Mach numbers of 2.5 and 3.0. As can be seen by comparing these photographs with the normal sonic jet, Figure 9, the complex barrel shock pattern does not exist. Thus, we expect that more dissipation has occurred by turbulence than in the normal sonic jet. Penetration was taken to the edge of the light zone running nearly horizontal in the pictures. This definition corresponds to the zero concentration point as determined by gas samples in the next section. Penetration was compared to the empirical correlation formula of Povinelli and Povinelli (Reference 11). The results are shown in Figure 35. The results for the high shear injector are correlated very well by the equation

$$\frac{Y_0}{D_{eff}} = 2.4 \left(\frac{q_f}{q_a}\right)^{0.35} \left(\frac{M_1}{M_f}\right)^{0.094} \left(\frac{X_1}{D_{eff}} + 0.5\right)^{0.277} \tag{209}$$

which is Equation 6 from Reference 6 with the slope increased by 25%. This equation was obtained by Povinelli using a regression analysis of experimental data using the dimensionless groups determined by Vranos and Nolan (Reference 12). Since the structure of this jet is different, it is somewhat surprising that this functional grouping works so well.

5.3.b. Concentration Measurement

The concentration profile normal to the wall is shown in Figure 36, 10 jet diameters downstream. This jet has the same mass flow rate as that in the coaxial test. A very large increase in mixing rate is observed. This profile also verifies the definition of penetration for the optical data. A correlation of downstream decay of normal sonic jets was obtained by Henry and presented in Reference 7. Mass fractions were correlated with downstream distance divided by the core length. Core length is defined to be the last downstream station for which the peak concentration is 100%. From the Schlieren photographs of the jet structure and the extrapolation of concentration data back to the 100% point, it is concluded that the core length for this jet is equal to the half width of the nozzle at the exit with distance measured from the jet centerline,

$$X_0 = \frac{\text{Width of Jet Nozzle}}{2} \tag{210}$$

Downstream decay of peak mass fraction was then plotted in Figure 37 for a comparison with the mixing rate of the sonic normal injector. The experimental data are represented by the formula

$$Y_f = \left(\frac{X_1}{X_0}\right)^{-1.2} \tag{211}$$

where the sonic jets were correlated in Reference 5 as

$$Y_f = \left(\frac{X_1}{X_0}\right)^{-0.6} \tag{212}$$

These exponents show a much faster mixing rate, in fact larger, by the square. It also appears that the mixing length is determined solely by the size of the injector and not by the dynamics; however, more data should be obtained to verify this conclusion. This result would be of great value in engine design.

5.4 SUMMARY OF IMPORTANT EXPERIMENTAL RESULTS

This experimental work has several important results that apply directly to both theoretical and practical design conclusions.

a. Large defects in mean static pressure are found in compressible turbulent shear flows. This defect is interpreted to be a direct measurement of the turbulence pressure.

b. The experimental laws relating eddy viscosity and dissipation of turbulent energy to the local turbulence energy and an appropriate scale can be applied directly to the formulation of an improved theoretical model of turbulent shear flow.

c. The scale of turbulence appears to be constant across the shear layer even though eddy viscosity, dissipation, and turbulent energy vary across the shear layer.

d. Turbulent energy can be frozen in a supersonic nozzle and thus cause performance losses.

e. The normal fuel injector design tested can apparently give short constant mixing lengths over a wide range of initial air velocities, thus simplifying combustor design.

SECTION VI

NUMERICAL RESULTS FOR FREE JETS

6.1 DESCRIPTION OF TURBULENCE PROGRAM EMPIRICAL INPUT

The equations for axisymmetric mixing were coded for solution on an IBM 7094 computer. The purpose of this calculation was to show that a coupled set of equations could adequately describe the turbulent shear flows. Many empirical inputs are needed since the detailed turbulent structure is unknown. The following incompressible eddy viscosity formula was used:

$$\epsilon_o = \frac{L_D}{16.5}\left(\frac{2}{3}K\right)^{1/2} \tag{213}$$

where

$$L_D = \frac{\bar{W}_{max} - \bar{W}_{min}}{\left(\frac{\partial \bar{W}}{\partial r}\right)_{max}}\,(2)^{1/2} \tag{214}$$

and

$$K = \frac{3}{2}\,\frac{\rho\gamma}{\bar{\rho}} \tag{215}$$

A constant mixing length seems appropriate in view of the results for the coaxial supersonic mixing length scales (Figure 32).

The dynamic viscosity was then calculated from the equation

$$\mu_T = \bar{\rho}\,\epsilon_o \tag{216}$$

The effects of heat transfer and diffusion on turbulent viscosity have been formulated by Corrsin in Reference 13 but were not applied in this study. The large Mach number effect was accounted for by the following formulas:

$$\frac{\epsilon}{\epsilon_0} = 1 - M^2 \quad (0 < M < 0.5) \tag{217}$$

and

$$\frac{\epsilon}{\epsilon_0} = (1 + 0.25M)^{-2} \quad (0.5 < M < \infty) \tag{218}$$

The first formula is derived from the definition of the Reynolds stress and the assumption that the covariant density velocity fluctuations are isentropic which should be valid for low Mach numbers (Figure 38). The second formula was obtained by fitting the solution to the data of Eggers (Reference 14), as shown in Figure 39. The dissipation function was calculated by the formula

$$d_k = \frac{3}{2} \frac{\rho \left(\frac{2}{3} K\right)^{3/2}}{L_D} \tag{219}$$

Thus there must be a relation between the viscosity scale and the large scale eddies, namely

$$\ell_{mix} = \frac{L_D}{16.5} \tag{220}$$

This value seems to be physically plausible. No compressibility or transport effects were incorporated into the calculation of dissipation.

The measured value of Prandtl number $P_r = 0.75$ was used for the calculations and the effective Lewis number was set equal to unity for intuitive reasons, and then the Schmidt number became 0.75 because of the relationship between Schmidt number and Prandtl and Lewis numbers. The diffusion of turbulent kinetic energy is analogous to turbulent heat and mass transfer. A Lewis number for turbulence defined below was set equal to 1.2 in the final calculations.

$$L_k = \frac{3}{5} \frac{\epsilon_k}{\epsilon_T} \tag{221}$$

6.2 SOLUTIONS FOR INCOMPRESSIBLE FLOW

The data of Laurence (Reference 15) were used as a comparison for the low speed calculation. The lower curve in Figure 39 shows the comparison of centerline velocity decay. The agreement is excellent. This model has correctly calculated the core length as well as the centerline decay in the

transition and self-preserving regions. Figure 40 shows a comparison of measured and calculated turbulence intensity in the initial shear layer near the end of the potential core at $\frac{Z}{D_j} = 3.8$. The agreement is good but two discrepancies are noted. First, the peak intensity is too low. This may be due to the nonisotropy of the shear flow, which is not accounted for by this theory. The second discrepancy is the large difference in centerline turbulence level between the calculated and measured values. The reason for this discrepancy is not known. Perhaps it is due to the assumption regarding the purely dissipative role of viscosity which may not be valid at the edges of the turbulent region. Some remarks in this regard may be found in Hinze (Reference 16). It is interesting that the turbulence intensity is larger at the outside edge of the shear layer than the mean velocity itself.

6.3 SOLUTIONS FOR COMPRESSIBLE FLOWS WITH CONSTANT TOTAL TEMPERATURE

Comparison of the theoretical calculations with the free jet data for Mach numbers of 0.8, 1.4, 2.0, 2.5 is shown in Figure 41. The agreement is generally good except for the Mach 2.5 case for which the decay rate is over-predicted in the transition region even though the potential core length is predicted closely. The reason for this deviation is not known. It is postulated, however, that this deviation may be due to the fact that the turbulence terms were not accounted for in the data reduction by Rayleigh's pitot formula. An examination of the Mach 2.0 results also shows a similar deviation but smaller when the turbulence pressure is significant.

6.4 FLOW WITH EXCESS TOTAL ENTHALPY

The low speed jets, M = 0.8 and M = 1.4, have heat transfer in the same direction as momentum transfer while the heat transfer in the high speed constant total enthalpy cases was opposite to the momentum transfer. Thus these cases should present a difficult test for the theoretical calculation. The results for two cases are shown in Figures 42 and 43. Good agreement was obtained. For these calculations the measured initial profiles were used as input. The calculation was performed with 14 input points on the profile and the calculation took less than two minutes, a run time characteristic of all these problems. The calculations at M = 2.0 and M = 2.5 did not agree as well with the data

(Figures 44 and 45). The data exhibit double structure with a centerline decay that existed through the nozzle itself. These data show that turbulence is not relaxed in the nozzle so that indeed frozen turbulence losses can be expected in supersonic propulsion nozzles. The present formulation of the mixing program is for only one shear layer, although in principle the flow can be divided into different regions with different scales. Despite these shortcomings it is felt that the present formulation of the turbulence program is more useful and consistent than previous turbulent calculations based on a velocity defect law for eddy viscosity. These calculations are also useful for the problem of calculating the noise generated by jets since turbulence intensity is a necessary input to Lighthill's theory of noise from submerged jets (Reference 17). The final Figure, 46, shows a comparison of computed and measured relative turbulence intensities on the centerline for two different Mach numbers. The agreement is quite good although the theory is a little low consistent with the low results obtained at the centerline in Figure 39 for the low speed jet of Laurence.

SECTION VII

CONCLUSIONS

The results of the theoretical and experimental study of supersonic mixing have led to the following conclusions.

1. Thrust losses due to freezing the turbulence kinetic energy of the combustor can be appreciable; however, these losses are not as large as originally presented by Swithenbank in Reference 2 and do not constitute a fundamental performance limitation to the supersonic combustion ramjet as previously thought.

2. Mixing rate and penetration of normal jets can be increased by designing injectors to make more energy available for turbulent dissipation as was done in these experiments by eliminating the strong internal shock structure and maximizing the jet velocity. It is concluded that normal fuel injection offers the designer advantages of the shortest and most constant mixing lengths for a very small loss of potential engine performance.

3. The theoretical model of turbulence based on the turbulent state concept should provide improved calculations, under widely different initial conditions, over the previous theoretical models.

APPENDIX A

TABLE OF EXPERIMENTAL CONDITIONS
FREE JET EXPERIMENTS

Experiment No.	M	P_o	T_o	Comments
1	2.0	115	531	Calibration
2	2.0	120	960	Calibration
3	2.0	113	558	Bad Pressure Data
4	2.0	117	997	
5	2.0	114	1209	
6	2.0	115	560	
7	2.5	250	900	
8	2.5	253	1500	
9	2.5	---	--	P_{t_2} Probe Failed
10	2.5	245	560	
11	1.0	26	535	Only Static Pressure Measured
12	1.0	27	1 [illegible]	Only Static Pressure Measured
13	1.0	25	1440	Only Static Pressure Measured
14	1.0	24	1100	
15	1.0	25	540	
16	1.5	50	1330	
17	1.5	52	1050	Data Acquisition System Malfunctions
18	1.5	50	550	
19	1.5	50	545	
20	1.5	50	1054	
21	1.5	104	555	
22	1.5	153	565	

Experiment No.	M	P_o	T_o	Comments
23	2.5	250	1350	
24	2.5	---	--	Cooling Check
25	2.5	---	--	Calibrate P_T
26	2.5	---	--	Calibrate P_T
27	2.0	95	1330	
28	2.0	50	1250	
29	2.0	120	560	P_T Only
30	2.0	120	560	P_T Only
31	2.0	115	1260	Naval Ordnance Laboratory Probe Used
32	2.0	220	1365	
33	2.0	200	560	Only Static Pressure Measured

APPENDIX B

FIGURES

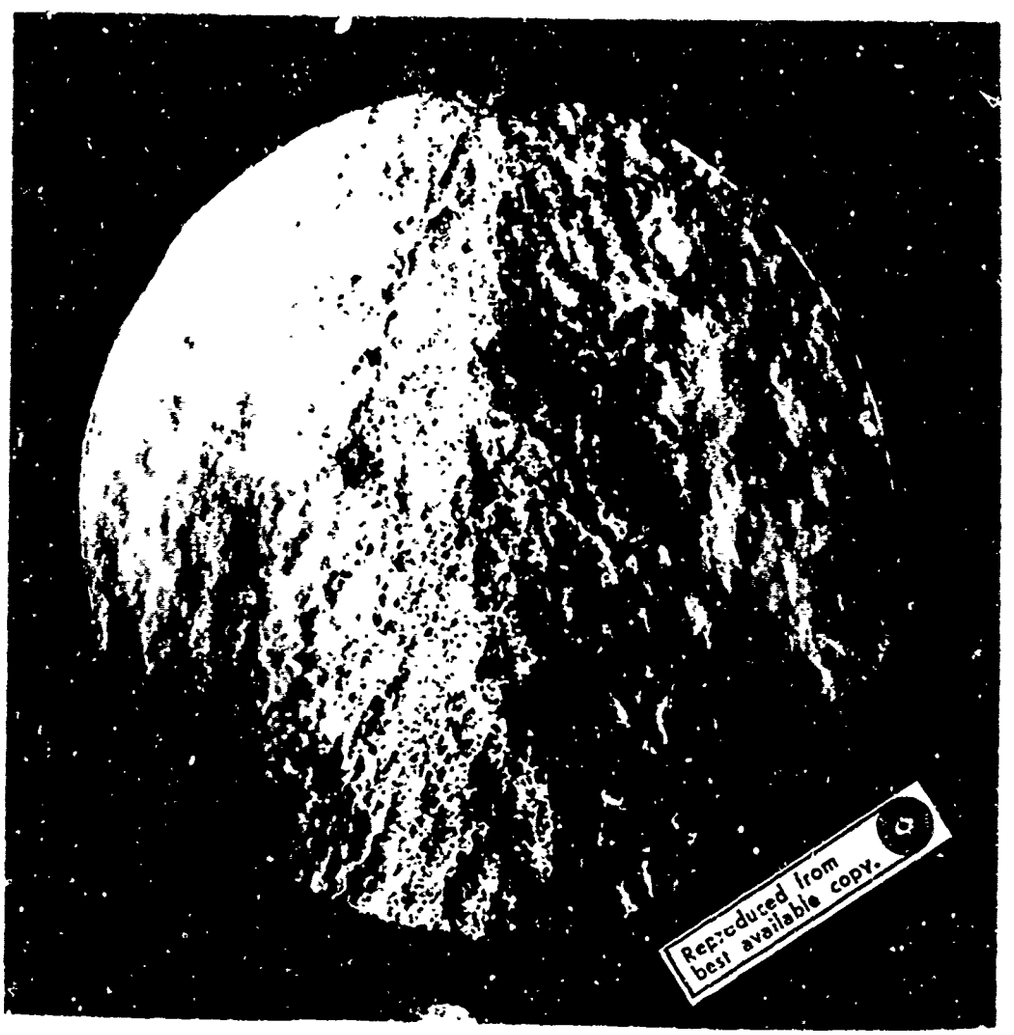

Figure 1. Schlieren of Free Jet Showing Turbulent and Nonturbulent Regions

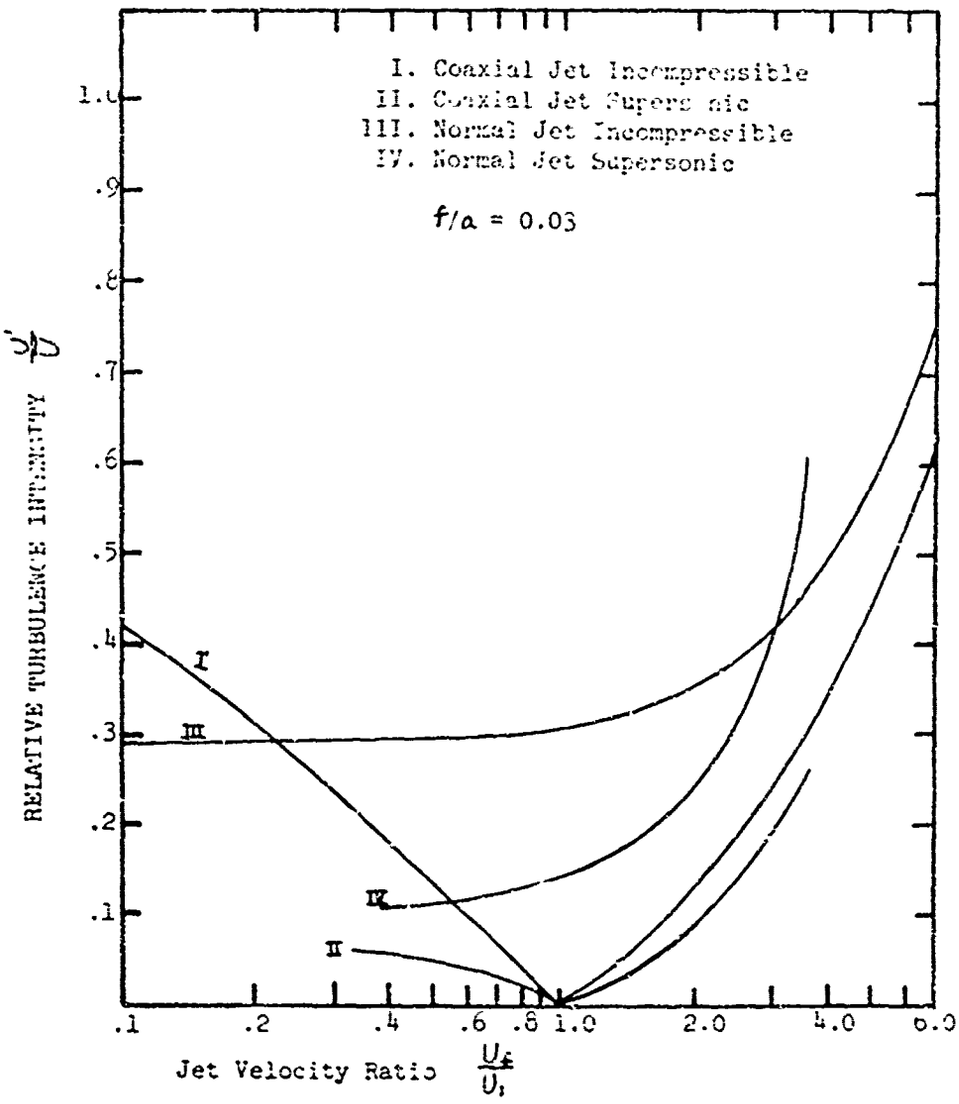

Figure 2. Turbulence Production in Internal Flow

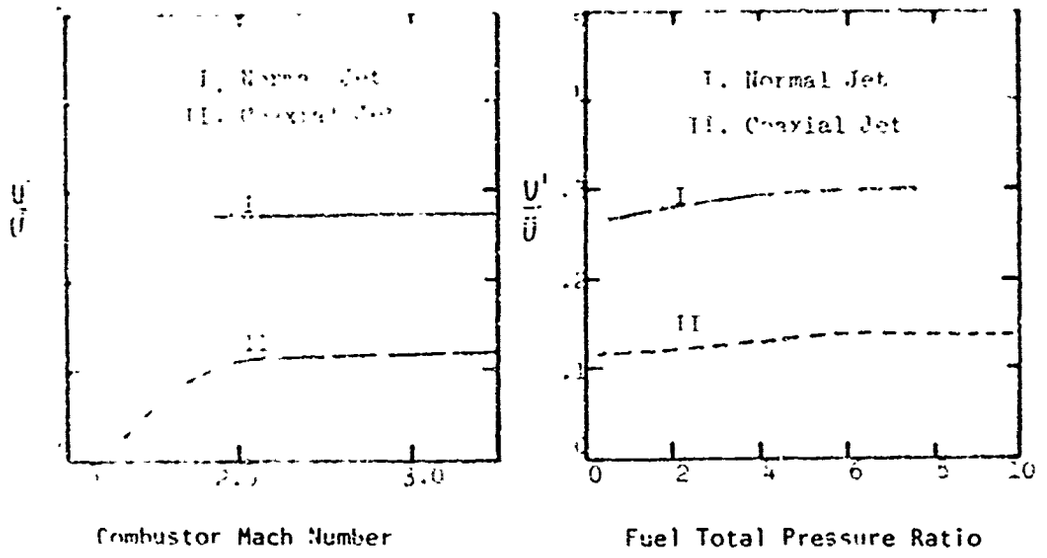

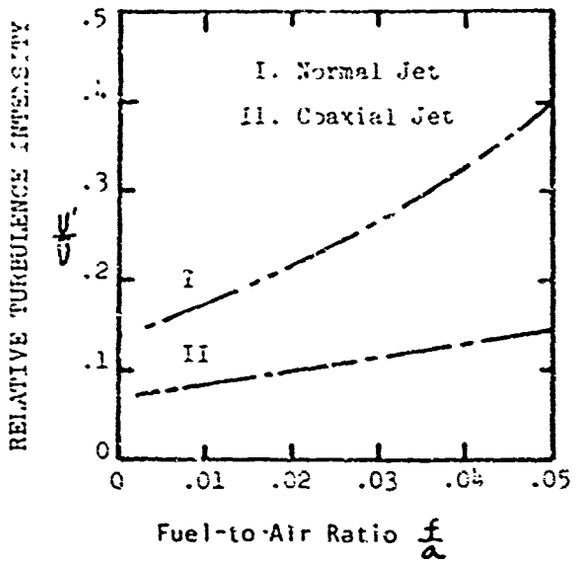

Figure 3. Effects of Initial Conditions on Turbulence Production

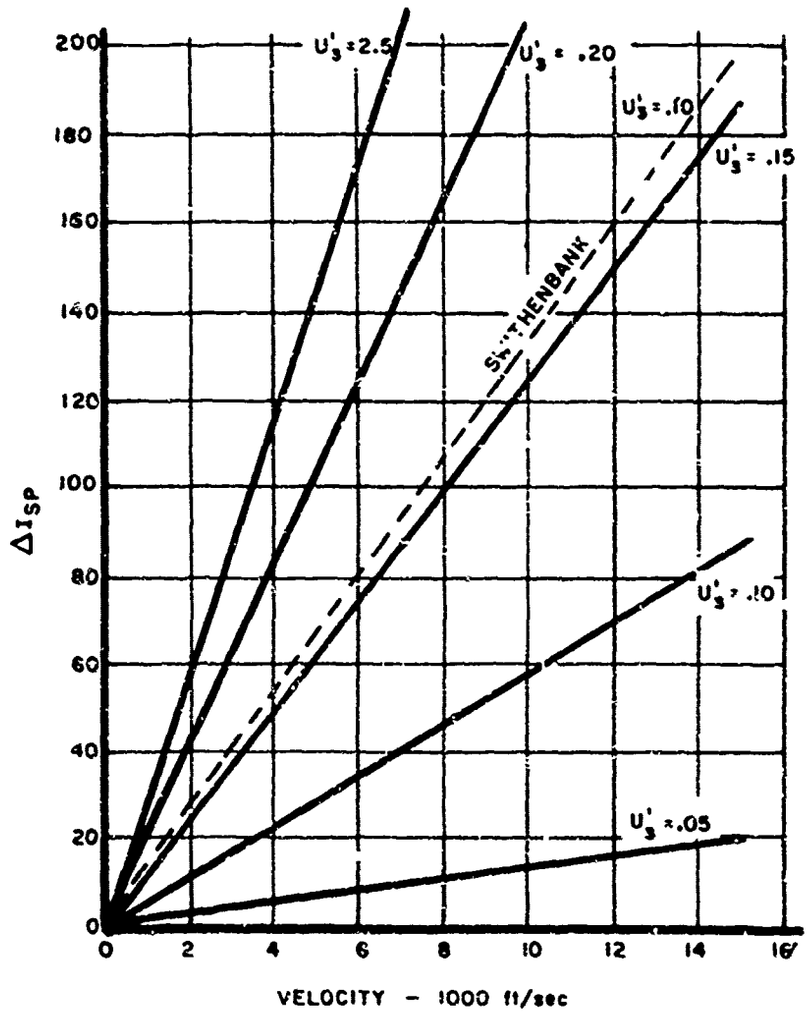

Figure 4. Specific Impulse Losses Due to Freezing Turbulence Generated by Mixing

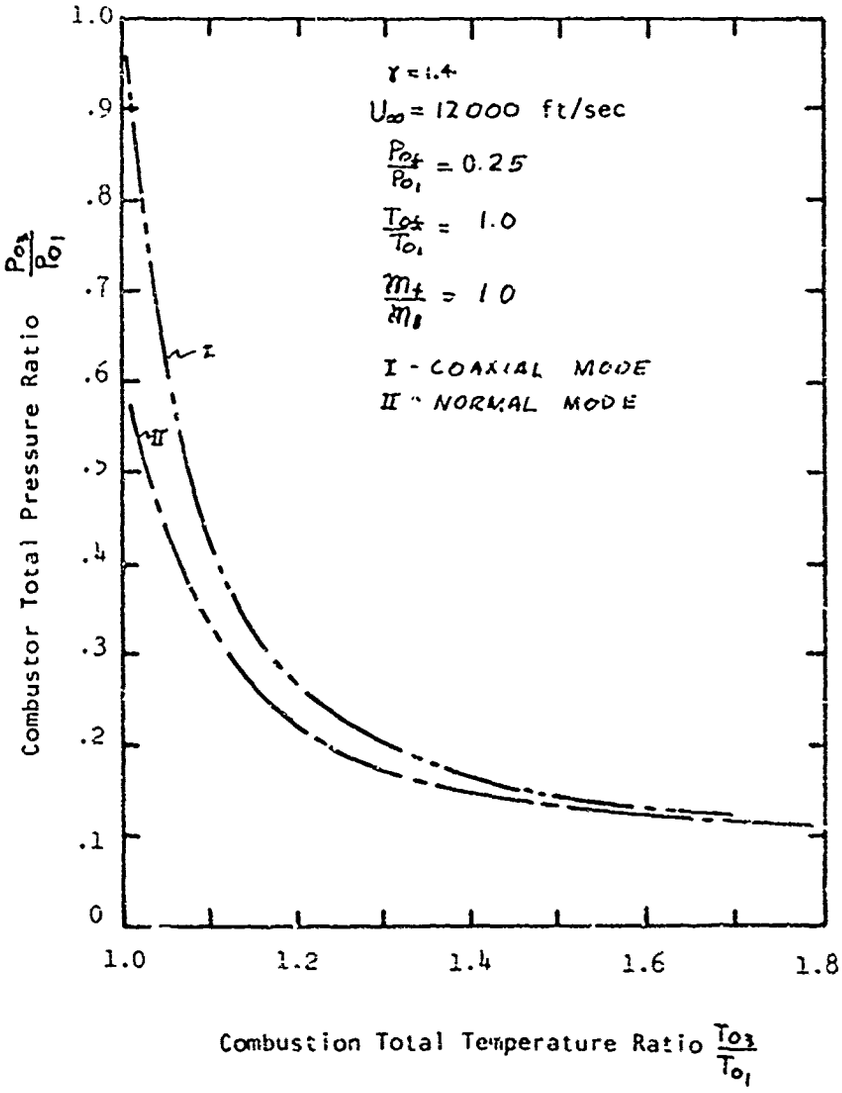

Figure 5. Effect of Fuel Injection Mode on Combustor Total Pressure Losses

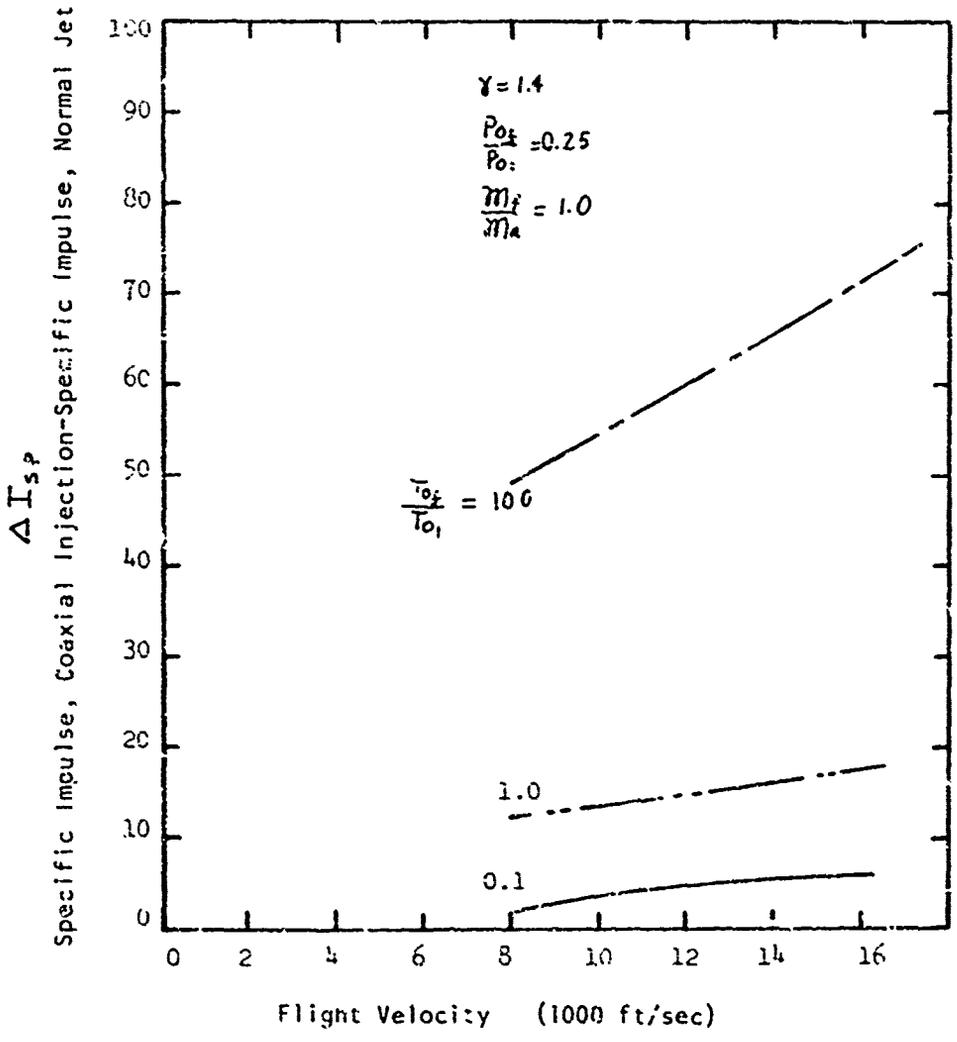

Figure 6. Effect of Fuel Injection Mode on Performance

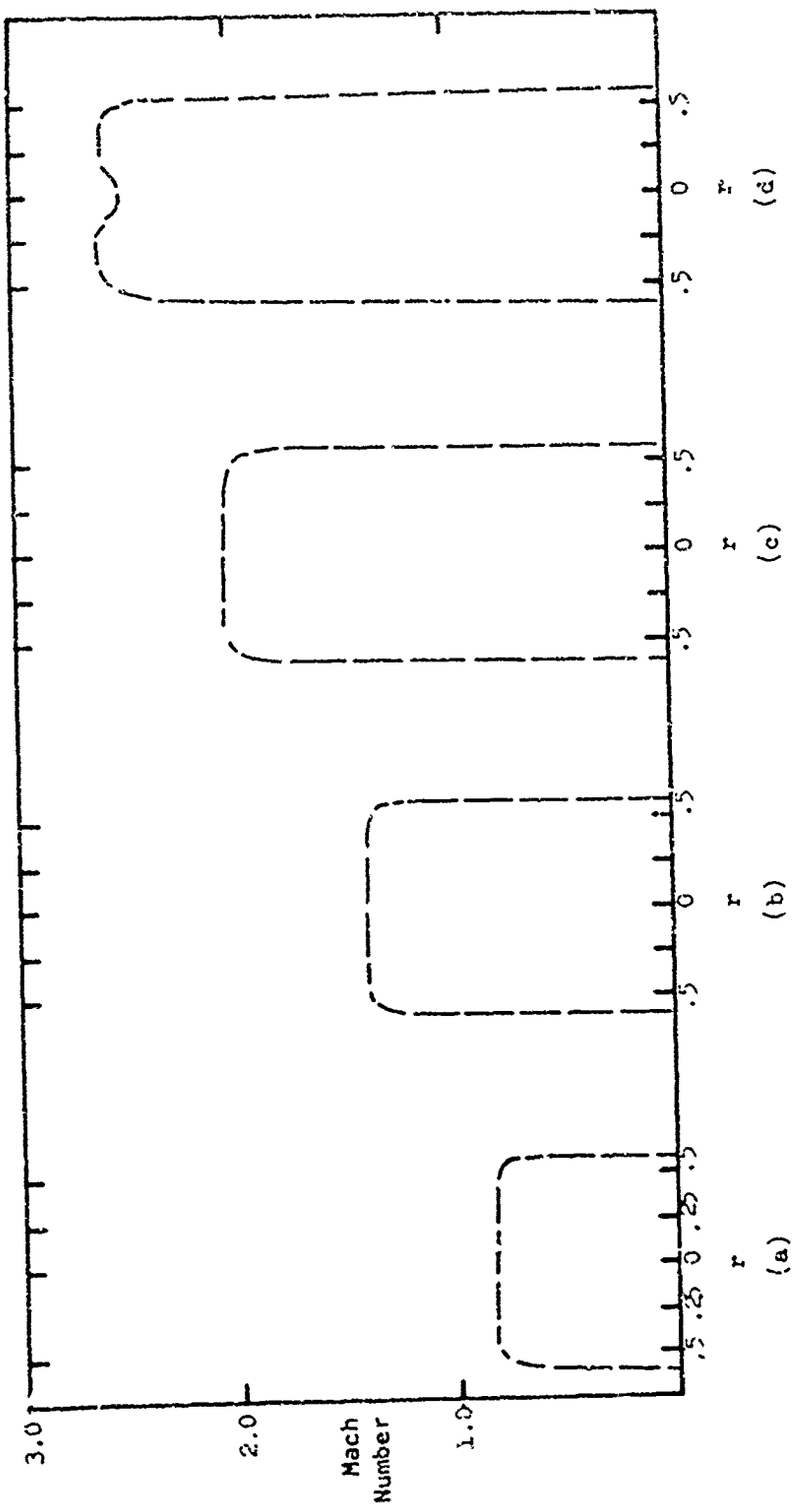

Figure 7. Free Jet Exit Mach Number Profile

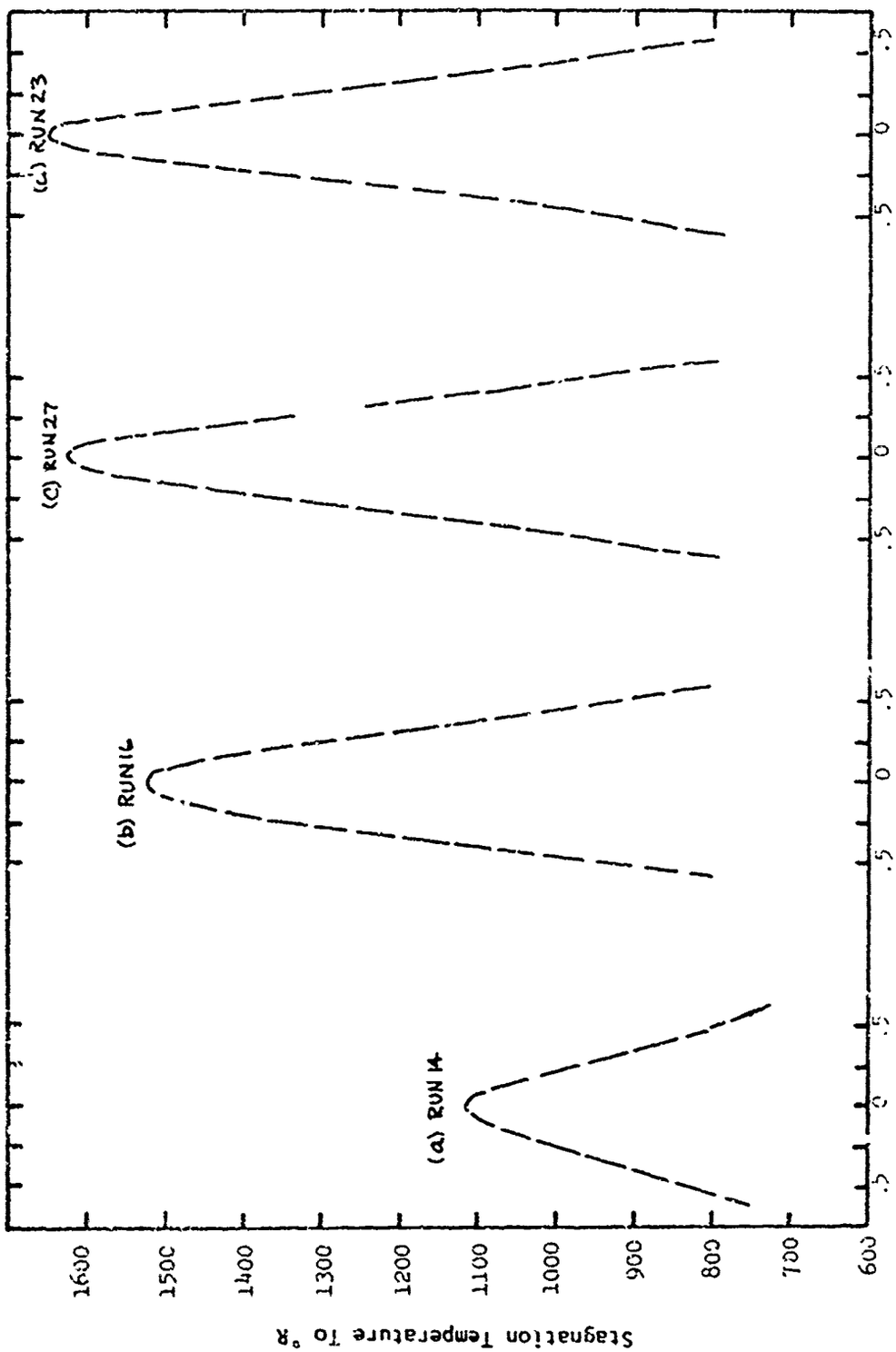

Figure 8. Free Jet Exit Total Temperature Profiles

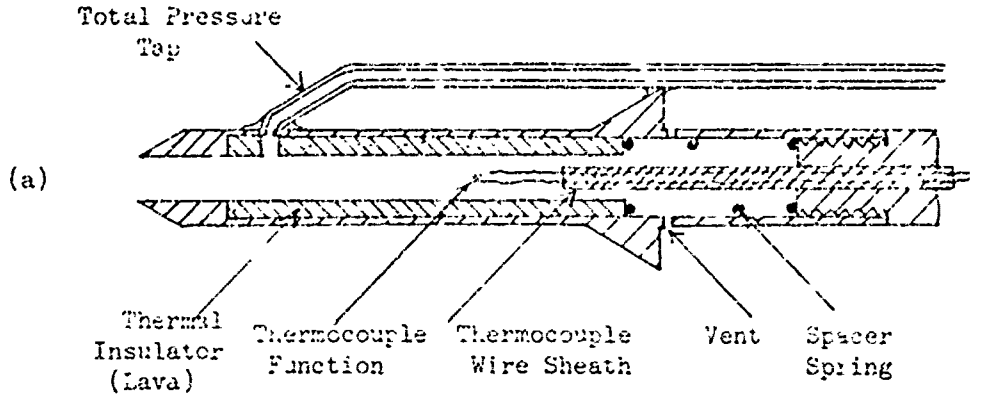

COMBINATION PROBE

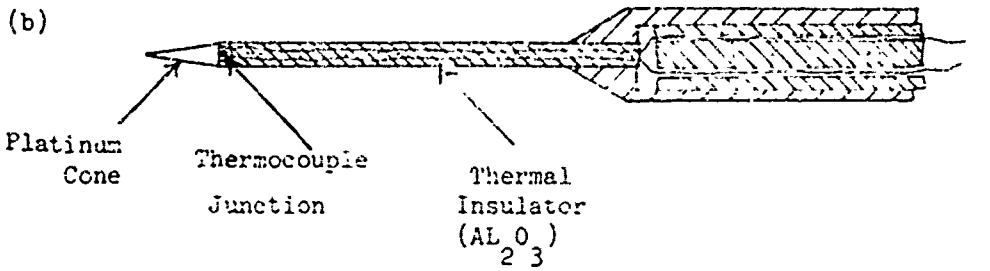

NAVAL ORDNANCE LAB RECOVERY PROBE

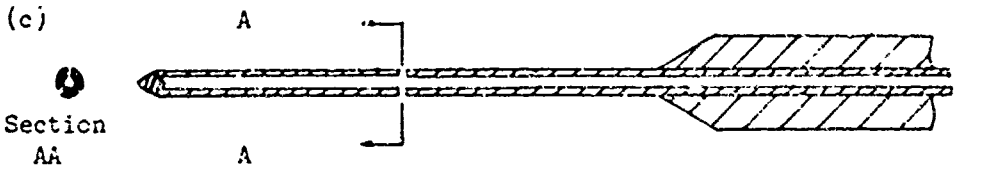

STATIC PRESSURE PROBE

Figure 9. Schematic Drawing of Instrumentation

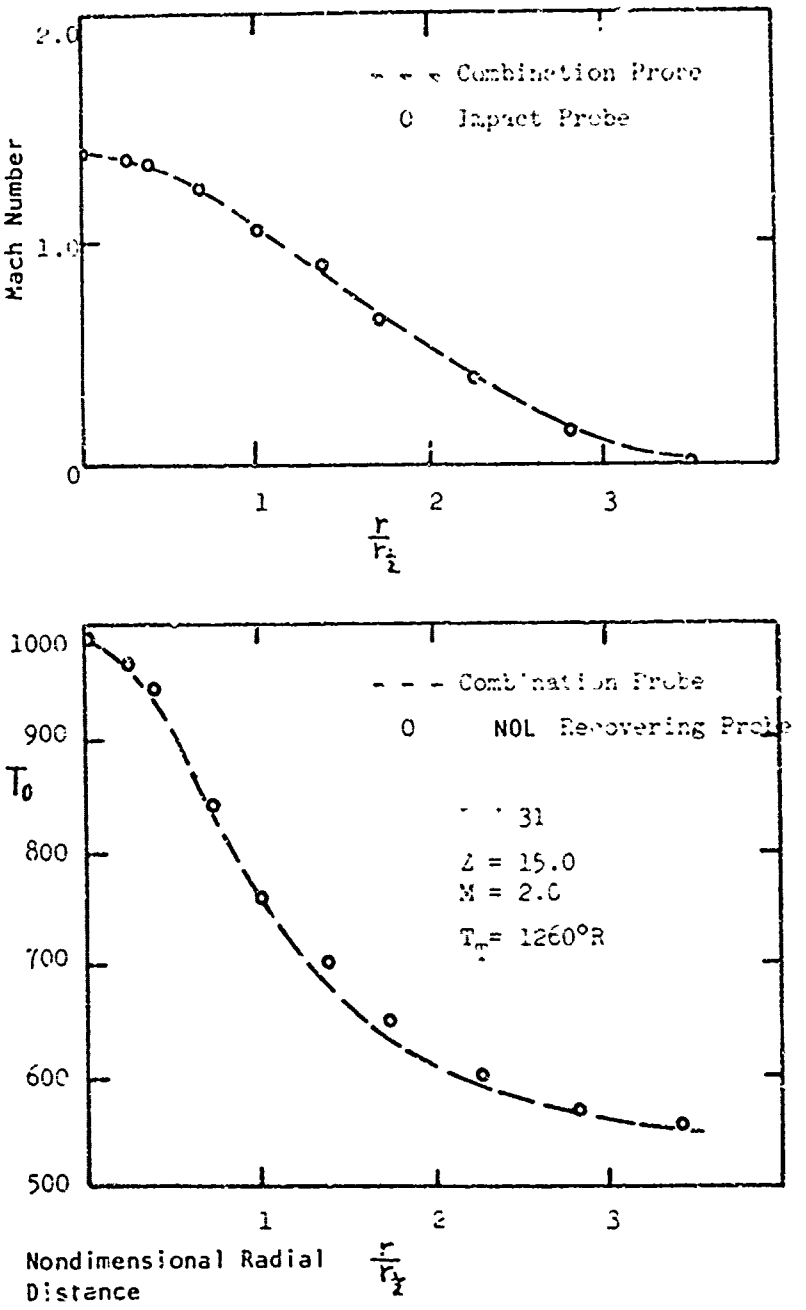

Figure 10. Comparison of Combination Probe and Naval Ordnance Laboratory Probe Data

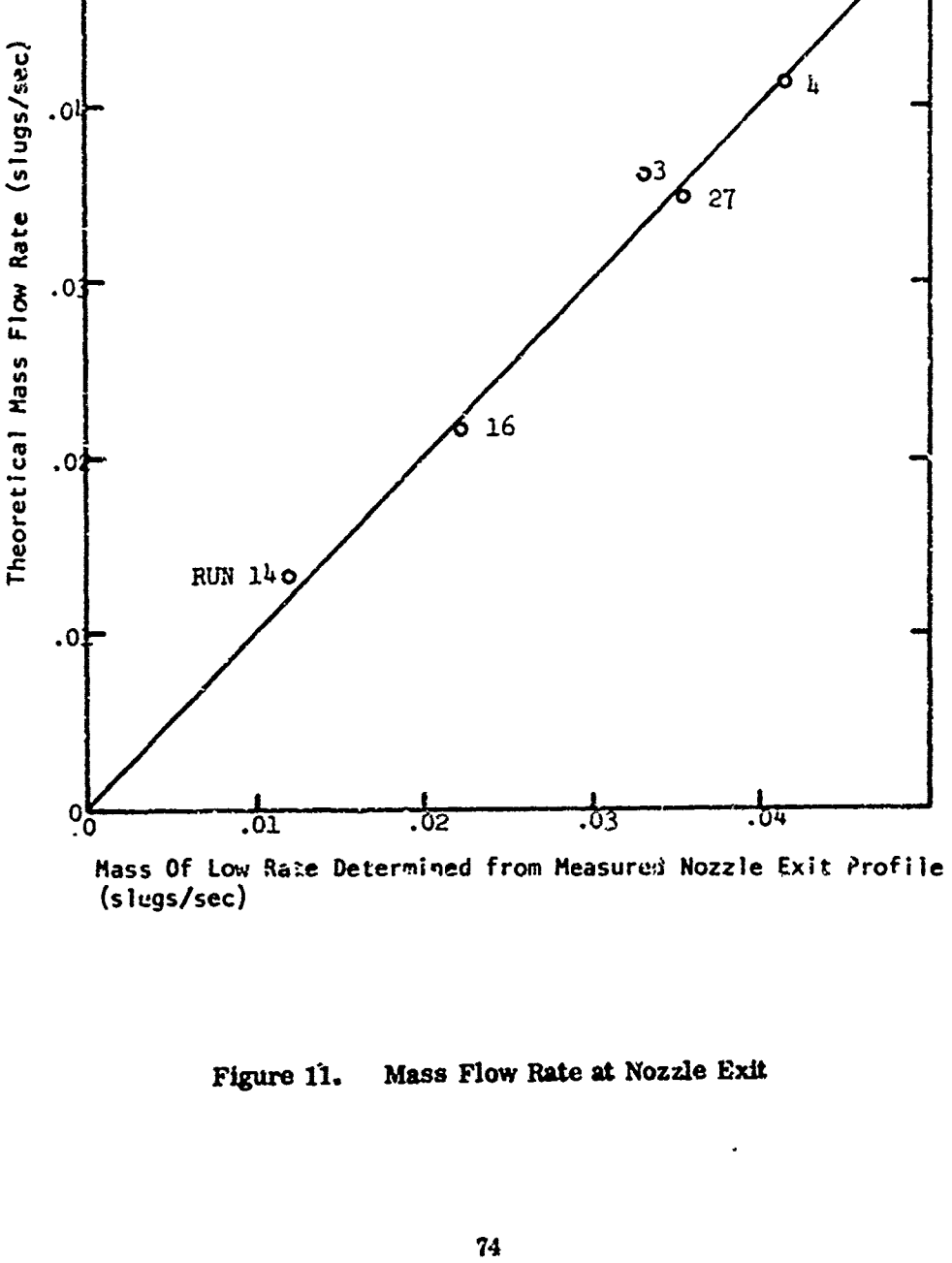

Figure 11. Mass Flow Rate at Nozzle Exit

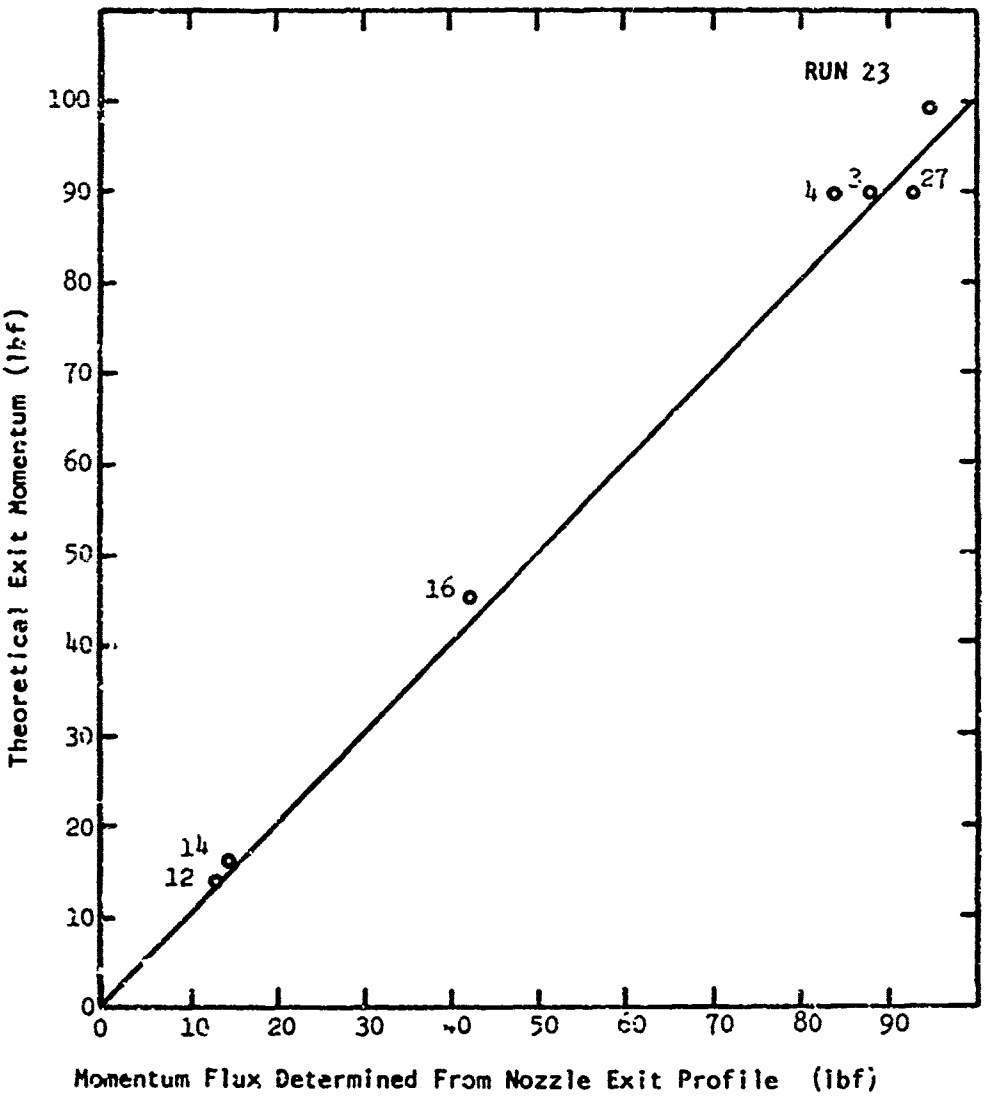

Figure 12. Accuracy of Exit Momentum Flux

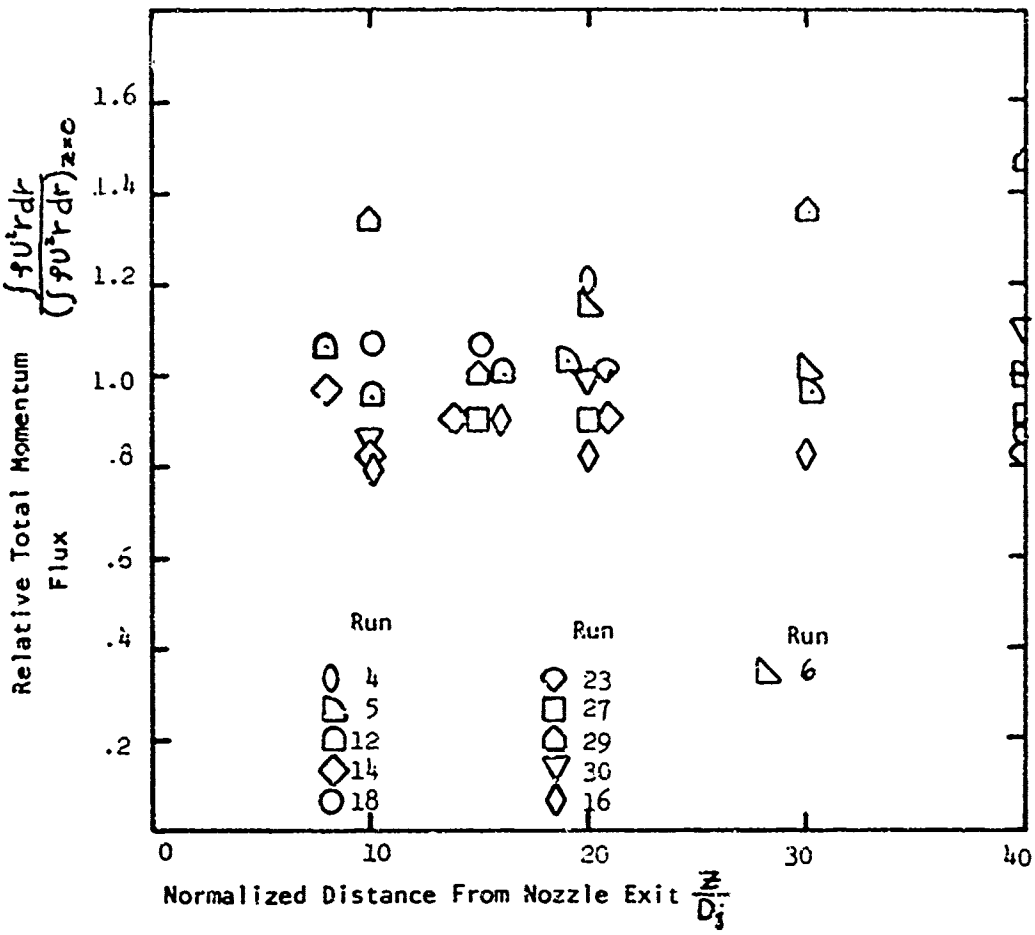

Figure 13. Accuracy of Normalized Jet Momentum

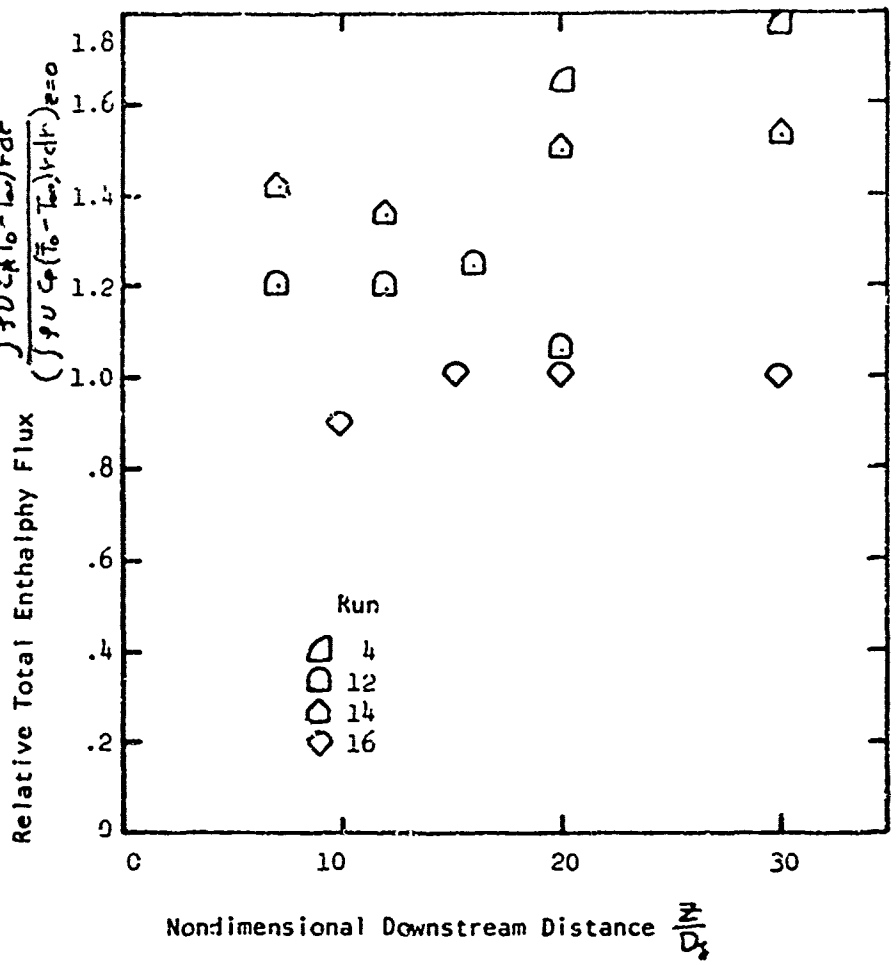

Figure 14. Accuracy of Normalized Enthalpy

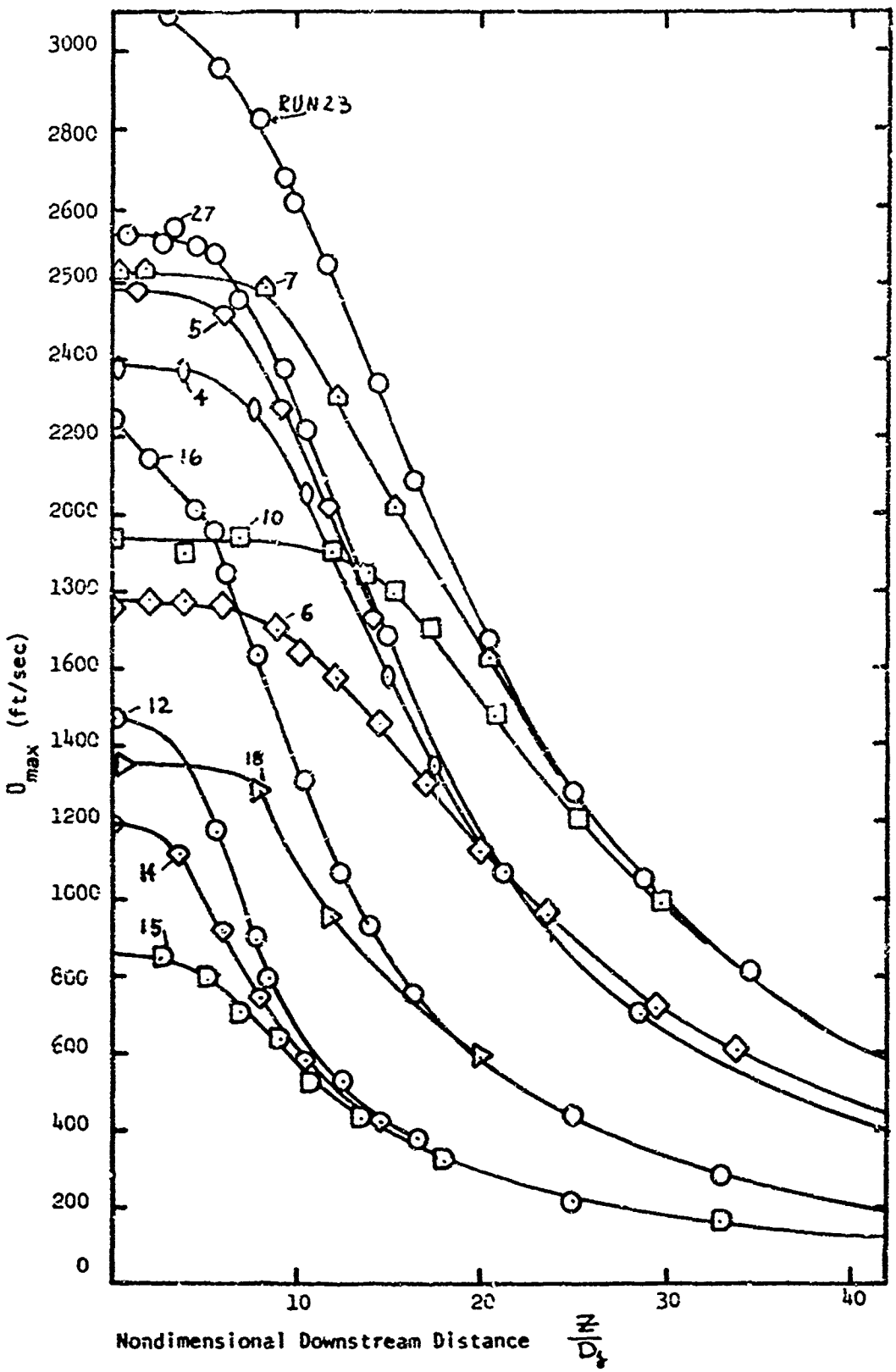

Figure 15. Free Jet Centerline Velocity Decay

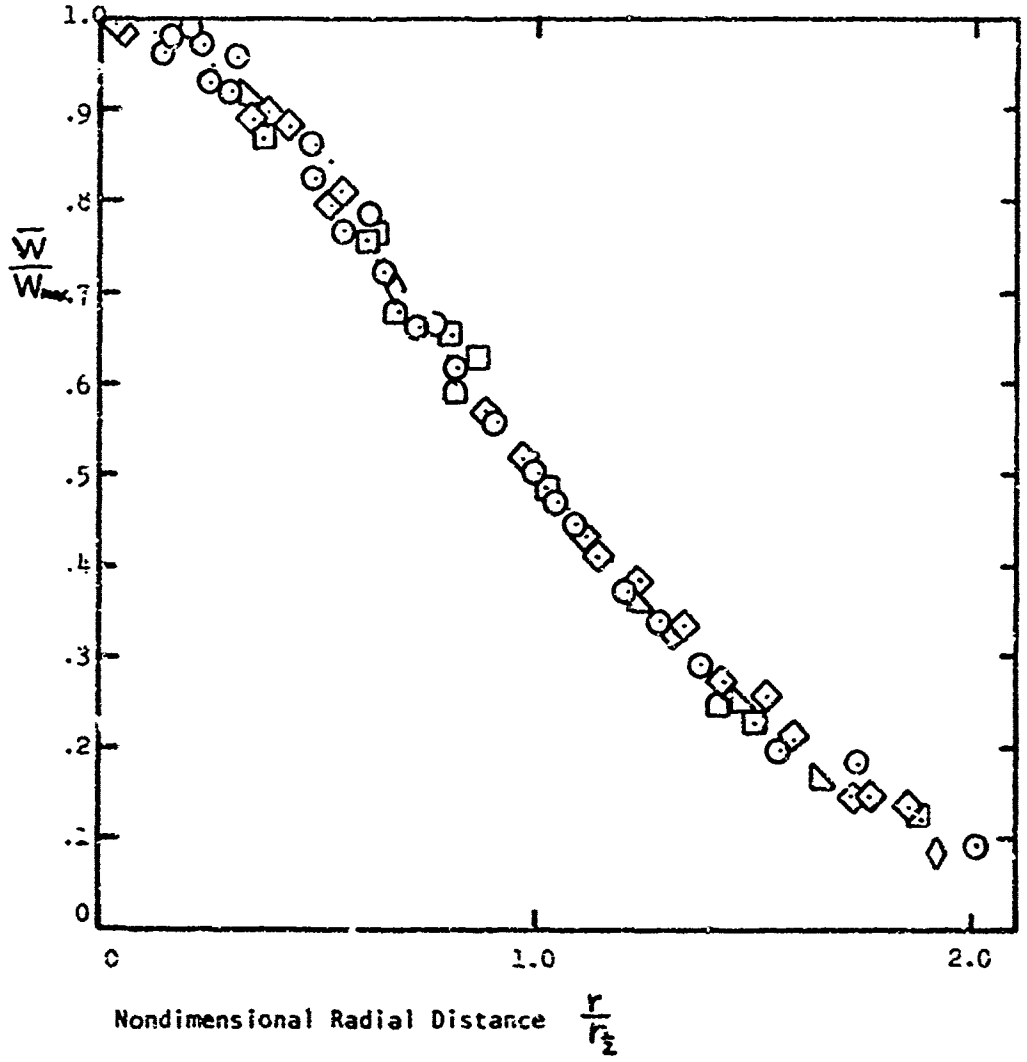

Figure 16. Similarity of Radial Velocity Profiles of Free Jet

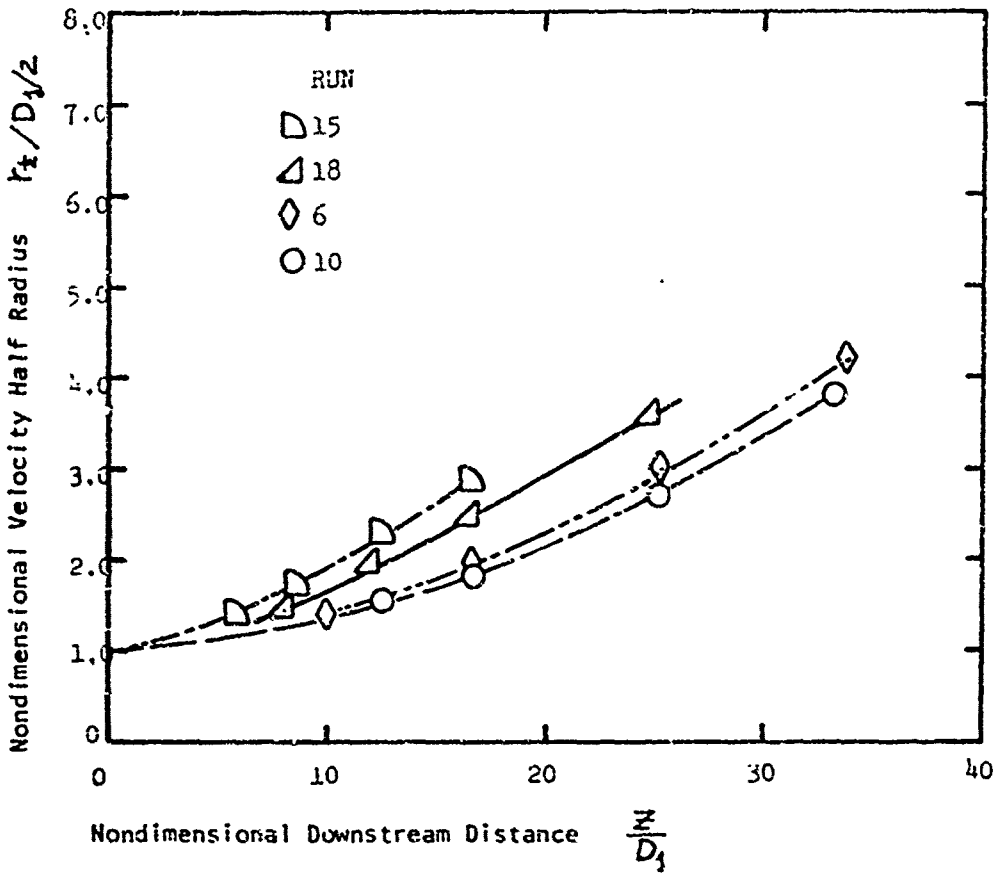

Figure 17. Experimental Velocity Half Width; $\bar{T}_o/T_\infty = 1.0$

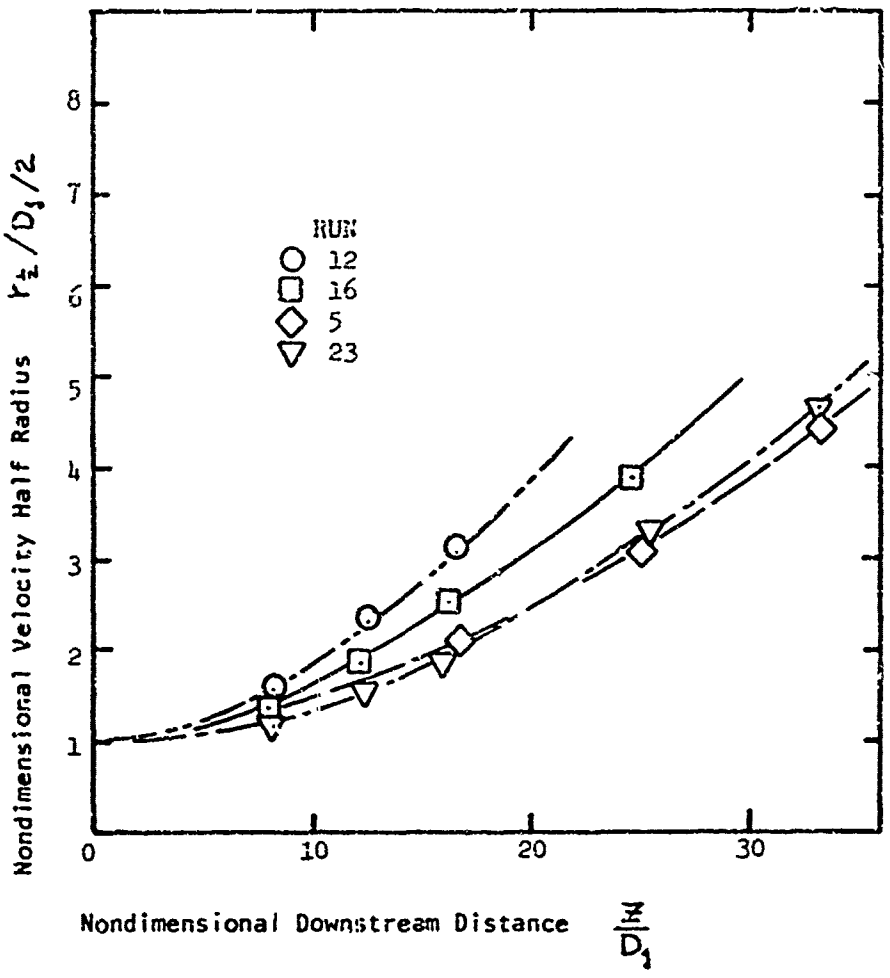

Figure 18. Experimental Velocity Half Width; $\bar{T}_o/T_\infty > 1$

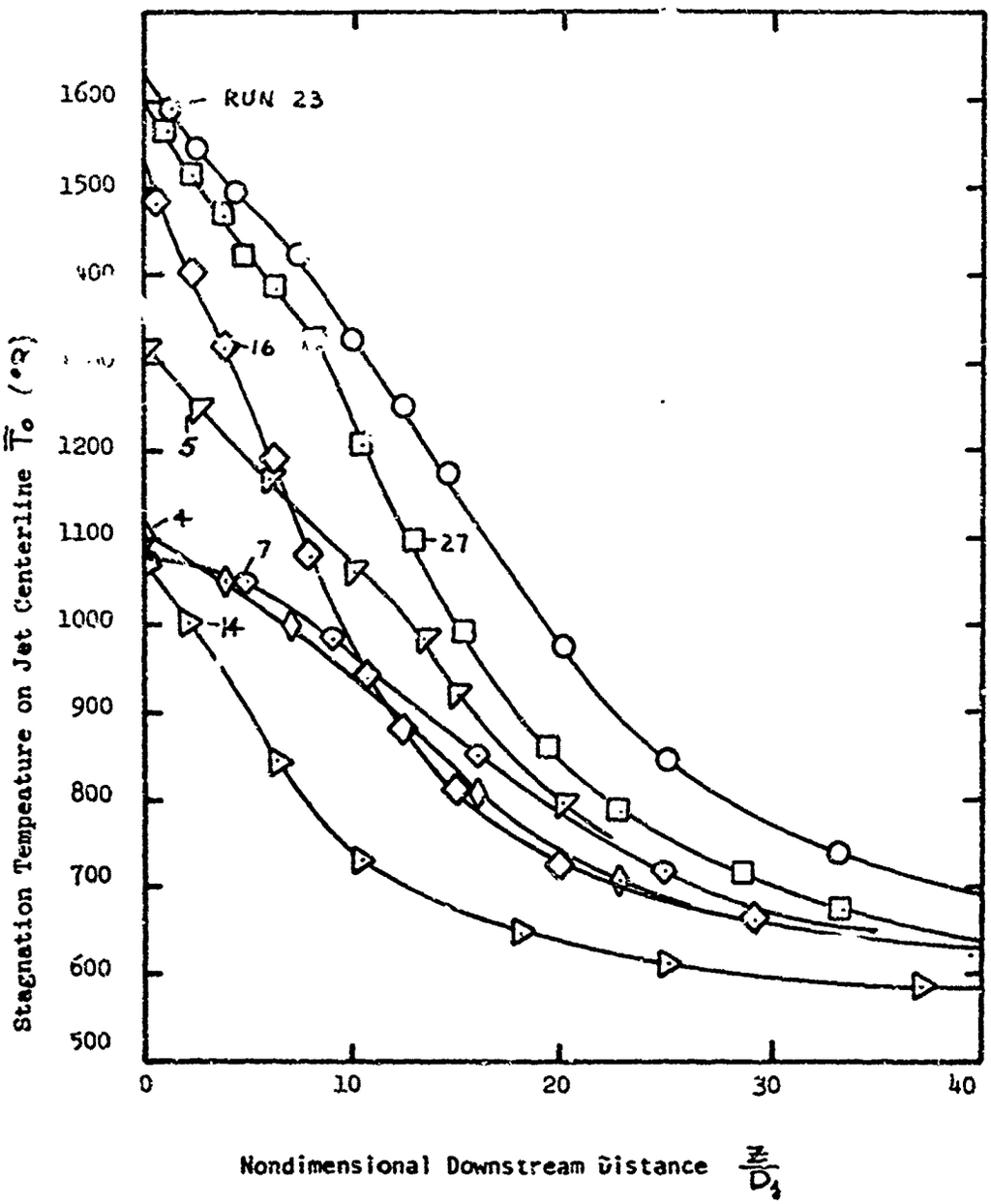

Figure 19. Free Jet Centerline Total Temperature Decay

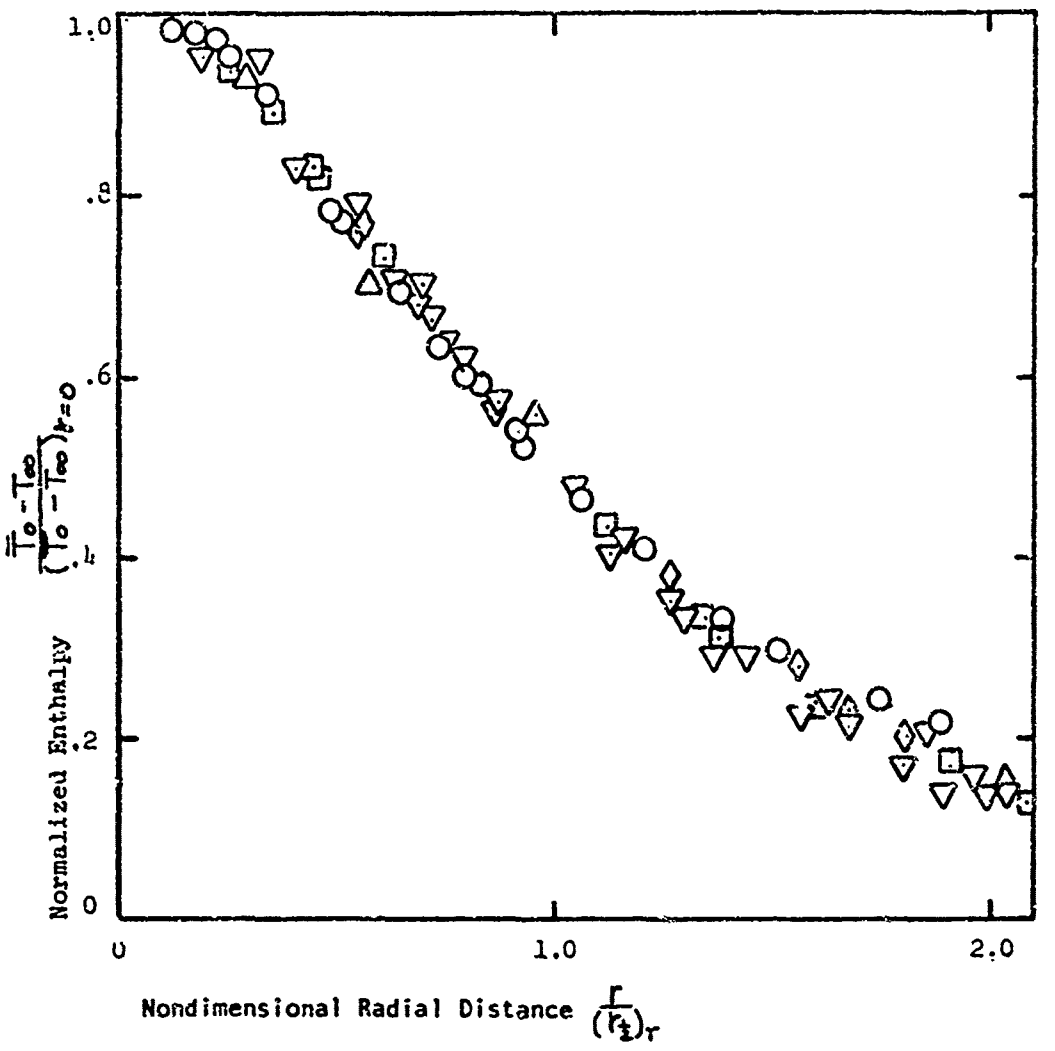

Figure 20. Similarity Profile of Normalized Enthalpy Free Jet

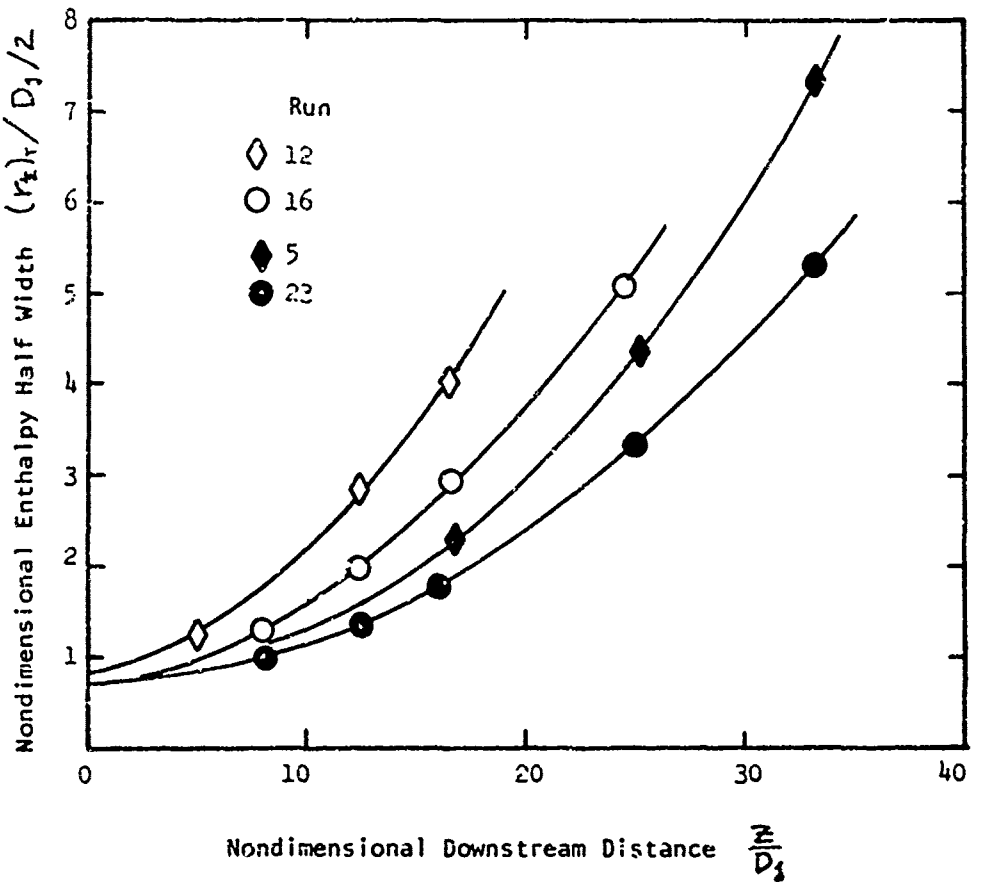

Figure 21. Normalized Enthalpy Half Width

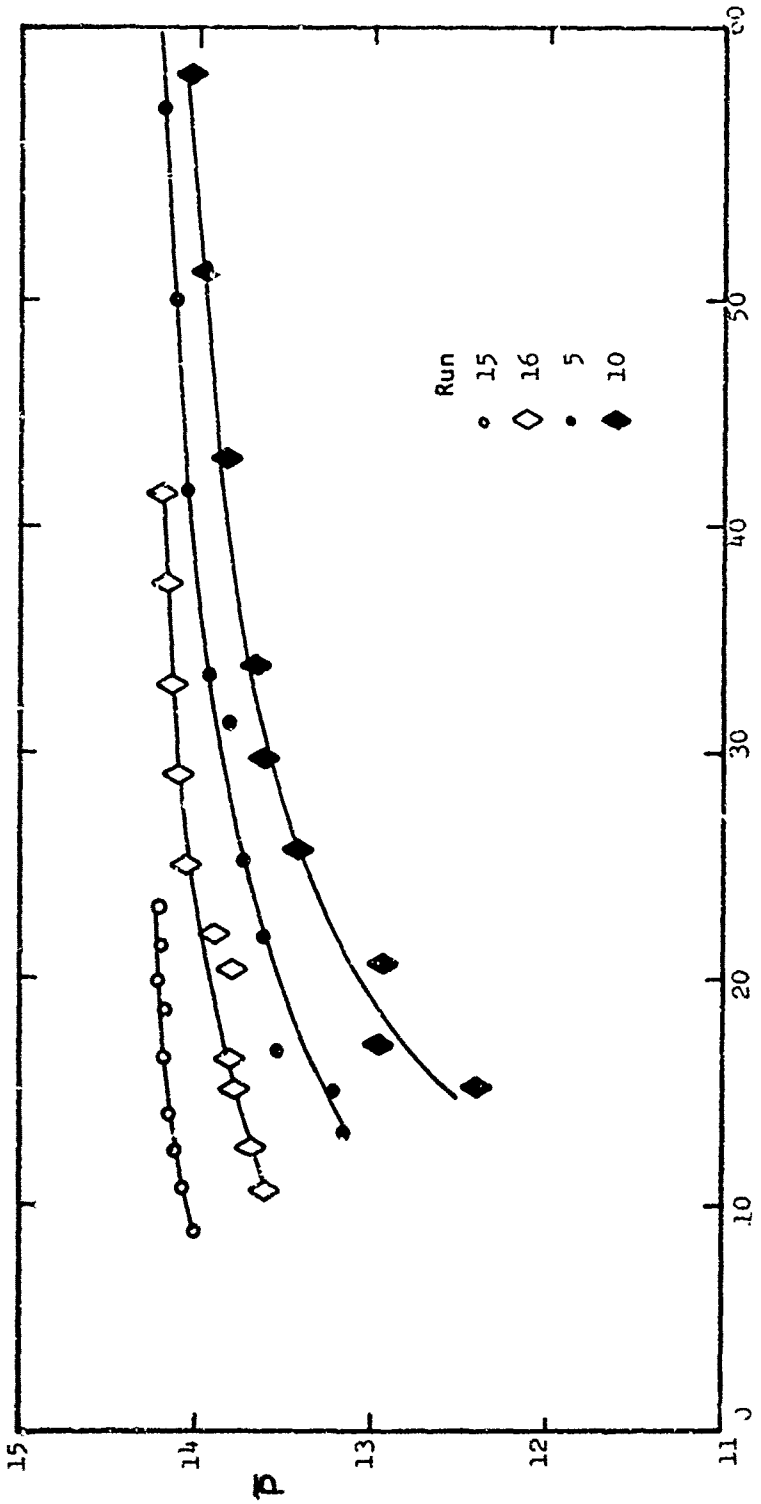

Figure 22. Experimental Free Jet Centerline Static Pressure

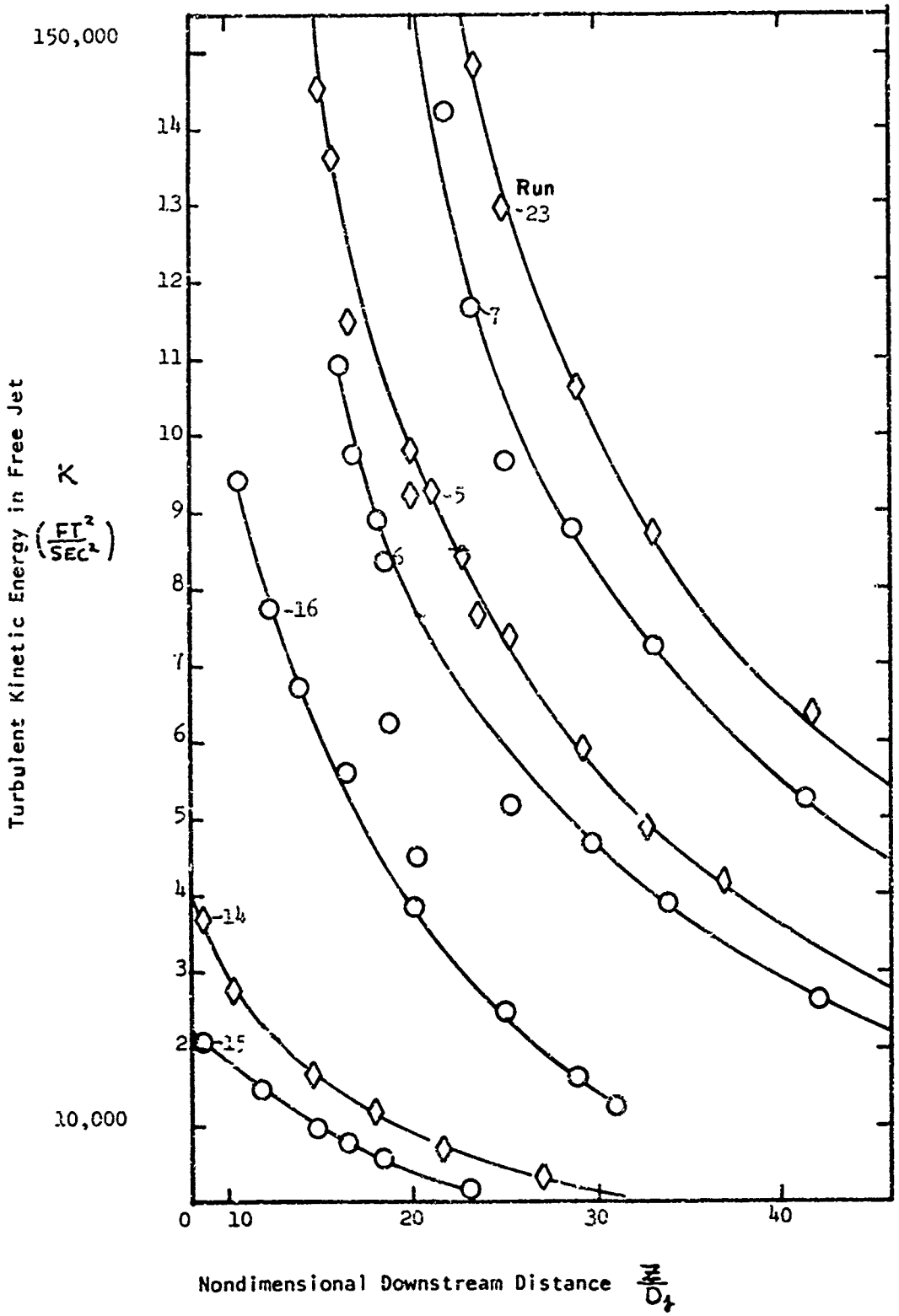

Figure 23. Free Jet Centerline Turbulent Kinetic Energy

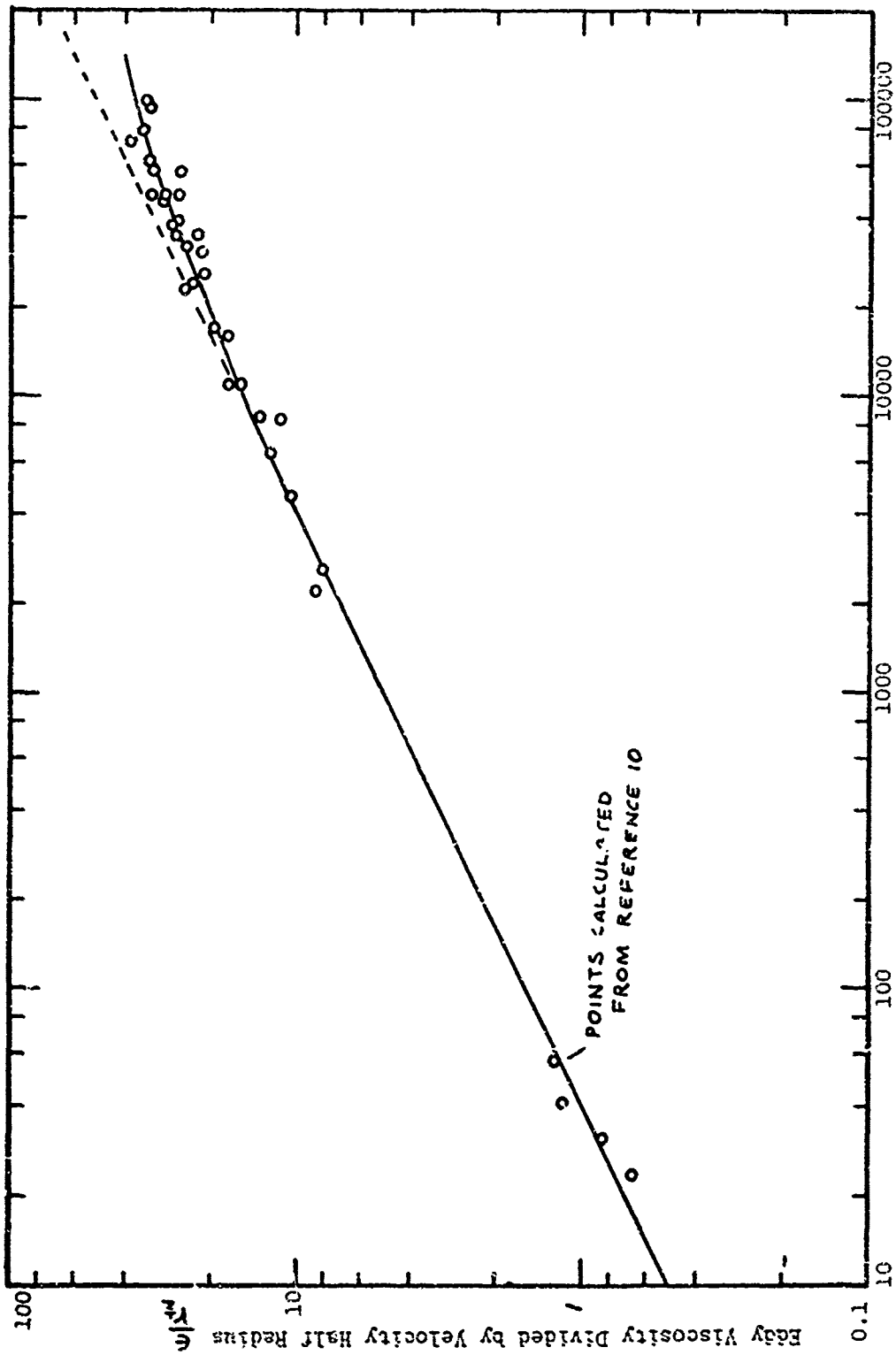

Figure 24. Eddy Viscosity Correlation With Turbulent Pressure

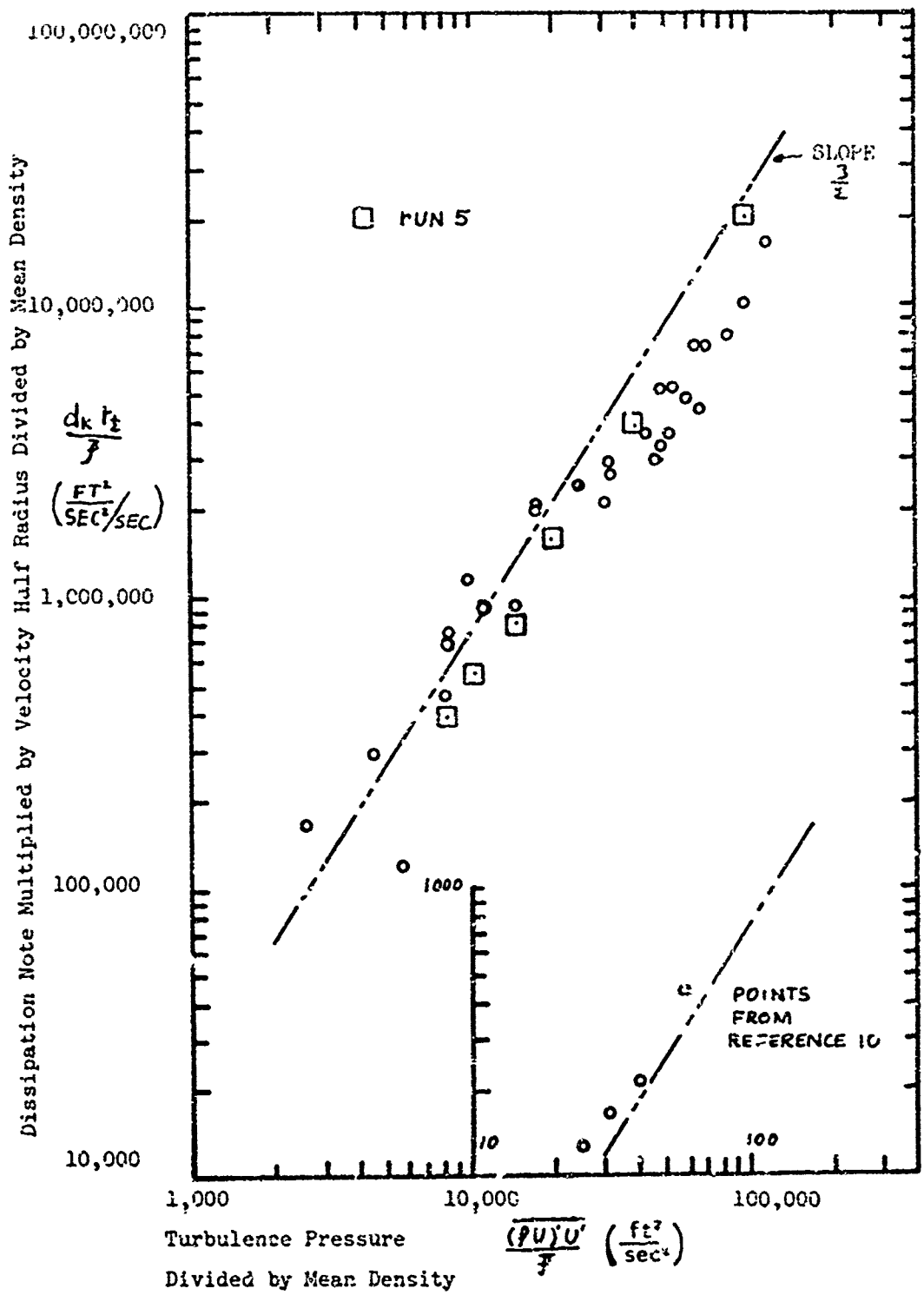

Figure 25. Turbulent Kinetic Energy Decay

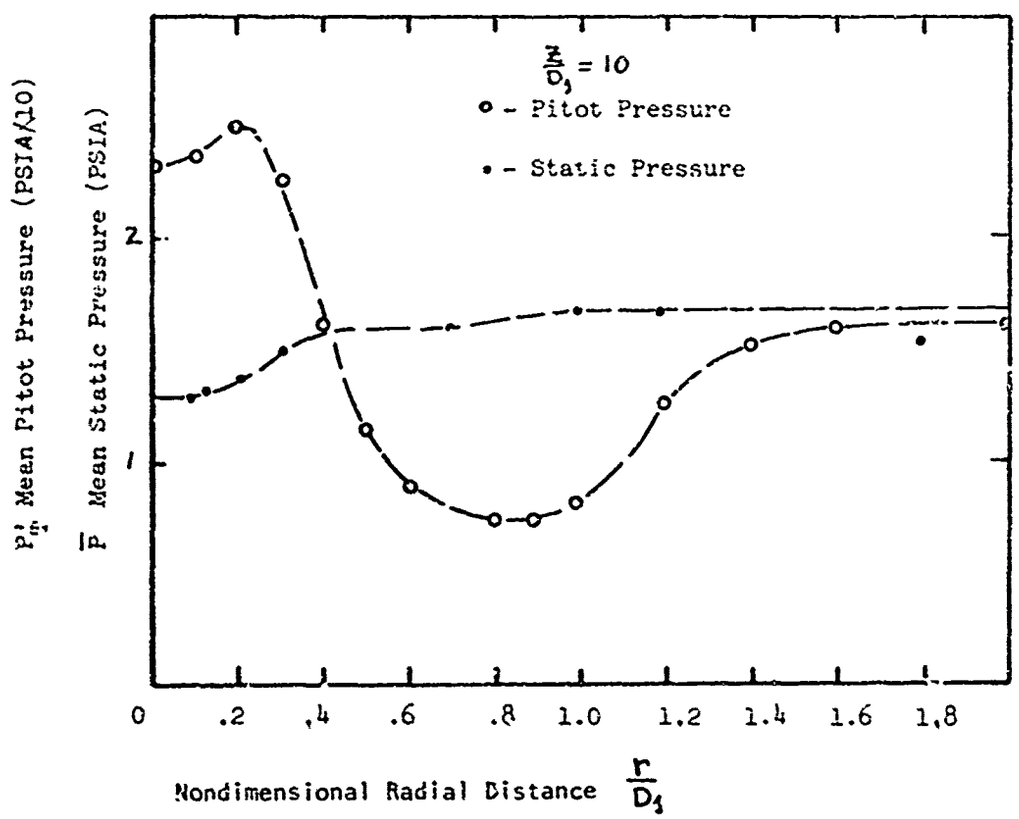

Figure 26. Coaxial Mixing Pitot and Static Pressure Profile

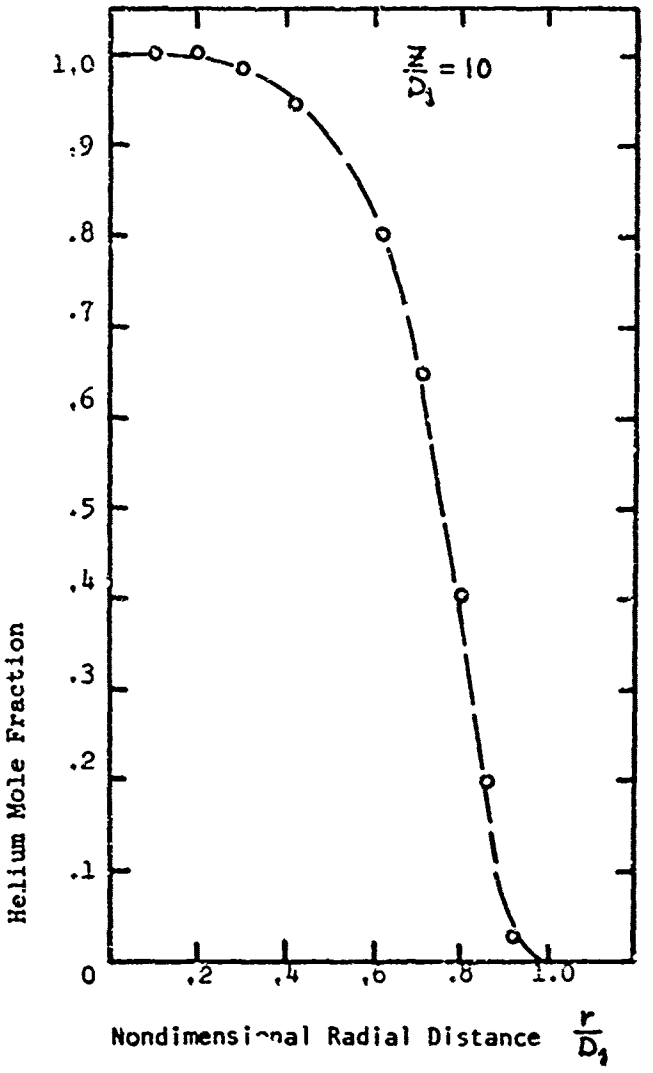

Figure 27. Profile of Helium Mole Fraction

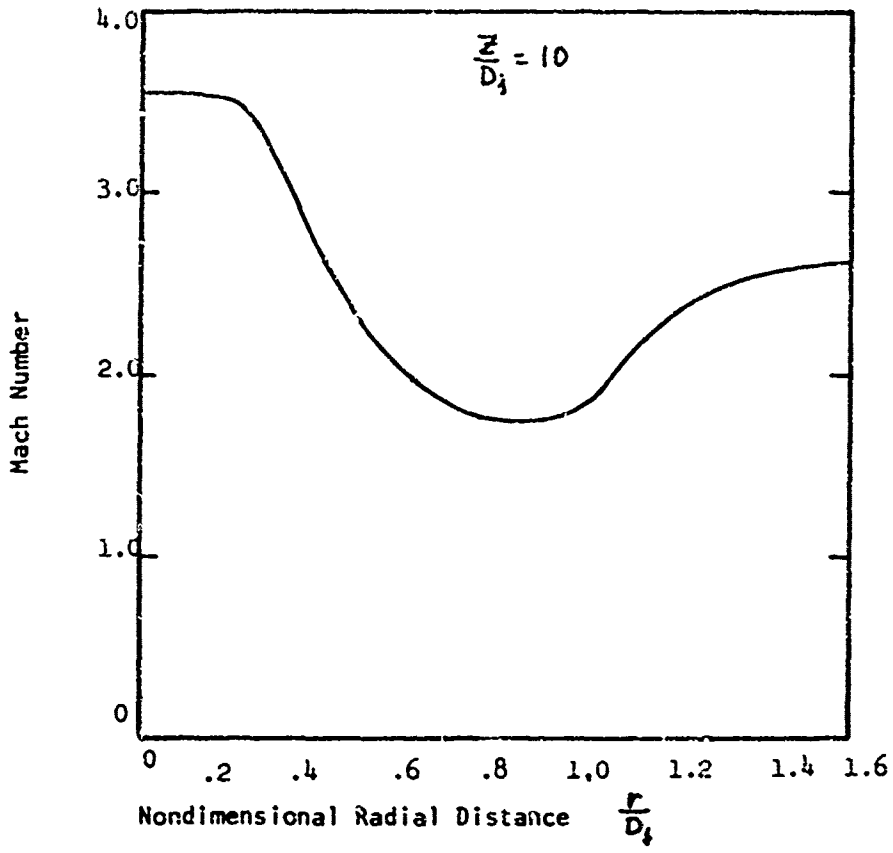

Figure 28. Computed Mach Number Profile

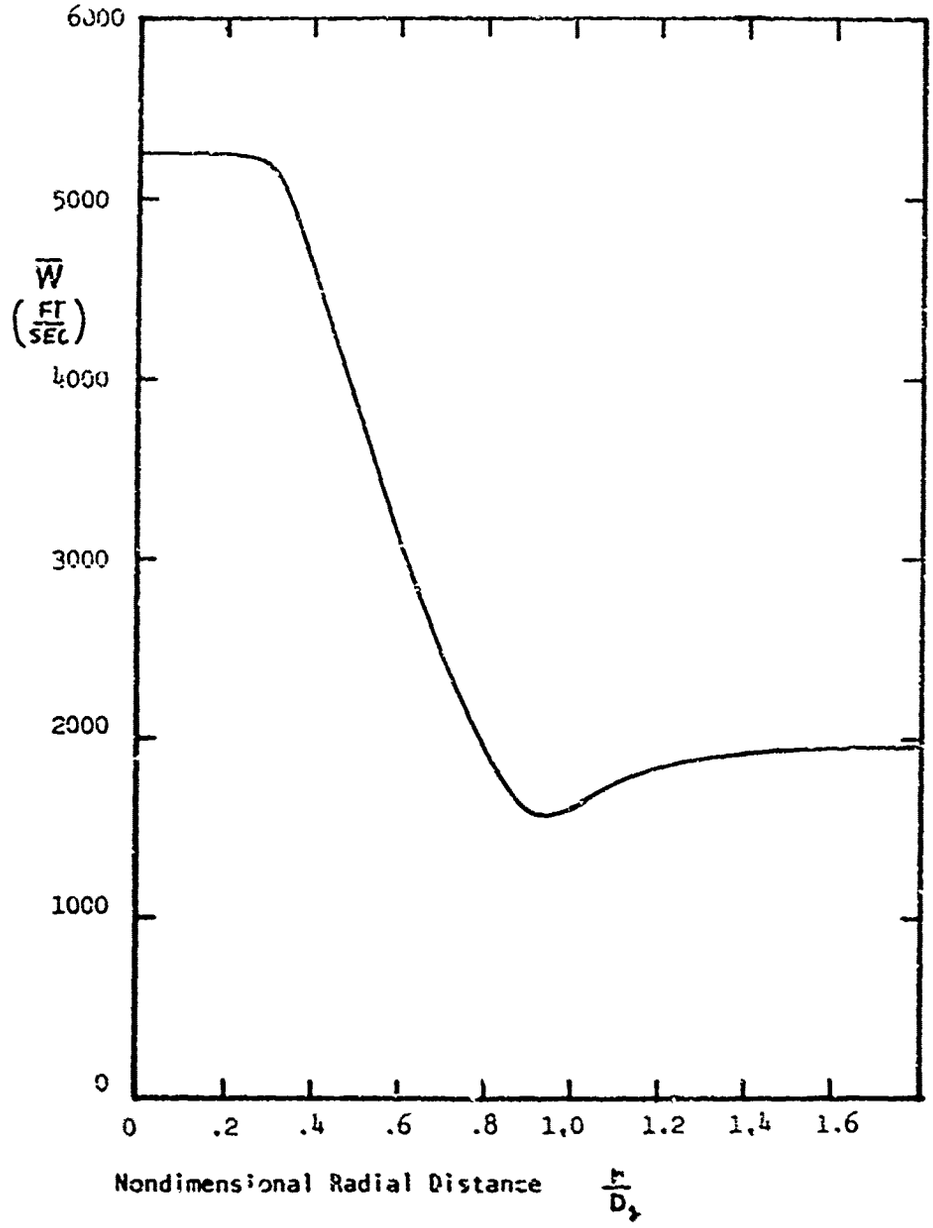

Figure 29. Computed Velocity Profile

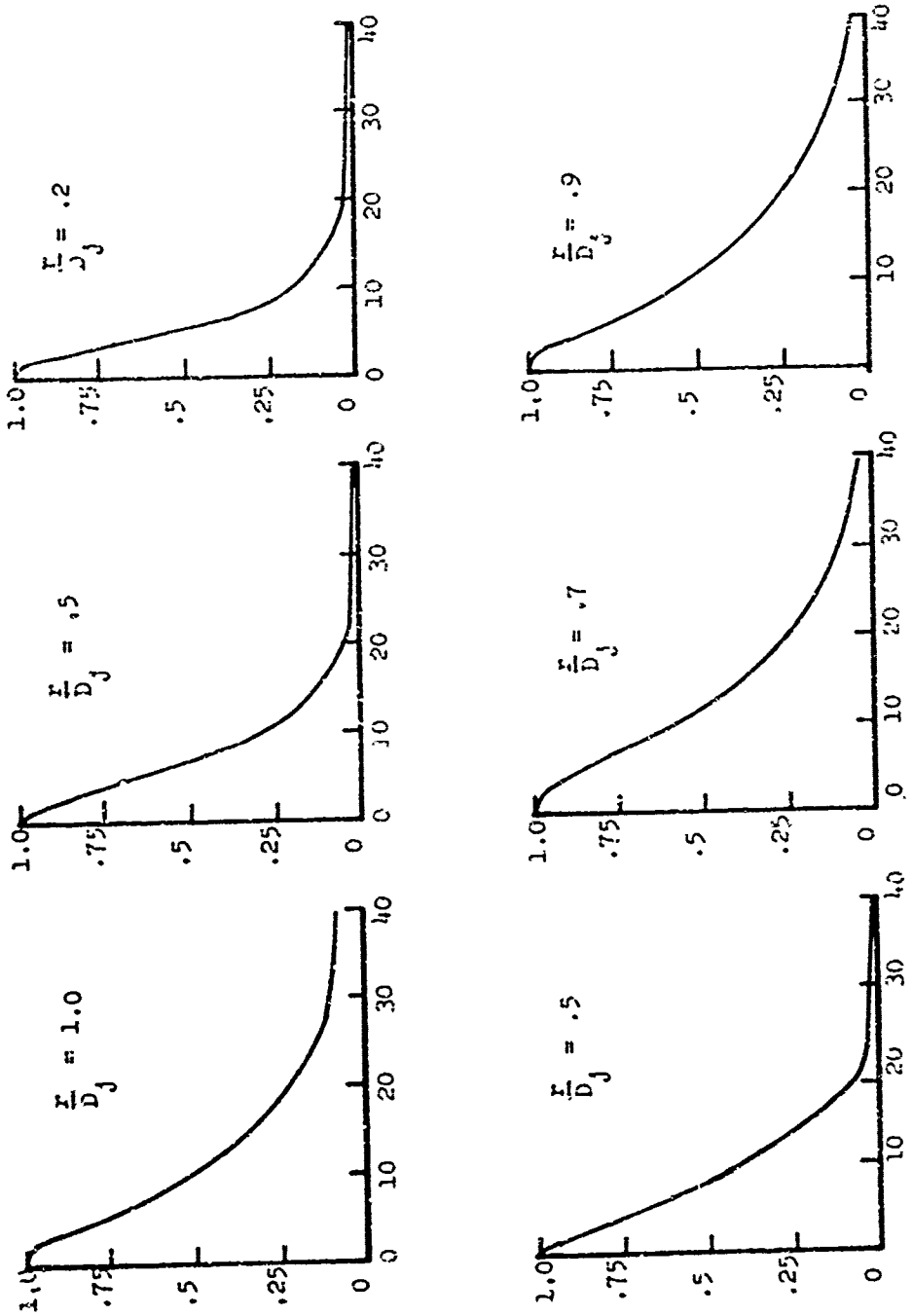

Figure 30. Autocorrelation Coefficients $\frac{Z}{D_j}$ = 10

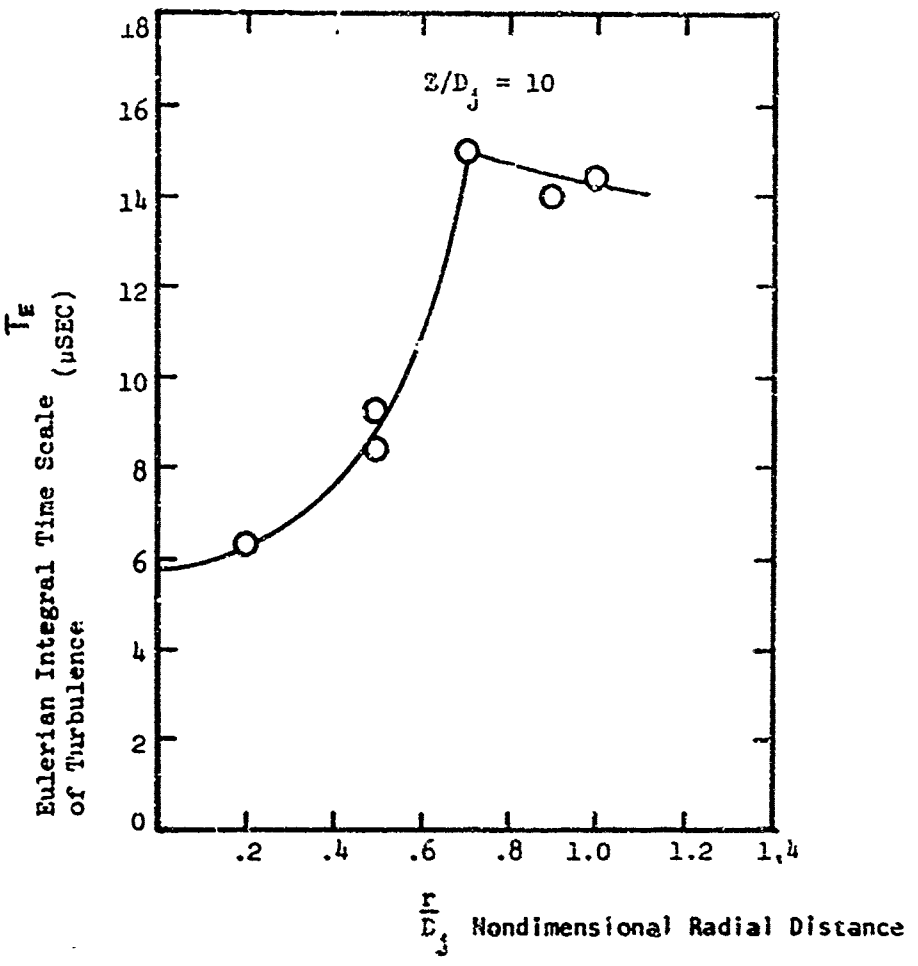

Figure 31. Eulerian Time Scale

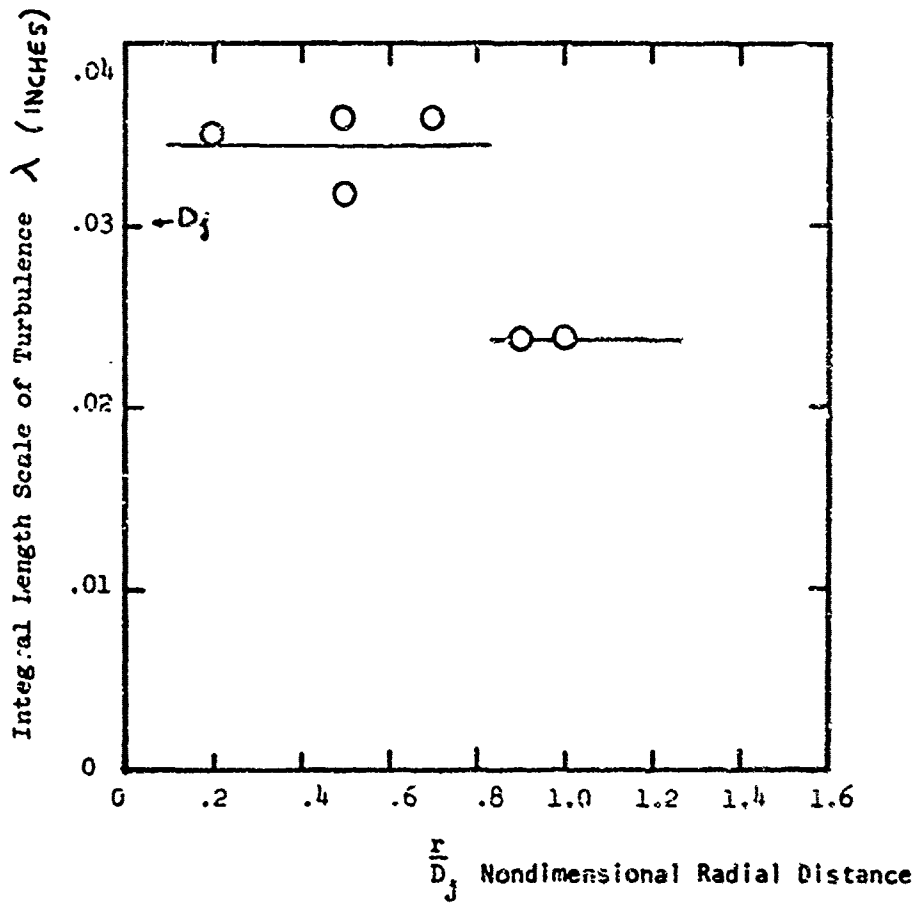

Figure 32. Integral Scale of Turbulence

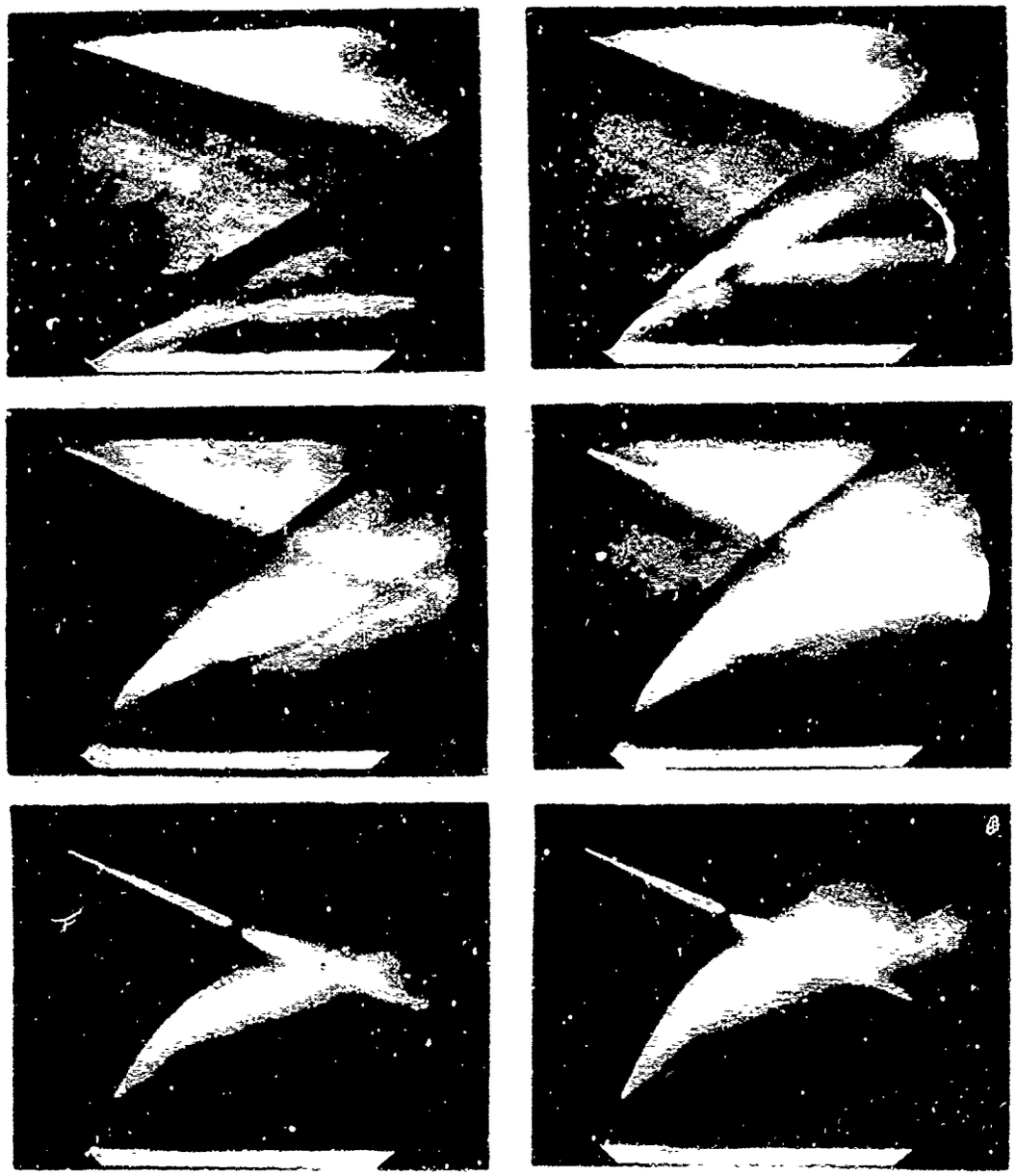

Figure 33. Schlieren Photographs of Helium Penetration into a Mach 2.5 Airstream (Jet to Stream Total Pressure Ratio)

$$\frac{P_{0_f}}{P_{0_a}} = 0.35 \text{ -- } 1.0$$

$$2.7 \text{ -- } 3.9$$

$$5.55 \text{ -- } 8.64$$

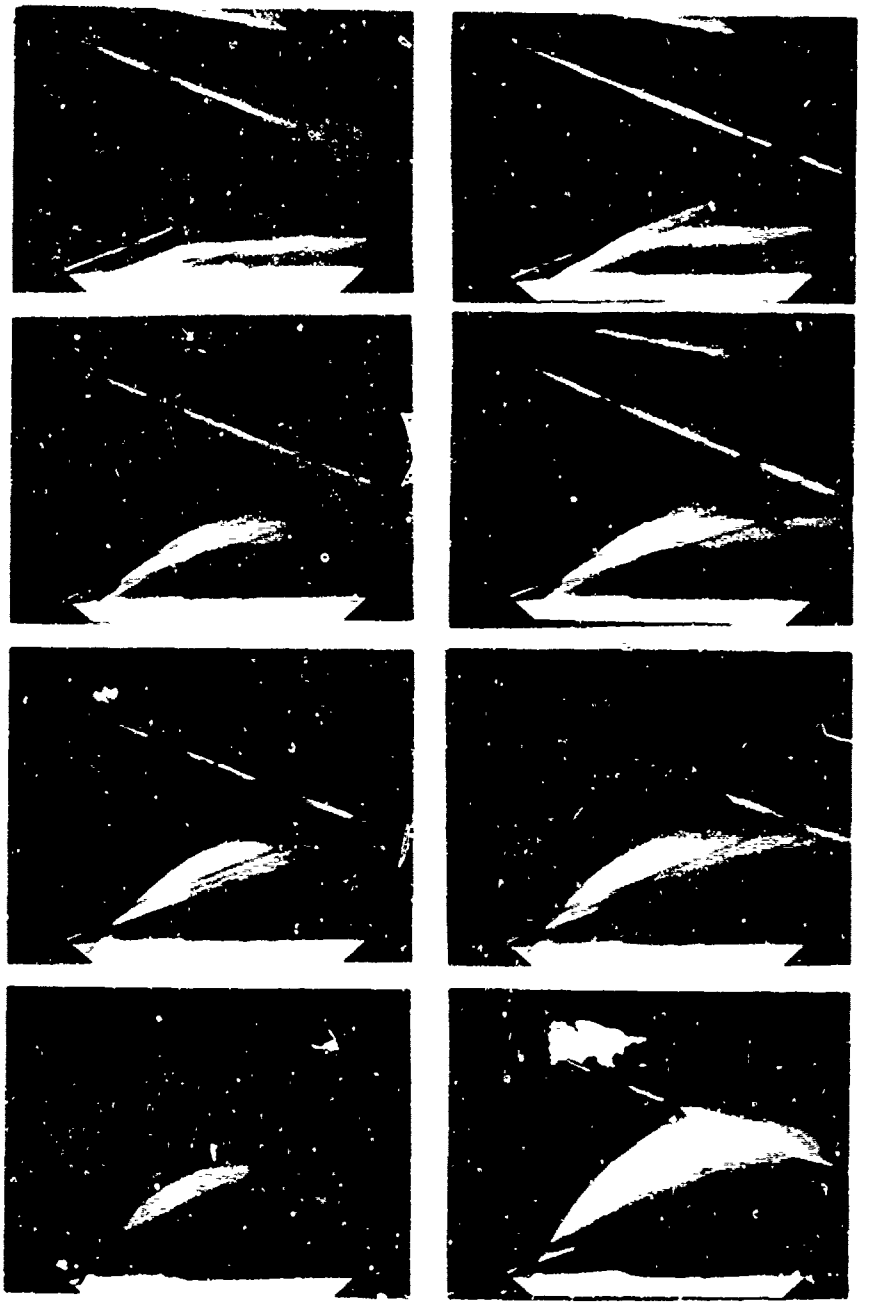

Figure 34. Schlieren Photographs of Helium Penetration into a Mach 3.0 Airstream (Jet to Stream Total Pressure Ratio)

$$\frac{P_{0_j}}{P_{0_a}} = \begin{array}{l} .35 - 0.6 \\ 1.0 - 1.3 \\ 1.8 - 2.7 \\ 3.9 - 5.55 \end{array}$$

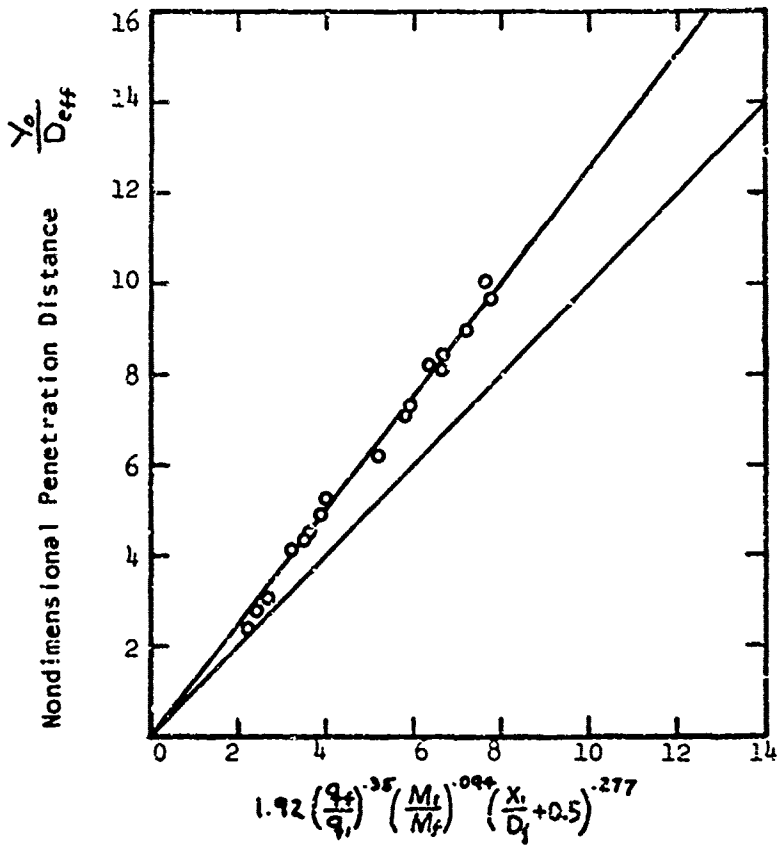

Figure 35. Observed Penetration Height

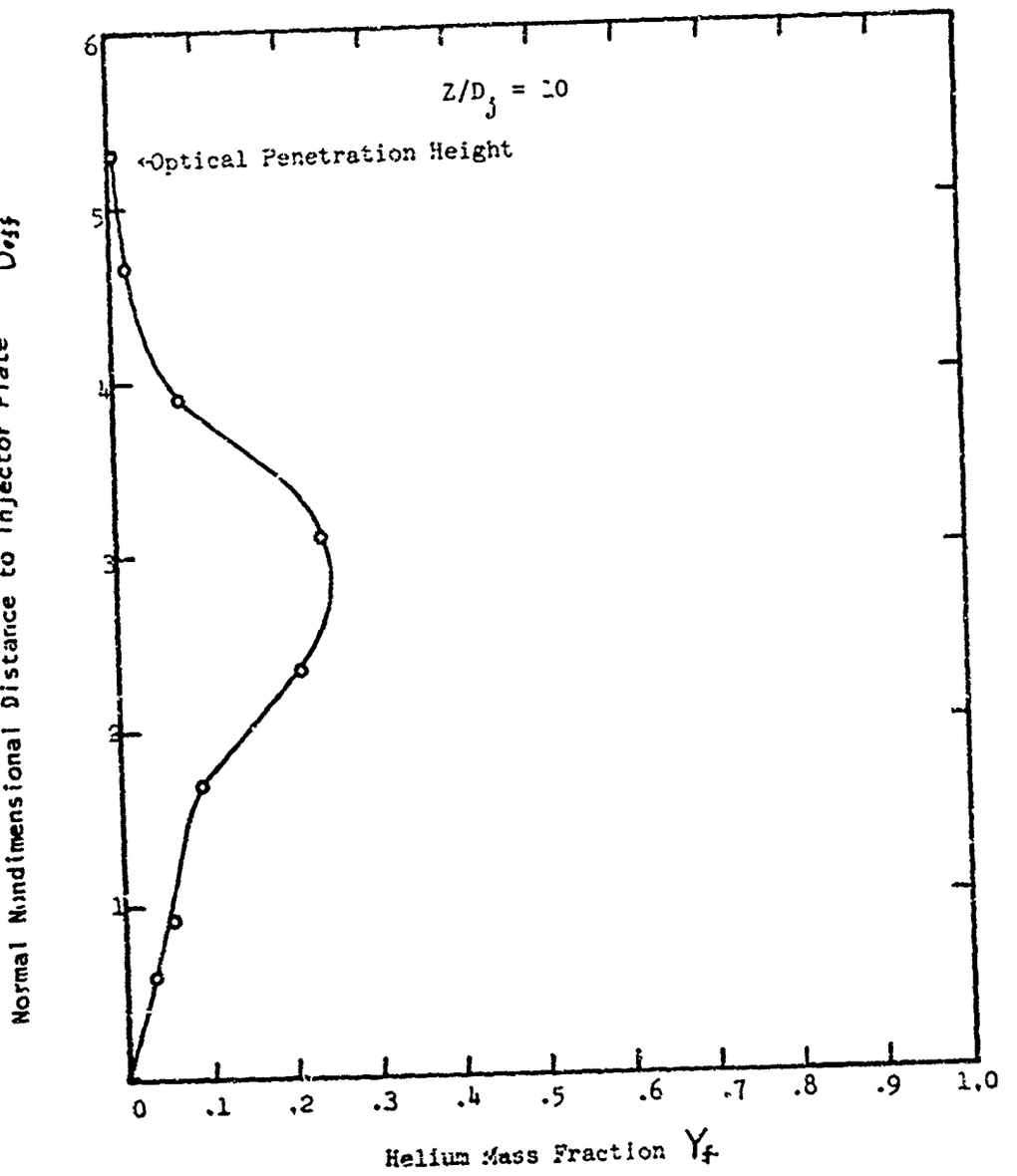

Figure 36. Profile of Helium Concentration

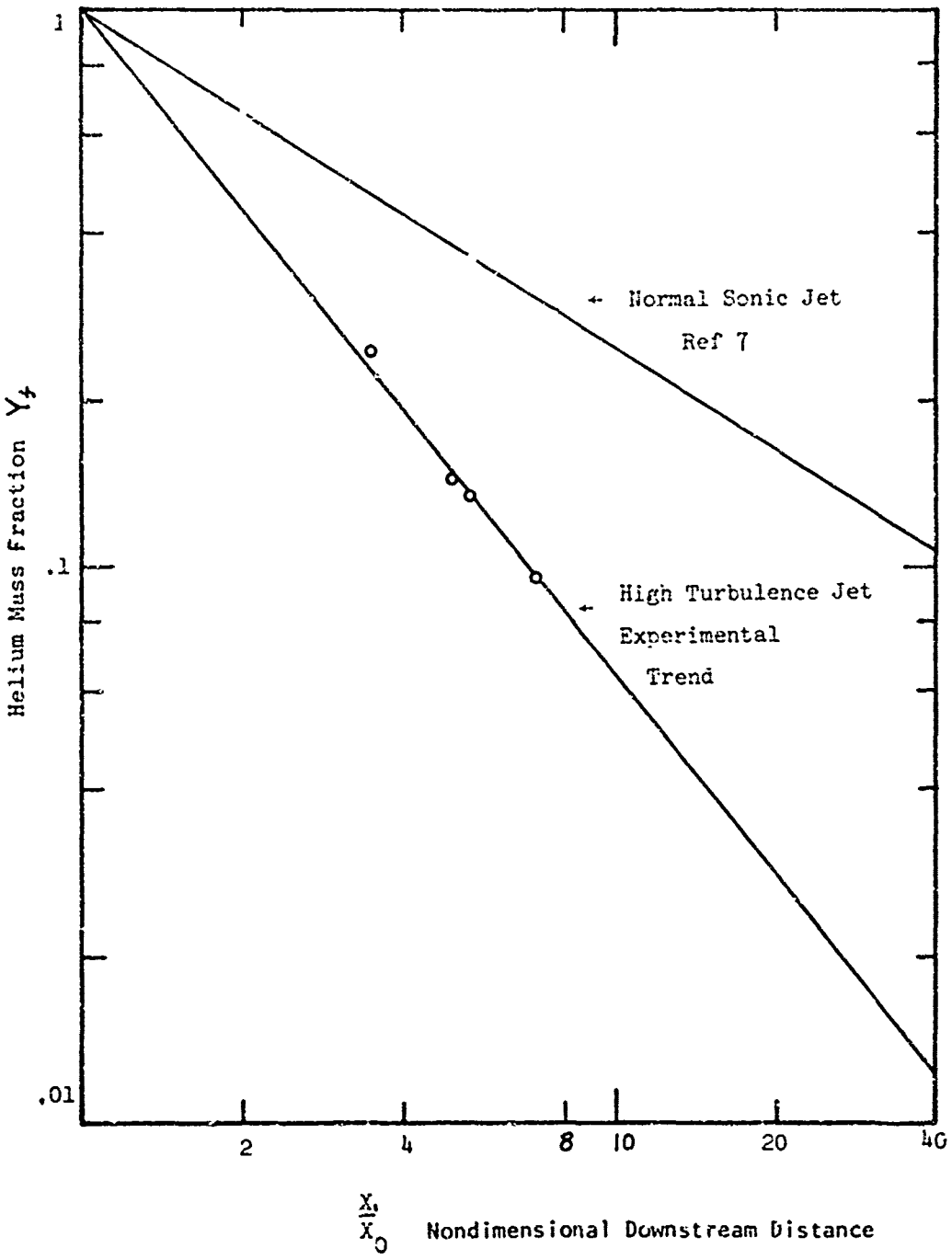

Figure 37. Experimental Mixing Rate of the Normal Injector

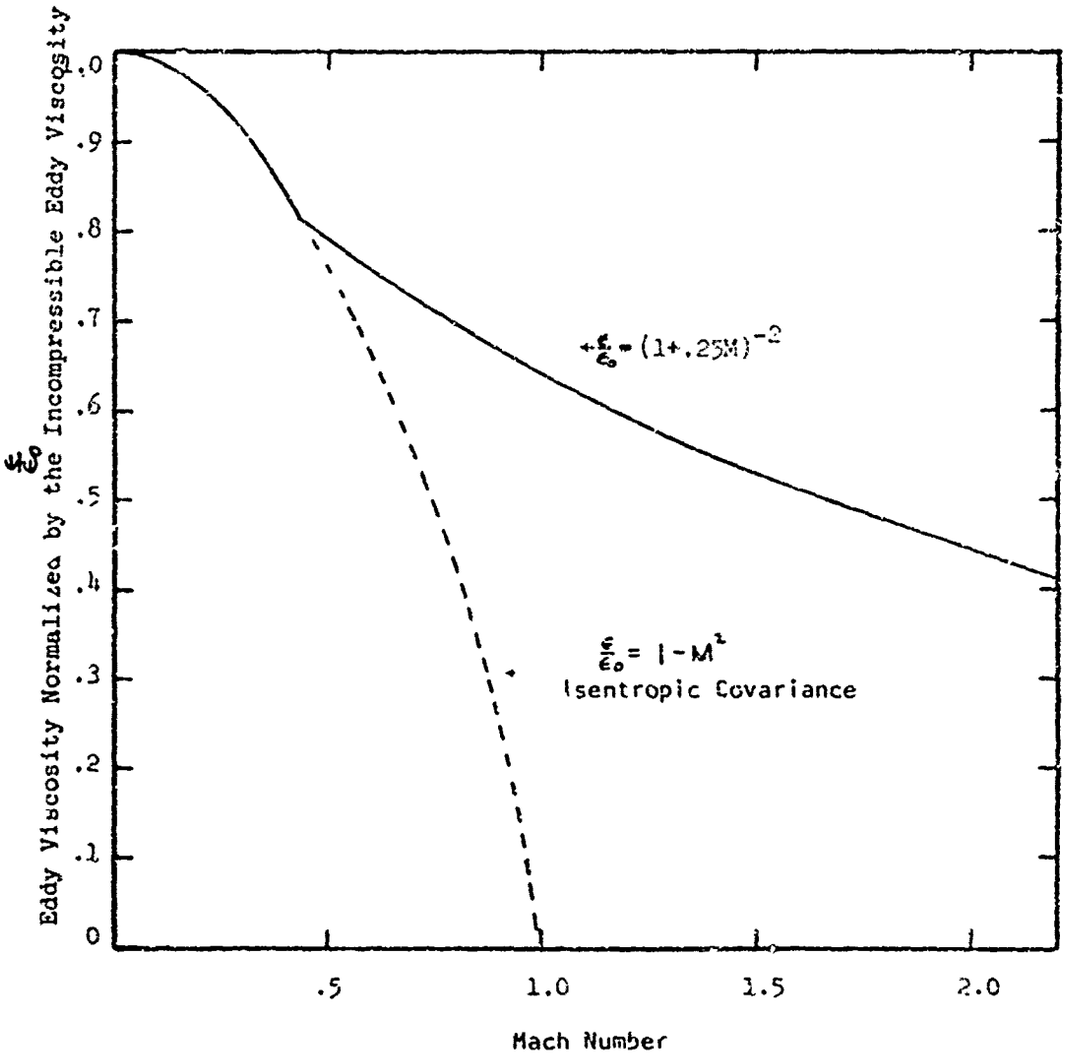

Figure 38. Effect of Compressibility on Eddy Viscosity

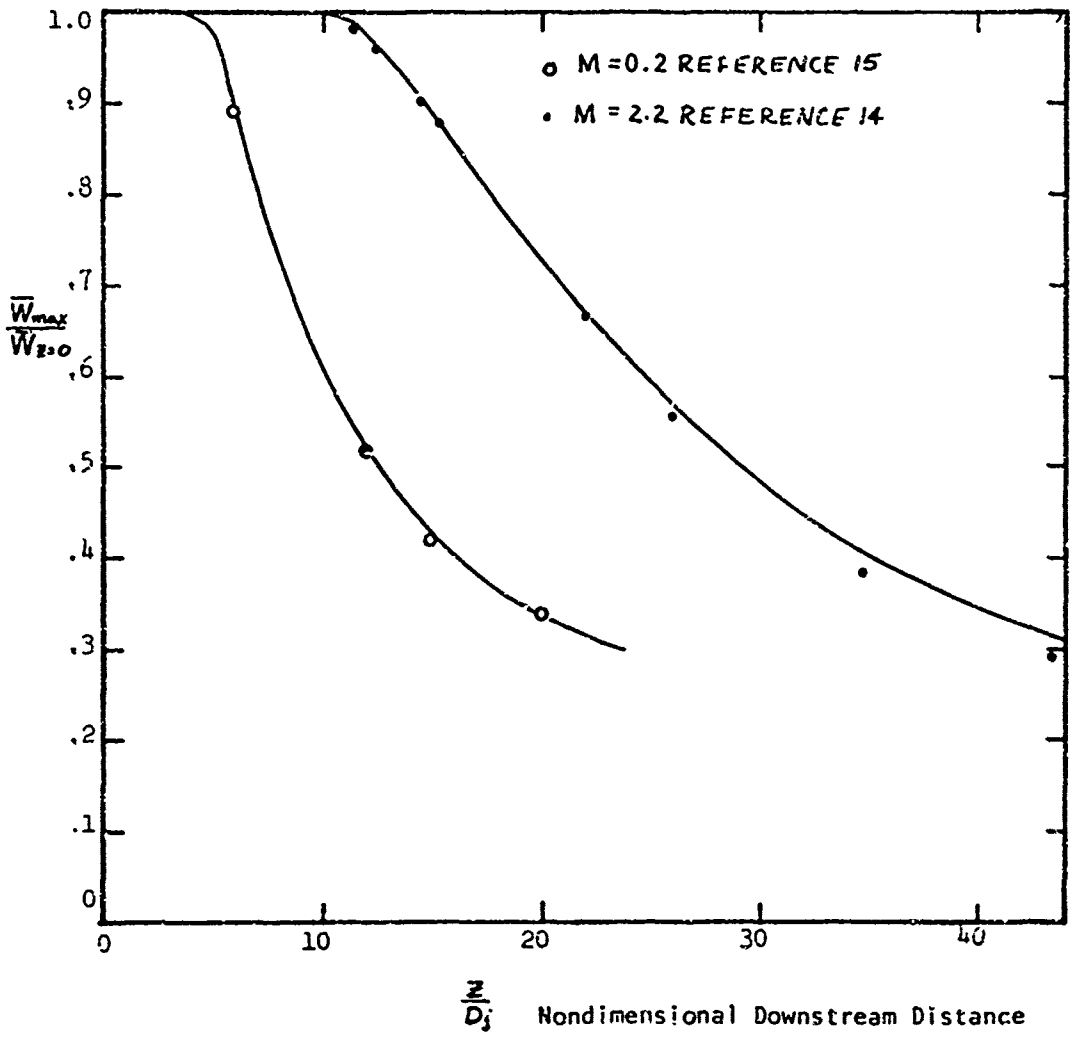

Figure 39. Data Used to Determine Mach Number Dependence of Eddy Viscosity

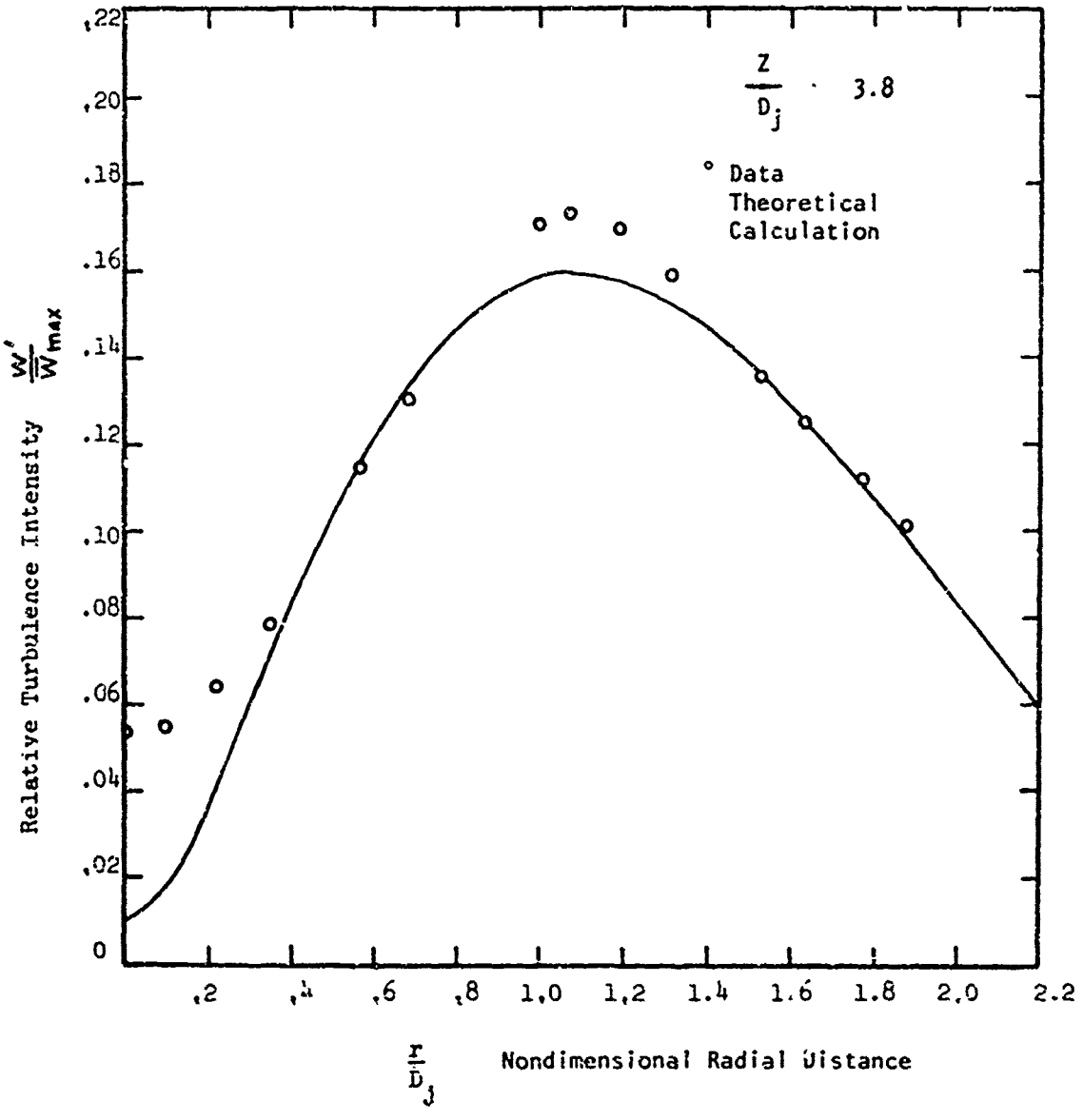

Figure 40. Comparison of Computed and Measured Turbulent Kinetic Energy from Reference 15

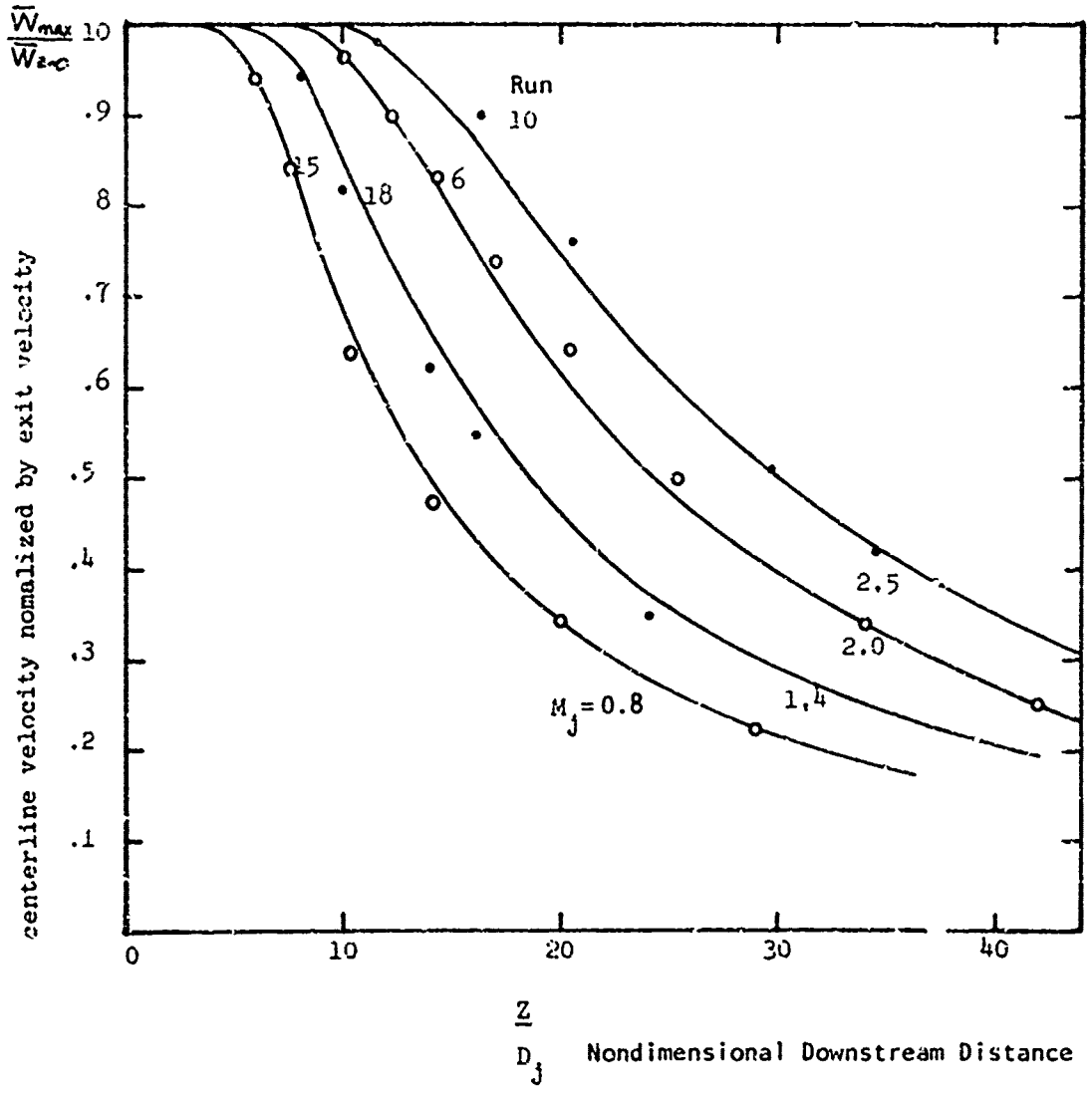

Figure 41. Comparison of Theoretical and Experimental Centerline Velocity Decay; $T_o/T_{oo} = 1$

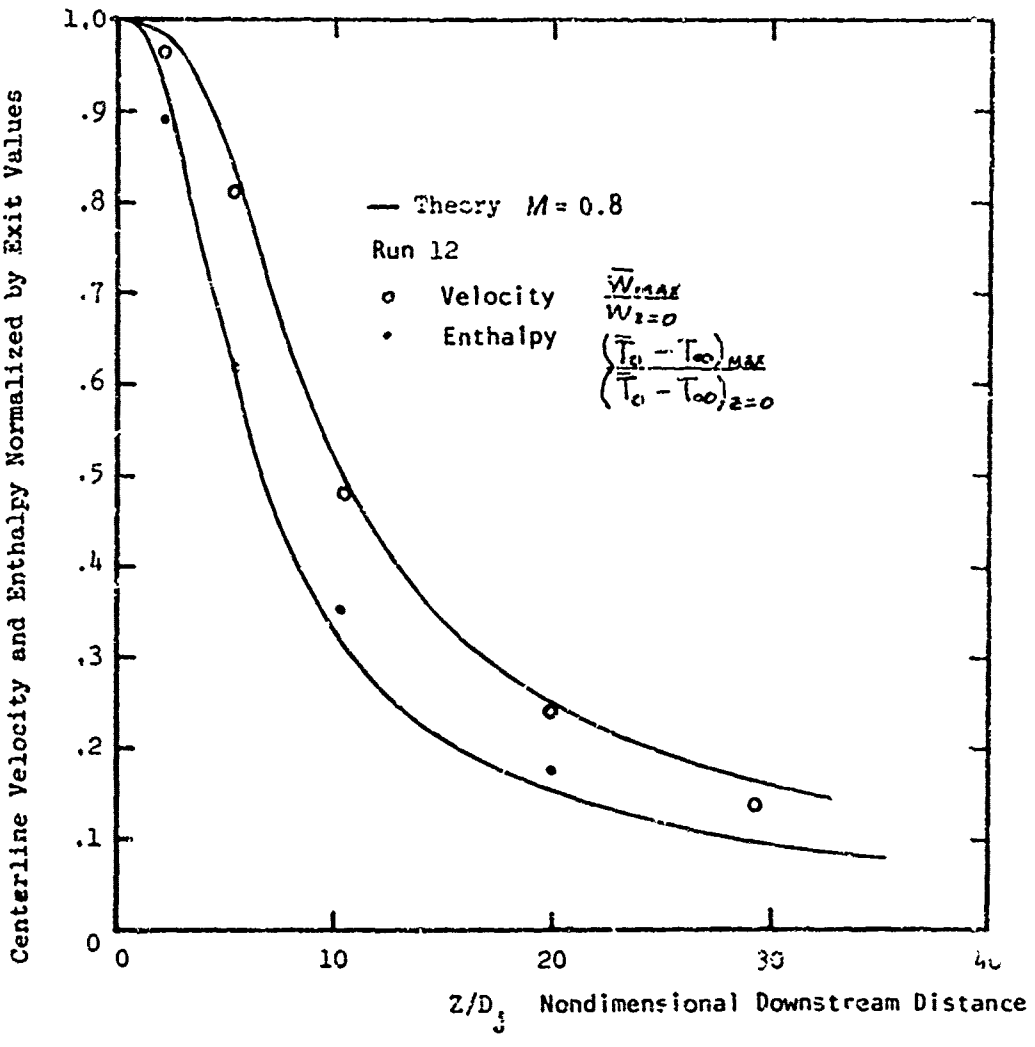

Figure 42. Comparison of Velocity and Normalized Enthalpy Decay

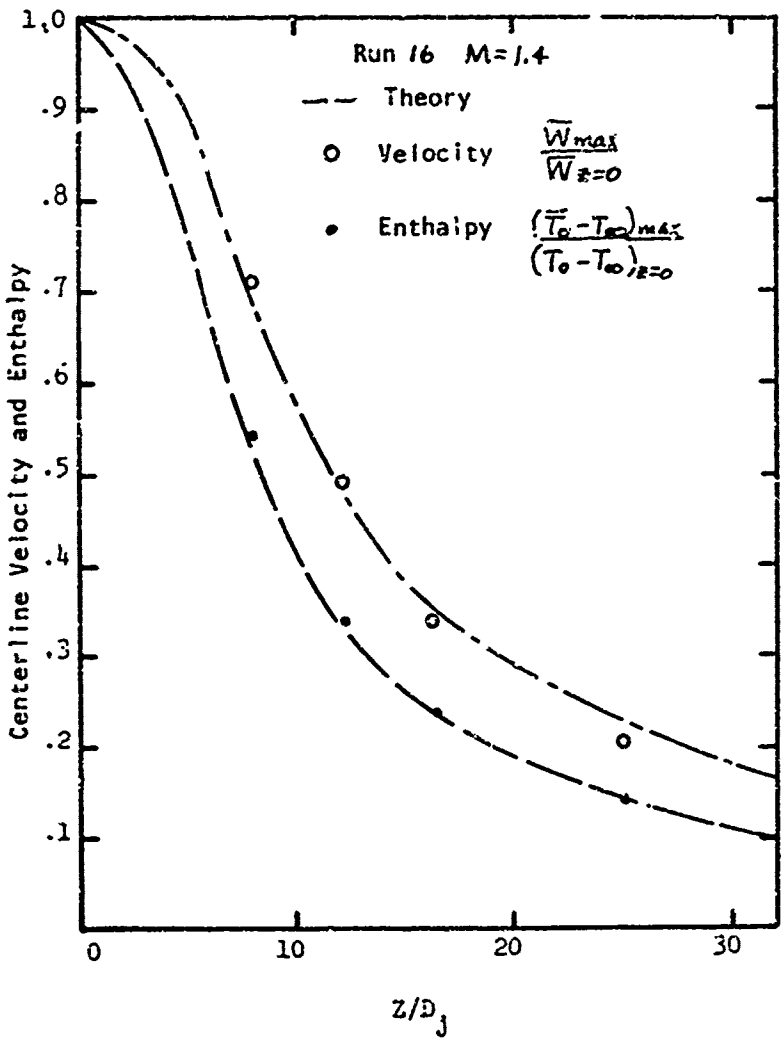

Figure 43. Comparison of Velocity and Normalized Enthalpy Decay

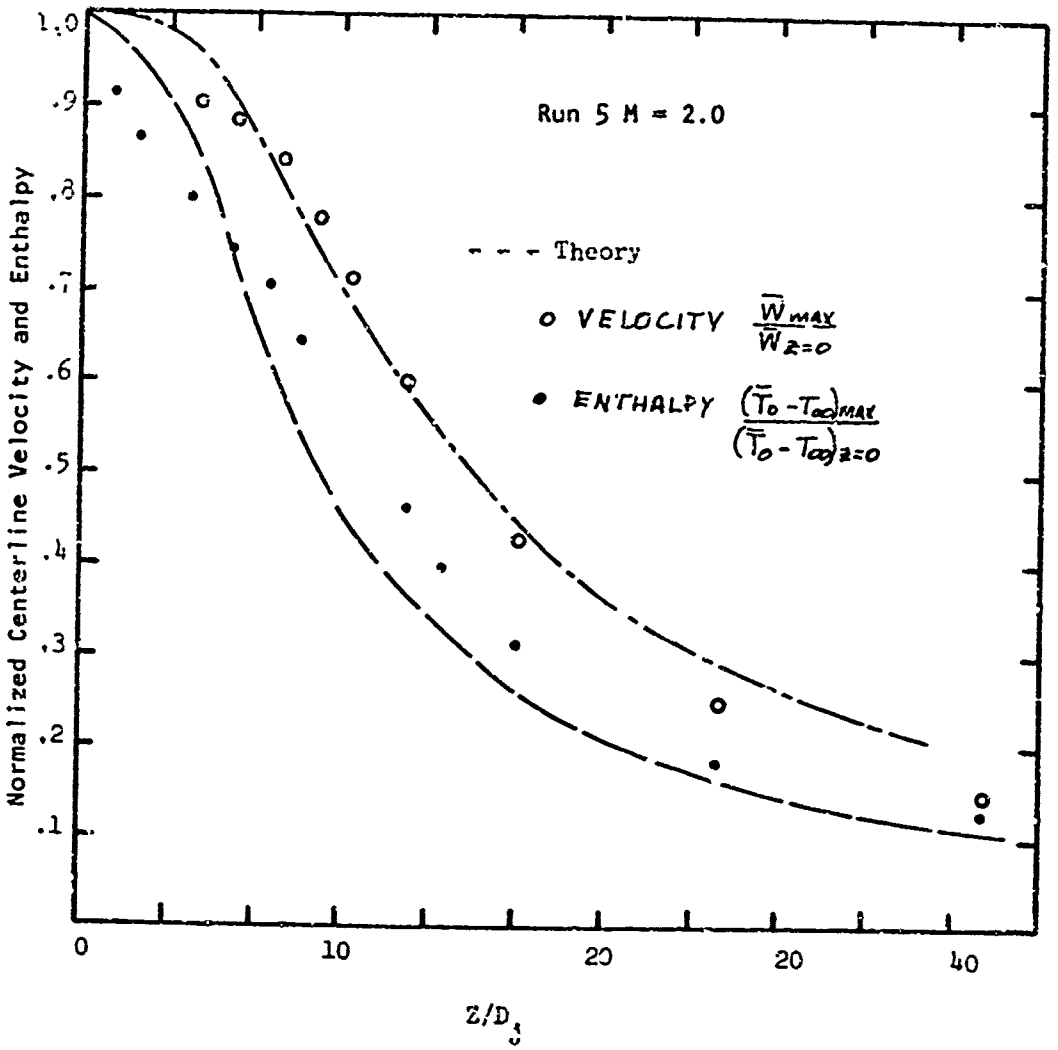

Figure 44. Theoretical and Experimental Free Jet Decay

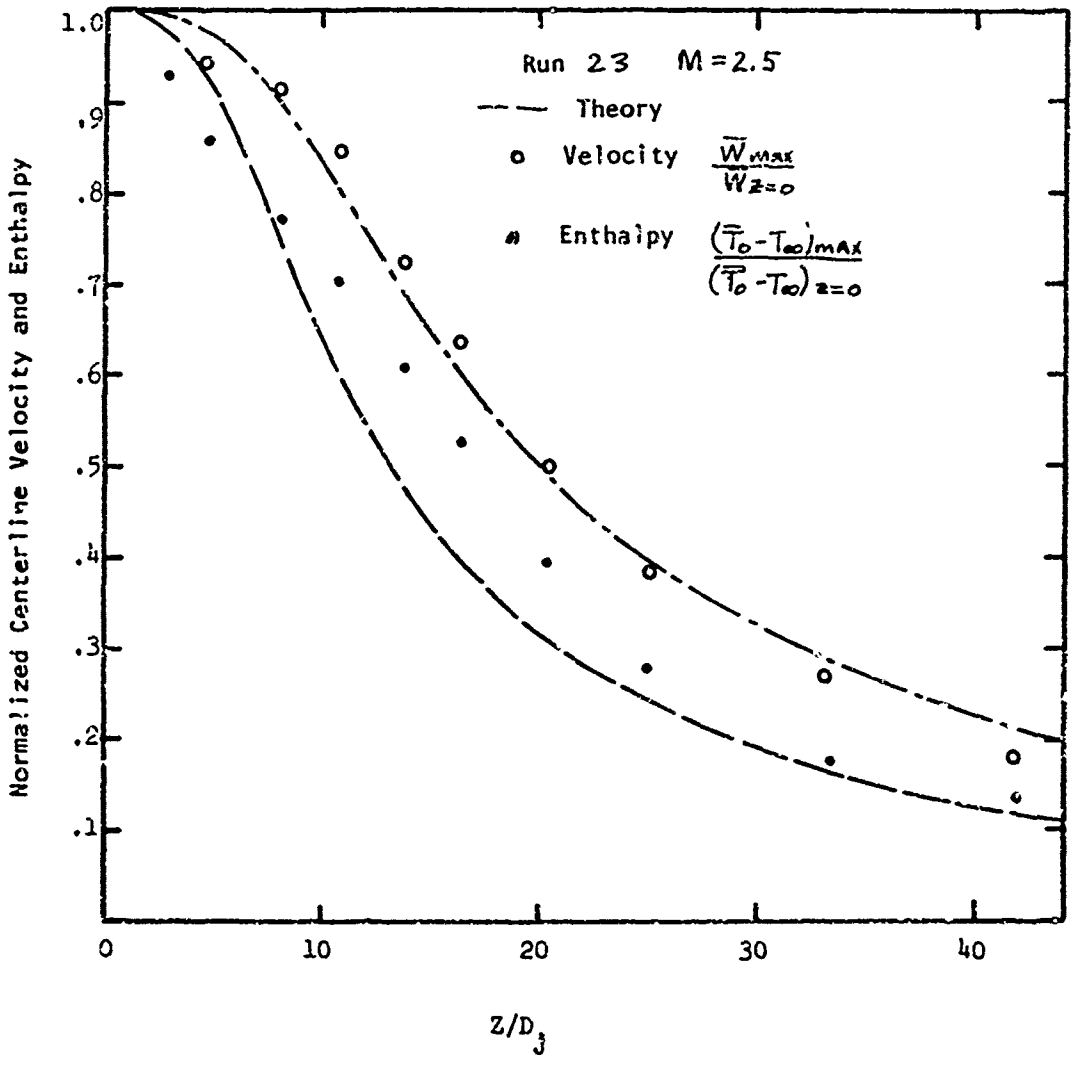

Figure 45. Theoretical and Experimental Free Jet Decay

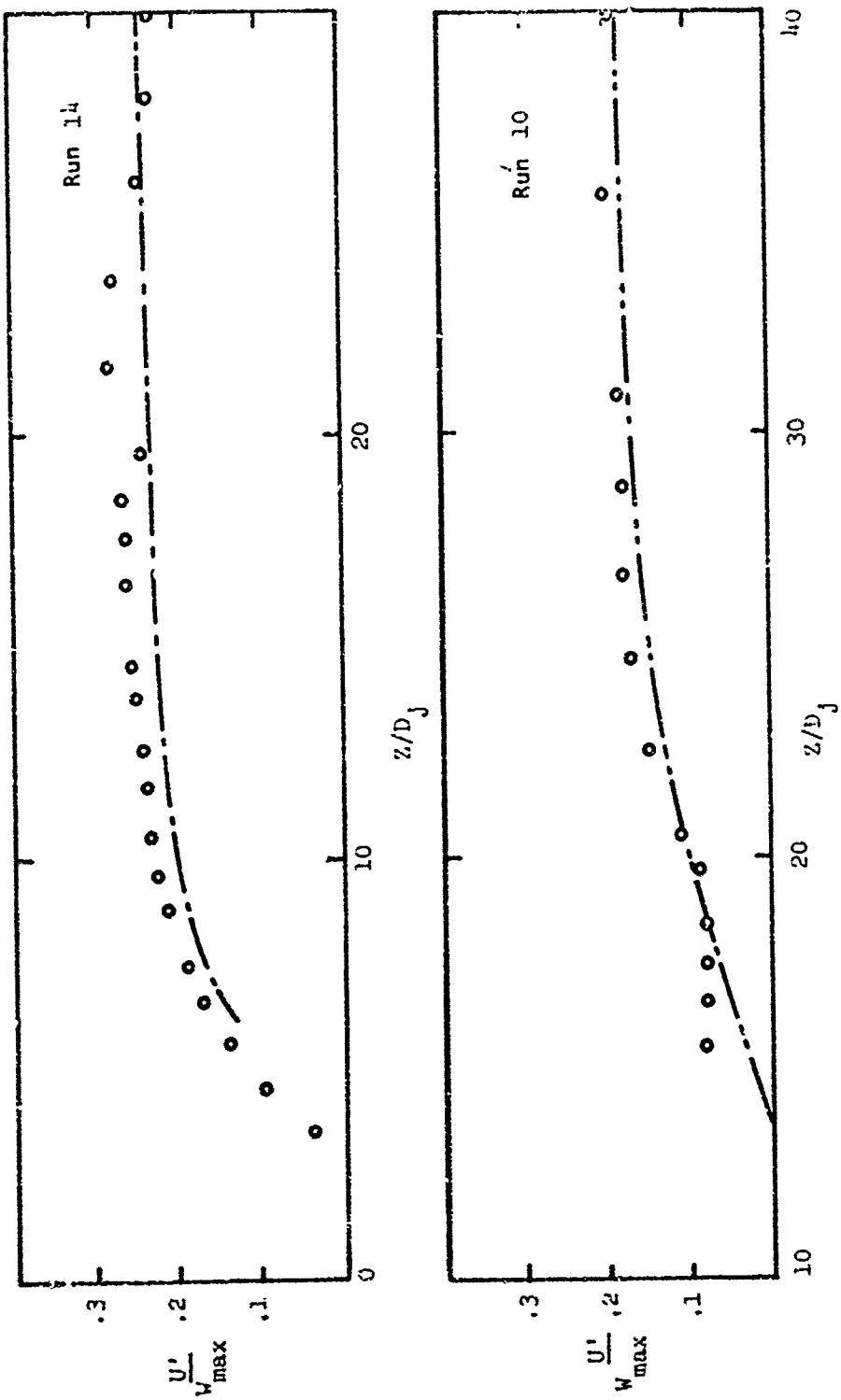

Figure 46. Comparison of Theoretical and Experimental Relative Turbulence Intensity on the Centerline

REFERENCES

1. J. Swithenbank, "New Developments in Supersonic Combustion Research," Proceedings of OAR Research Applications Conference. 13 March 1969.

2. J. Swithenbank and N. A. Chigier, "Vortex Mixing for Supersonic Combustion." Twelfth Symposium (International)on Combustion. The Combustion Institute. 1969.

3. J. A. Shetz, Unified Analysis of Turbulent Jet Mixing. NASA CR-1382. July 1969.

4. P. Bradshaw, D. H. Ferriss, and N. P. Atwell. "Calculation of Boundary Layer Development Using the Turbulent Energy Equation. "Journal of Fluid Mechanics, Vol. 28, pt 3. 1967. 593-616.

5. S. C. Lee and P. T. Harsha, "Use of Turbulent Kinetic Energy in Free Mixing Studies." AIAA Journal, Vol. 8, No. 6, June 1970. 1026-32.

6. F. S. Billig and R. C. Orth, "A Unified Approach to the Problem of Gaseous Penetration into a Supersonic Stream." AIAA Paper No 70-93.

7. J. R. Henry, "Recent Research on Fuel Injection and Mixing and Piloted Ignition for Scramjet Engines. "Twelfth Symposium (International) on Combustion. The Combustion Institute. 1969.

8. Townsend. "Structure of Turbulent Shear Flow." Cambridge University Press. 1956.

9. R. Edelman and O. Fortune. "An Analysis of Mixing and Combustion in Ducted Flows." AIAA Paper No. 68-114, AIAAth Aerospace Sciences Meeting, New York, New York. January 1968.

10. N. V. Arseyeva, et al. "Investigation of Free Submerged Jets. FTD-HT-23-990-68. May 1969.

11. F. R. Povinelli and L. A. Povinelli, "Supersonic Jet Penetration (Up to Mach 4) into a Mach 2 Airstream." AIAA Paper 70-92.

12. A. Vranos and J. J. Nolan. "Supersonic Mixing of a Light Gas and Air. "AIAA Propulsion Joint Specialist Conference, Colorado Springs, Colorado. 14-18 June 1965.

13. S. Corrsin "Extended Applications of the Hot Wire Anemometer." NACA TN 1864. April 1949.

14. J. M. Eggers. "Velocity Profiles and Eddy Viscosity Distribution Downstream of a Mach 2.22 Nozzle Exhausting to Quiescent Air." NACA TN D-3601. September 1966.

15. J. C. Laurence. "Intensity, Scale, and Spectra of Turbulence in Mixing Region of Free Subsonic Jet. "NACA R 1292. 1956.

REFERENCES (Contd)

16. Hinze. "Turbulence." McGraw-Hill Book Company. 1959.

17. M. J. Lighthill. "Jet Noise." AIAA Journal, Vol. 1, No. 7. July 1963.